Digital Hydraulic Actuator Study

Phase III

Final Report

Sponsored by:
Air Programs, Office of Naval Research
Contract Nonr 4375(00)

By:
G. W. Scott

IBM NO. : 66-L03-005

IBM Electronics Systems Center, Owego, New York

November 1966

DIGITAL HYDRAULIC ACTUATOR STUDY

Phase III

Final Report

Sponsored By
Air Programs, Office of Naval Research
Contract Nonr 4375(00)

By
G. W. Scott

IBM No: 66-L03-005

November 1966

IBM *Federal Systems Division, Electronics Systems Center, Owego, New York*

ABSTRACT

To further support the practicability of the digital hydraulic actuator as a control component, IBM has successfully demonstrated operation of the Phase III laboratory model in a simulated digital flight control system. Performance using the laboratory model is compared with the performance when using a mathematical model. Recorded transients and the values obtained for a maximum stable step and gain change are presented. The effect of varying the actuator parameters and the validity of a linearized model is also established. Agreement of the results shows the mathematical model to accurately represent the actual hardware. Hence, this study verified the results of both Phase I and Phase II.

ACKNOWLEDGEMENTS

Mr. J. W. Raider, the originator of the digital hydraulic concept investigated, significantly contributed to the success of this program by his participation during the initial part of Phase III and the earlier phases.

The mathematical model and simulated flight control system was programmed by Mr. N. L. Pleszkoch.

TABLE OF CONTENTS

Section			Page
	ABSTRACT		iii
	ACKNOWLEDGEMENTS		iv
I	INTRODUCTION		1-1
	A.	SUMMARY	1-1
	B.	PURPOSE AND OBJECTIVES OF PROGRAM	1-1
	C.	DESCRIPTION	1-2
	D.	CONCLUSIONS	1-5
	E.	RECOMMENDATIONS	1-5
II	TECHNICAL APPROACH		2-1
	A.	EQUIPMENT - ARRANGEMENT AND DESCRIPTION	2-2
		1. Valve Control Logic	2-2
		2. Position Control Logic	2-4
		3. Digital Hydraulic Actuator	2-4
		4. Coulomb Friction	2-6
	B.	METHOD OF SIMULATION	2-6
		1. Digital Autopilot	2-6
		2. Digital Hydraulic Actuator (Digital Portion)	2-11
		3. Digital Hydraulic Actuator (Analog Portion)	2-15
		4. Comparison	2-17

Table of Contents (cont)

Section			Page
III	MATHEMATICAL MODEL EVALUATION		3-1
	A.	PARAMETER VALUES	3-1
	B.	RESULTS	3-4
		1. Effect of the Parameter C	3-9
		2. Effect of the Parameter β/V	3-10
		3. Gain-Phase	3-14
IV	DIGITAL FLIGHT CONTROL SIMULATION		4-1
	A.	DESCRIPTION	4-1
	B.	RESULTS	4-1
		1. Effect of Leakage Parameters	4-1
		2. Effect of Compensation Gain, K	4-8
		3. Comparison with Analog Flight Control	4-8
		4. Gain-Phase	4-8
V	LINEARIZED MODEL		5-1
	A.	DEVELOPMENT	5-1
	B.	RESULTS	5-4
REFERENCES			5-5
APPENDIX	Title		A-1
A	DIGITAL HYDRAULIC ACTUATOR OPERATIONAL CONCEPT		A-1
B	CIRCUITS CONTROL LOGIC		B-1
C	LIST OF SYMBOLS		C-1
D	DISTRIBUTION LIST-NONR 4375(00)		D-1

LIST OF ILLUSTRATIONS

Figure	Title	Page
1-1	Simulation Arrangement	1-3
1-2	Laboratory Arrangement	1-4
2-1	Arrangement of Equipment	2-3
2-2	Flow Curve for Digital Unit	2-4
2-3	Phase III Control Logic	2-5
2-4	Mathematical Model of Digital Autopilot, Digital Actuator, and Missile Dynamics	2-7
2-5	Digital Autopilot	2-8
2-6	Pulse Logic	2-9
2-7	Flow Calculations	2-11
2-8	Timing Chart	2-13
2-9	Digital Integration	2-14
2-10	Method of Obtaining Limiting Values for the Digital Integrator	2-15
2-11	Actuator Dynamics	2-16
2-12	Simulation of Coulomb Friction (Phase I)	2-16
2-13	Simulation of Coulomb Friction (Phase III)	2-17
2-14	Recorded Transients for ψ_o = -1/2° Run 207 Table 2-1	2-19
3-1	Recorded Motion of Ram with Digital Hydraulic Actuator in Simulated Control Loop (ΔF = 60 lbs)	3-6
3-2	Ram Motion for a Yaw Step Command (N_y = 10)	3-7
3-3	Simulation Arrangement	3-8
3-4	Block Diagram for DHA Load Dynamics	3-9
3-5	Recorded Transients Showing Actual Motion of Digital Hydraulic Actuator and the Motion Generated with the Mathematical Model	3-10
3-6	Recorded Transients for a Yaw Step Command (N_y = 10) Using Mathematical Model	3-11
3-7	Limit Cycle Generated with the Mathematical Model in the Simulated Control System	3-11
3-8	Recorded Transients for a Yaw Step Command (N_y = 10) Using Actual Hardware with Mathematical Model Operated Open Loop (Ref - Figure 3-3)	3-12

List of Illustrations (cont)

Figure	Title	Page
3-9	Response to a Yaw Step Command with C = 6 lb sec/in.	3-13
3-10	Response to a Yaw Step Command with C = 18 lb sec/in	3-14
3-11	Limit Cycle	3-15
3-12	Response to a Yaw Step Command for (a) β/V = 13,300 lb/in^5 (b) β/V = 100,000 lb/in^5	3-16
3-13	Limit Cycle	3-17
3-14	Closed Loop Amplitude and Phase Characteristics of Simulated Digital Control System when Closing the Loop with the Laboratory Model	3-18
3-15	Closed Loop Amplitude and Phase Characteristics of Simulated Digital Flight Control System Using Mathematical Model (See Table 3-1)	3-19
4-1	Recorded Transients for a Yaw Step Command N_y = 10 (See Table 4-1)	4-4
4-2	Recorded Transients for an Initial Yaw Condition, ψ_o = -1/2° (Ref: Table 4-1)	4-5
4-3	Recorded Transients for an Initial Yaw Condition (ψ_o = -1/2°) and no Leakage (q_L = q_{LC} = 0)	4-6
4-4	Recorded Transients for an Initial Yaw Condition (ψ_o = -1/2°), Assuming the "Worst" Case Leakage (q_L = 0.150 in^3/s, q_{LC} = -0.0165 in^3/s)	4-7
4-5	Recorded Transients for a Yaw Step Command (Ny = 10) Showing Steady State Error of ψ when K → 0 (K = 2^{-16})	4-9
4-6	Recorded Transients for a Yaw Condition (ψ_o = -1/2°) with K = 2^{-5}	4-10
4-7	Recorded Transients Using Analog Flight Control for a Yaw Step Command (N_y = 10)	4-12
4-8	Recorded Transients Using Analog Flight Control System for an Initial Yaw Condition (ψ_o = +1/2°)	4-13
4-9	Recorded Transients for a Yaw Step Command (N_y = 10) with K = 2^{-9} (Ref - Table 4-1)	4-14
4-10	Recorded Transients for an Initial Yaw Condition (ψ_o = -1/2°) with K = 2^{-9} (Ref - Table 4-1)	4-15

List of Illustrations (cont)

Figure	Title	Page
4-11	Closed Loop Amplitude and Phase Characteristics of Simulated Polaris Digital Flight Control	4-16
5-1	Block Diagram of Digital Flight Control System Neglecting Load Dynamics	5-2
5-2	Block Diagram Equivalent of Figure 5-1 when Neglecting Quantization and Restricting Input to Small Signals	5-2
5-3	Identity Used to Reduce Figure 5-2 to Figure 5-4	5-3
5-4	Equivalent Form of Figure 5-2	5-3
5-5	Linearized Model of Digital Flight Control System	5-3
5-6	Closed Loop Amplitude and Phase Characteristics of Linearized Model (Ref Fig. 5-5)	5-4
5-7	Computed Response to a Yaw Command (N_y = 10) Using Linearized Model	5-5
A-1	Schematic of the Basic Digital Hydraulic Actuator	A-3
A-2	Digital Hydraulic Actuator	A-4
A-3	Pilot Drive Schematic	A-6
B-1	Clock Pulses - Function and Time Relation (Revised)	B-3
B-2	Central Logic	B-4
B-3	Clock Generation	B-5
B-4	Current Driver	B-5
B-5	Negative Current Driver	B-6
B-6	Positive Current Driver	B-6
B-7	Sign Pulse Generation	B-7
B-8	Small Pulse Generation	B-7
B-9	Large Pulse Generation	B-8
B-10	Amplifiers and Command Inverters	B-8
B-11	Sign Driver	B-9
B-12	Delay Generation Logic	B-9
B-13	Small Actuating Driver	B-10
B-14	Large Actuating Driver	B-10
B-15	Error Detector	B-11

LIST OF TABLES

Table	Title	Page
2-1	Simulation Runs to Determine Agreement Between the Methods of Implementing the Mathematical Model	2-18
3-1	Parameter Values	3-2
3-2	Performance of Simulated Flight Control System	3-4
4-1	Parameter Values for Simulation of Digital Flight Control	4-2
4-2	Summary of Results - Simulation of Digital Flight Control	4-3
4-3	Results of Analog Flight Control Simulation (Phase I)	4-11

Section I

INTRODUCTION

A. SUMMARY

Completion of Phase III yields results which further support the practicability of a digital hydraulic actuator (DHA) for flight control. A laboratory model of the DHA was operated in a closed loop simulating the digital flight control of the Polaris missile. Performance of the simulated control system using the actual hardware is compared with the performance obtained with the mathematical model. Results presented show the mathematical model to accurately describe hardware dynamics.

Due to the ram area ratio, the system performance could not be determined with the required friction load. However, having established the validity of the mathematical model, the performance of the system with the required ram area and friction load was determined by simulation. The effect of varying the actuator parameters and the performance for a "worst" case parameter condition was also established. Analog flight control, which was simulated in Phase I, is used to provide a basis for evaluating the digital flight control.

A linearized model of the DHA is derived. The model is shown to be a valid approximation when operation is not velocity saturated and quantization is ignored. Frequency response, phase shift, and response to a step command is used as a basis to show the linearized model is a good approximation.

B. PURPOSE AND OBJECTIVES OF PROGRAM

Control of an aerospace vehicle can potentially be simplified by using the capabilities of the digital guidance computer for performing those control functions now being accomplished by analog techniques. To study the impact of digitally controlled actuators on flight control systems and to ascertain those requirements of the DHA, ONR initiated Contract No. Nonr 4375(00). The total objective of this program is to demonstrate the feasibility of a DHA as a flight control component. The program consists of three phases whose objectives are:

- Phase I - To ascertain those DHA requirements that are necessary in an aerospace application such as Polaris

- Phase II - To design and evaluate DHA meeting the requirements found necessary in Phase I

- Phase III - To demonstrate the performance of the DHA hardware in a simulated digital flight control system and to establish the accuracy of the mathematical model.

The use of an incremental DHA will result in:

- System simplification by the elimination of digital-to-analog conversion equipment required for communicating between the digital computer and the actuator

- Elimination of an output transducer and a summing amplifier in the analog hydraulic servo loop

- Substitution of bi-stable control valves for the analog control valves, the latter being more susceptible to null shift and oil contamination

- Increased versatility to perform such operations as programmed gain changes or adaptive functions

- A significant step toward realizing an all-digital control system.

C. DESCRIPTION

The IBM Digital Metering Unit complemented by a hydraulic actuator make up the DHA. The metering unit actuated by digital commands produces a required change of position by the transfer of calibrated fluid volumes. Each digital command produces a volume of fluid equal to one quantum of position. The DHA thus provides a capability of transforming digital commands without conversion into related output positions. A detailed description of the operational concept is presented in Appendix A.

A mathematical model of the DHA is compared with the actual hardware by the arrangement depicted schematically in Figure 1-1. The arrangement provides a capability of monitoring the unused model. Equations describing the flight control system and the DHA are implemented by a hybrid combination of an IBM 709 EDPM and a EAI Analog Computer. The arrangement of the hardware is shown in Figure 1-2.

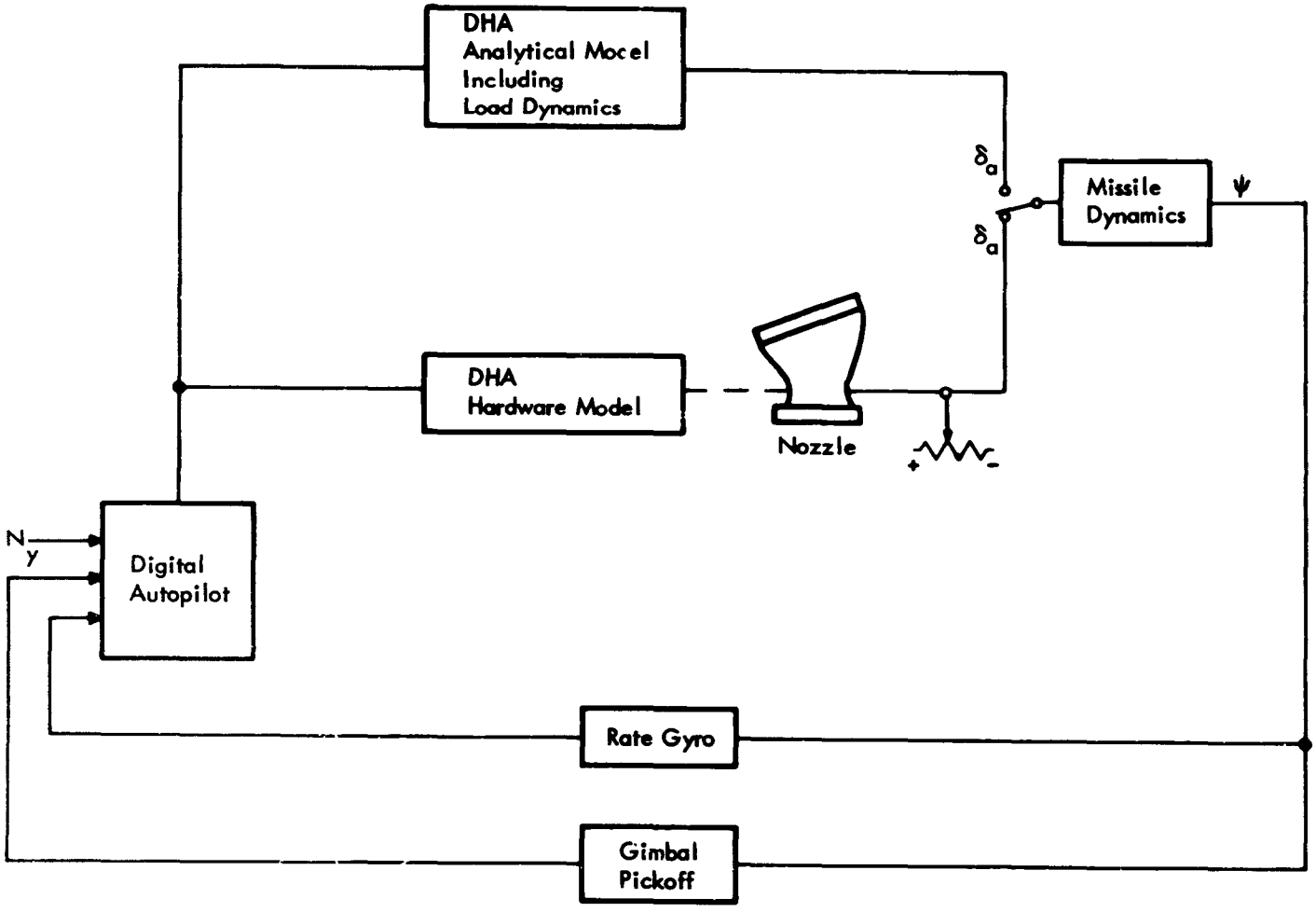

Figure 1-1. Simulation Arrangement

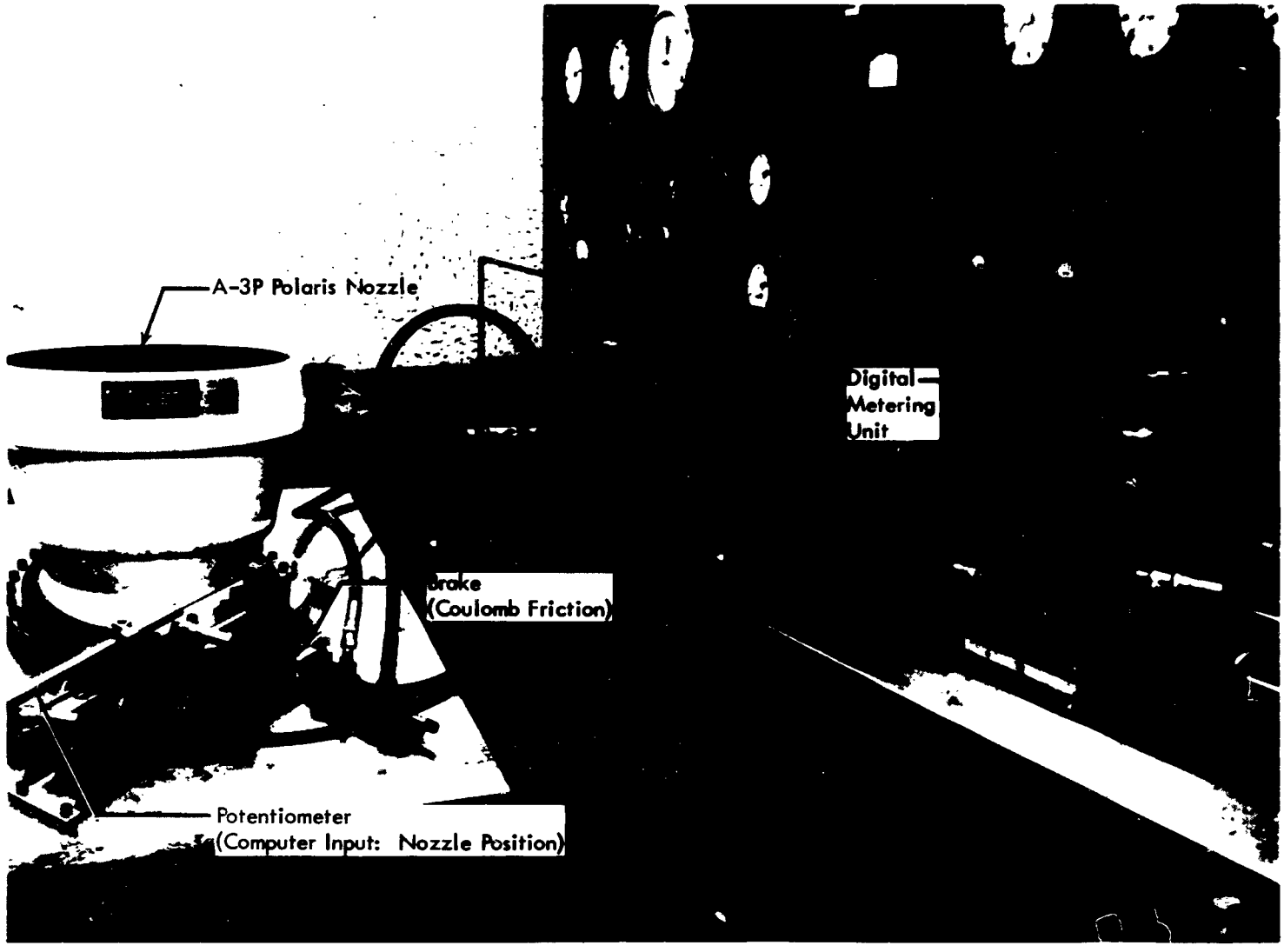

Figure 1-2. Laboratory Arrangement

D. CONCLUSIONS

Completion of Phase III yielded the following conclusions:

- The mathematical model of the DHA is an accurate representation of the actual hardware
- Results obtained by the Phase I simulation are valid
- Parameter values to attain a required system performance can be accurately determined with the mathematical model is a simulated system.
- A DHA is feasible for an aerospace application, such as Polaris
- For an application such as the Polaris, the acceptable tolerance on the leakage parameters, q_L, and q_{LC}, is relatively large. Hence leakage variation due to production tolerances and wear should not present a problem
- The suitability of the DHA to a given application can be initially determined by means of a linearized model.

E. RECOMMENDATIONS

The DHA for this study was tailored to the requirements of the Polaris Missile. Other applications may require a DHA capable of producing a smaller resolution and a higher velocity. For some applications such as aircraft, a two-speed actuator may be necessary to achieve both high resolution and high velocity of the controlled surface.

The following is recommended for future study:

- Ascertain by simulation the requirements and performance when using a DHA for the control of an aircraft, including the effect of the oscillatory motion of the control surface during steady state on the vibratory modes of the structure.
- Evaluate the performance of a two-speed actuator having the capability of changing the direction of drift*

*Raider, Scott, "Digital Hydraulic Study Engineering Summary Report Phase II; Contract No. Nonr 4375(00), IBM No. 66-928-7.

- **Evaluate the design of the laboratory model of the DHA. Based on the results design a DHA which is representative of a deliverable item, meeting reliability and environment specifications.**

- **Design of a metering unit which uses a double-ended ram. This will increase the output power of the actuator for any selected flow and pressure.**

Section II

TECHNICAL APPROACH

This section describes the equipment, and implementation of the equations. The Phase III Study consisted of the following effort:

- Design logic interface between the hardware and simulated flight control system
- Implement equations defining the DHA and flight control system
- Compare performance of simulated control system when using actual hardware with the performance when using the mathematical model
- Establish the performance of the Polaris missile when using a DHA which provides a force independent of the direction of motion and opposed by a 600-pound coulomb friction load
- Ascertain the effect of parameters on performance of the simulated system
- Determine the validity of approximating a DHA and digital control system by a linearized model.

Phase III is consistent with Phase I in that:

- Missile dynamics are when the missile is subjected to maximum aerodynamic pressure which corresponds to the least controllable portion of the flight trajectory
- The yaw angle, the loop of highest gain, is studied
- Feedback components are assumed to be ideal in that no error is contributed to the system by the resolution or drift of the attitude sensors

- The transfer function of the Polaris missile is derived for the short period oscillation mode, assuming:
  - Rigid Structure
  - Stationary environment
  - Small perturbations
  - Missile aligned with the equilibrium position of the velocity vector (zero sideslip)
  - Constant mass.

A. EQUIPMENT - ARRANGEMENT AND DESCRIPTION

Arrangement of the equipment for the Phase III simulation is shown in Figure 2-1. Two modes of operation are provided, the analog mode and simulation mode. The analog mode permits the DHA to be operationally checked without the computer. A commanded position is compared with the actual position to produce an error signal which is converted into digital signals; a sign, and a volume command. The simulation mode permits the DHA to be operated open loop to control a simulated plant (the Polaris missile). Position error is determined by the control loop about the plant.

1. VALVE CONTROL LOGIC

The control logic permits evaluation, in either the simulation or analog mode, of a single-speed actuator, two-speed actuator or an actuator for achieving accurate positioning, i.e., operation at the discontinuous point of the flow curve (Figure 2-2). Schematic and detailed logic is presented in Appendix B.

Logic required for the Phase III Study is depicted in Figure 2-3. The logic requires that a sign command be received in parallel with each volume command. Sign commands following the last sign change produce the gating signal, $\overline{\Delta}$. A volume command when accompanied with the signal, $\overline{\Delta}$, is gated to the actuating driver. The actuating driver, upon receipt of a digital command, de-energizes the valve latch to initiate the transfer of a calibrated fluid volume. When changing the direction of motion, the signal, $\overline{\Delta}$, does not occur, and the volume command in parallel with the sign command is inhibited. The sign command switches the sign driver, and the transfer of a calibrated volume follows the switching of the sign valve. Sign commands following the last sign change are transmitted to the same sign driver. However, the sign valve is now controlled by the sign driver associated with the latch magnets holding the armature.

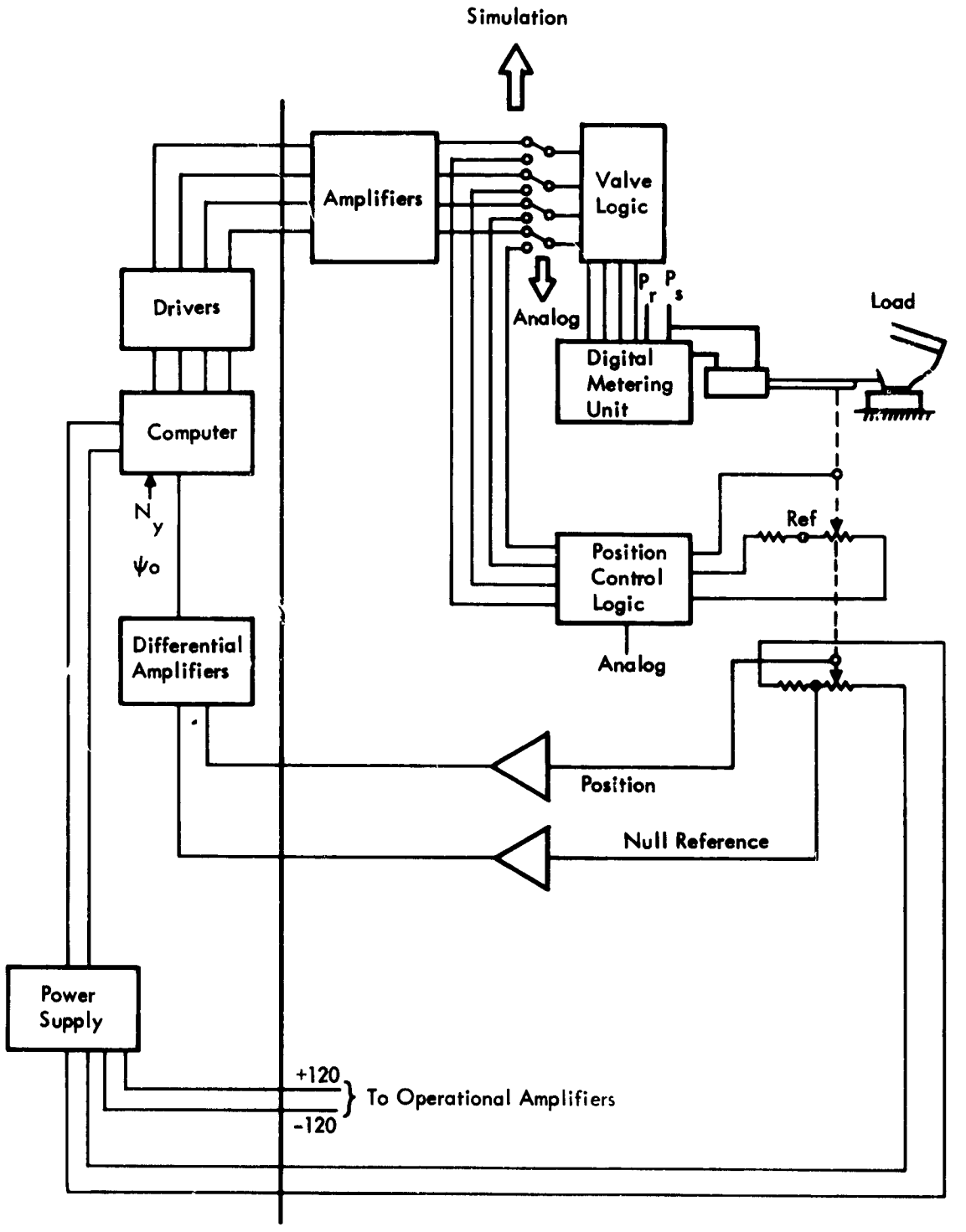

Figure 2-1. Arrangement of Equipment

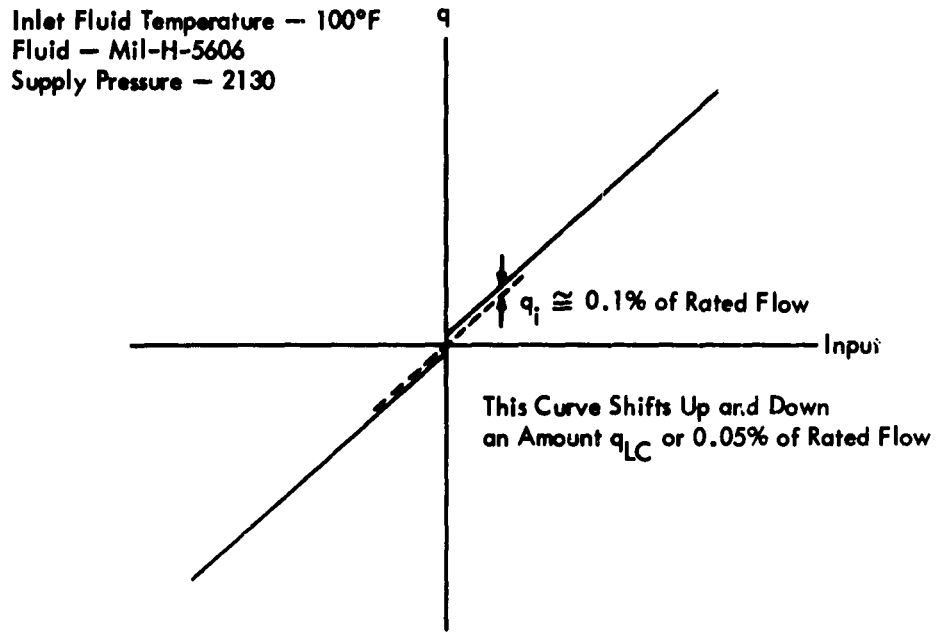

Figure 2-2. Flow Curve for Digital Unit

2. POSITION CONTROL LOGIC

The position control logic shown in Figure 2-3 is used when operating in the analog mode to produce the sign and volume commands. The error detector determines the correction required by predicting the error that will exist after effecting the last command. This is accomplished by updating the error signal, based on present position, with the signal produced by the current driver, representing the position change commanded. Hence, the time-lag due to the time required to position the load does not introduce a false error. The error detector outputs (sign and volume commands) are gated to the pulse generators to produce pulses compatible with the valve logic input requirements.

3. DIGITAL HYDRAULIC ACTUATOR

As previously stated, the DHA consists of the prototype digital metering unit and a commercial actuator cylinder. The following modifications were

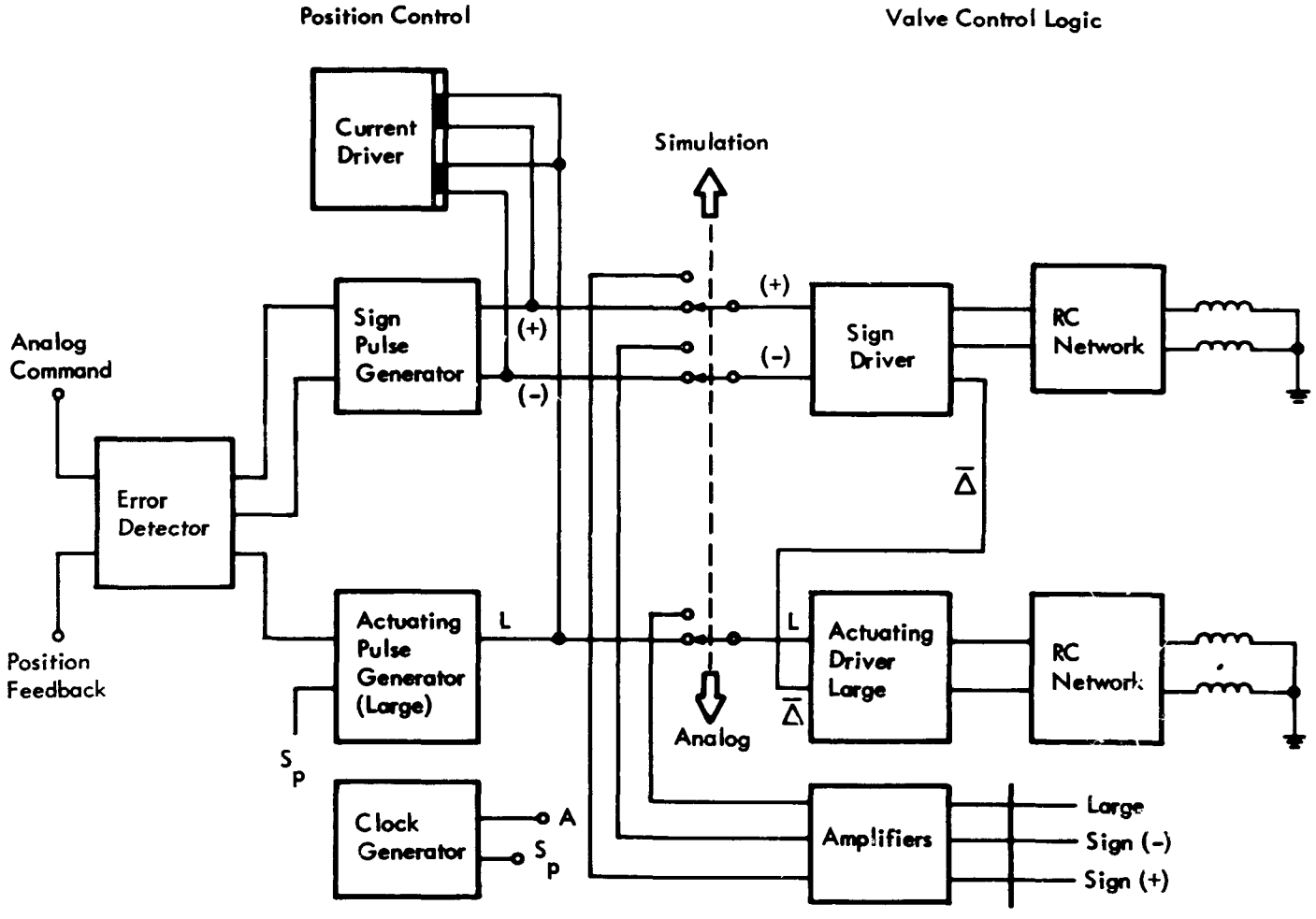

Figure 2-3. Phase III Control Logic

incorporated to improve performance and overcome operation problems experienced during Phase II:

- Relative motion between the pilot spools and armature bearing play was minimized by the use of shims and removing the bearing located on the eccentric
- New magnets were designed to provide a larger holding force and to eliminate the problem of lead wire breakage
- A new manifold was designed to eliminate the excessive leakage due to the location of the port to ram. In addition, the manifold provides ports for an additional valve unit and calibrating cylinder. Hence a capability for two-speed operation.

A commercial cylinder having a ram area of 0.994 square inch and an area ratio of 1.59:1 was used. Since this ratio differs from that required, the force produced is not the same for positive and negative motion.

4. COULOMB FRICTION

Coulomb friction is generated by the bearing and seals when firing the nozzle. To simulate coulomb friction, a phenolic pad was hydraulically loaded against an aluminum drum segment connected to the nozzle. Radial loading of the bearings was minimized by placing the back of the drum segment against the outer race.

Because the area ratio of the ram limited the force capability, the required coulomb friction could not be used when operating with the hardware.

B. METHOD OF SIMULATION

The mathematical model for the Phase III Study of the digital autopilot, DHA and missile dynamics is shown in Figure 2-4.

1. DIGITAL AUTOPILOT

The digital autopilot is programmed as shown in Figure 2-5. The yaw command, $N_y(t)$, can be either a step $|N_y|$ at $t = 0$ or $|N_y| \sin \omega t$.

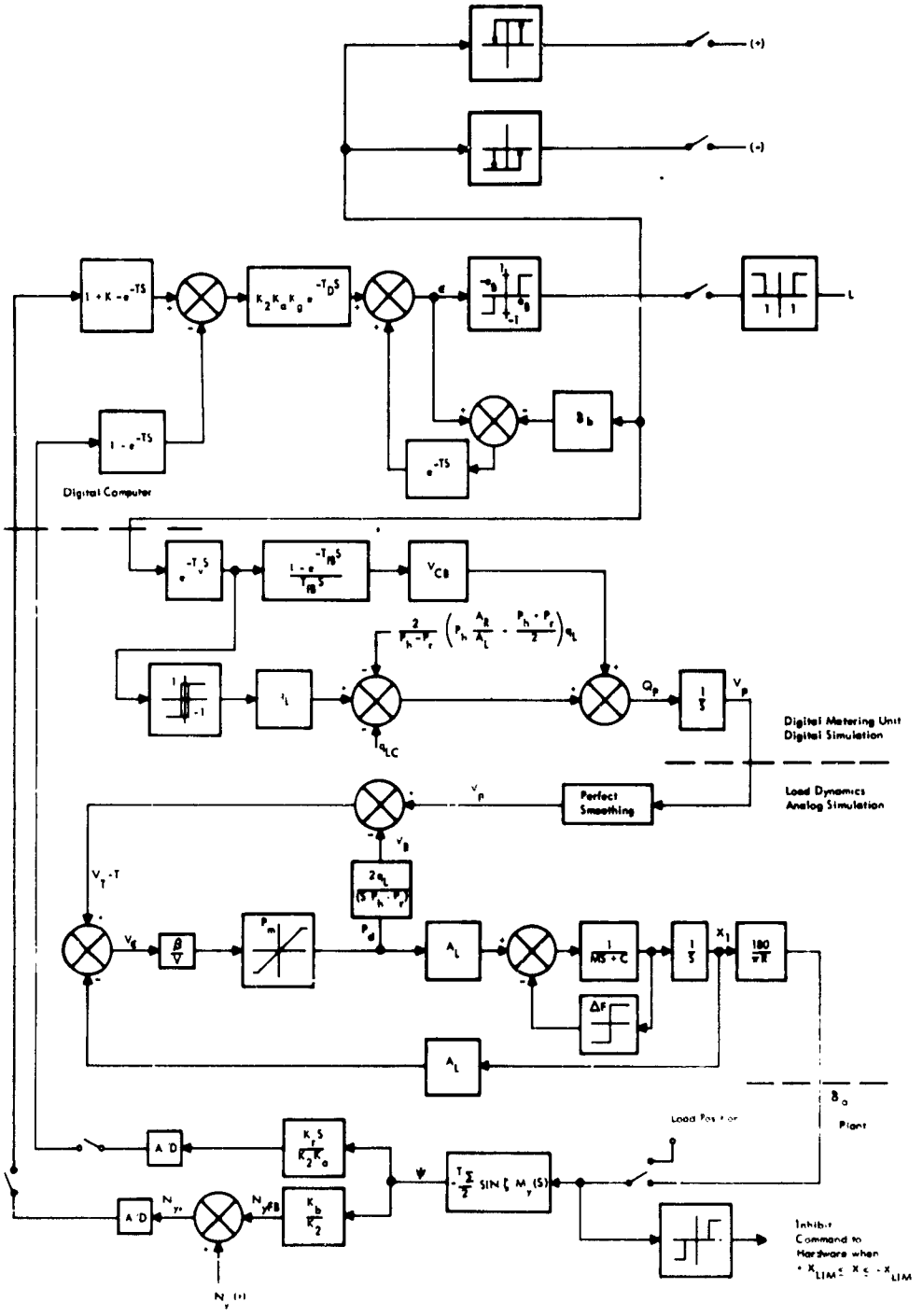

Figure 2-4. Mathematical Model of Digital Autopilot, Digital Actuator, and Missile Dynamics

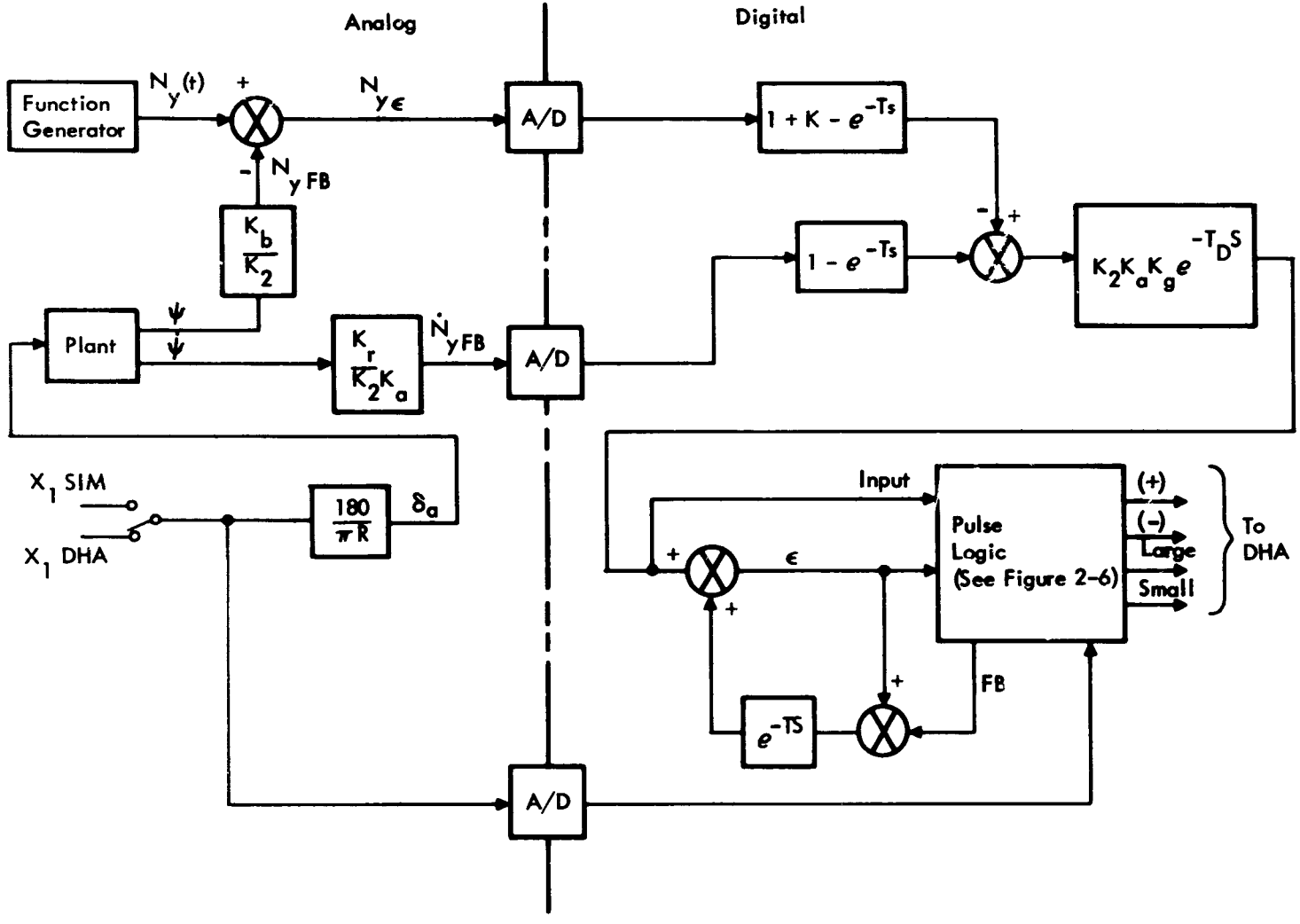

Figure 2-5. Digital Autopilot

The pulse logic box, which is depicted in detail in Figure 2-6, has been generalized to allow for the following autopilot options:

- Single-Speed Operation — Single-speed operation was used for the Phase III Study. This option is attained by setting $e_s = e_b$. Note that the condition imposed on ϵ to select a small volume command is then $e_b > |\epsilon| > e_s$ which cannot be satisfied since $e_s = e_b$.
- Two-Speed Operation — This option makes it possible to simulate an actuator having two volume sizes, a large volume for slew, and a small volume for fine quantization.

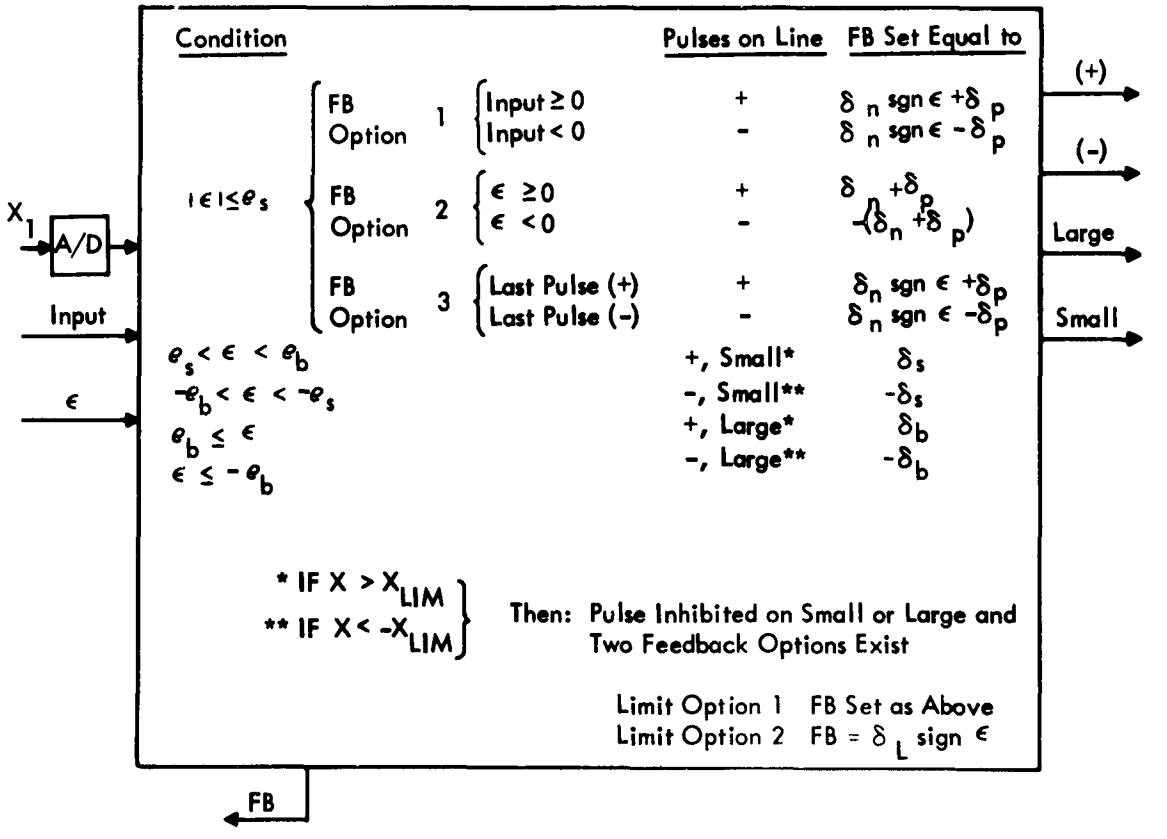

Figure 2-6. Pulse Logic

- Accurate Positioning (Precision Mode) — This option provides the capability of changing the direction of ram motion without displacing a calibrated volume.

  If $|\epsilon| \leq e_s$ the drift option allows the drift polarity to be determined by the polarity of "Input", ϵ, or the last command.

- Feedback Flexibility — The polarity of ϵ may be the opposite of the DHA sign pulse for $|\epsilon| \leq e_s$. To provide the flexibility of attaining a feedback (FB) polarity equal to the polarity of ϵ or the polarity of the sign pulse, FB is set equal to

  $$\delta_n \text{ sgn } \epsilon + \delta_p \text{ sgn (sign pulse)}.$$

  For small volume commands

  $$FB = \delta_s \text{ sgn } \epsilon,$$

  and for large volume commands

  $$FB = \delta_b \text{ sgn } \epsilon.$$

Hammering of the actuator into its stops by the control computer is prevented during check out and stability check runs by inhibiting the volume commands if the ram position magnitude, $|X_1|$, exceeds X_{Limit}. A value of X_{Lim} was selected so that $|X_1| = X_{Lim}$ when the ram is 0.3 inch from the stop. (This distance allows for the displacement produced by the volume stored by the auxiliary pistons.) Since the plant may recover from short periods of δ_α saturation, two limit options are provided. Limit option 1 assumes the control computer has no feedback from the actuator and does not alter FB. Option 2 allows for a special FB equal to δ_L sgn ϵ assuming some sort of limit detection. In summary, Phase I is duplicated if:

$$\epsilon_b = e_s = \frac{1 \text{ quantum} + \text{hysteresis}}{2} = 0.681 \text{ for a quantizer hysteresis of } \delta_{q/4}$$

drift option = 3

limit option = 1

2. DIGITAL HYDRAULIC ACTUATOR (DIGITAL PORTION)

After transmitting the DHA pulses, the digital computer calculates Q_{p1}, Q_{p2}, Q_{p3} and ΔV as shown in Figure 2-7. Where:

Q_{p1} is the flow for t in the interval (t_v, t_{fs})

Q_{p2} is the flow for t in the interval (t_{fs}, t_{fB})

Q_{p3} is the flow for t in the interval (t_{fB}, t_v)

$$\Delta V = \int_{t_v}^{t_v + T} Q_{p_i}\, dt \qquad (i = 1,\ 2,\ 3)$$

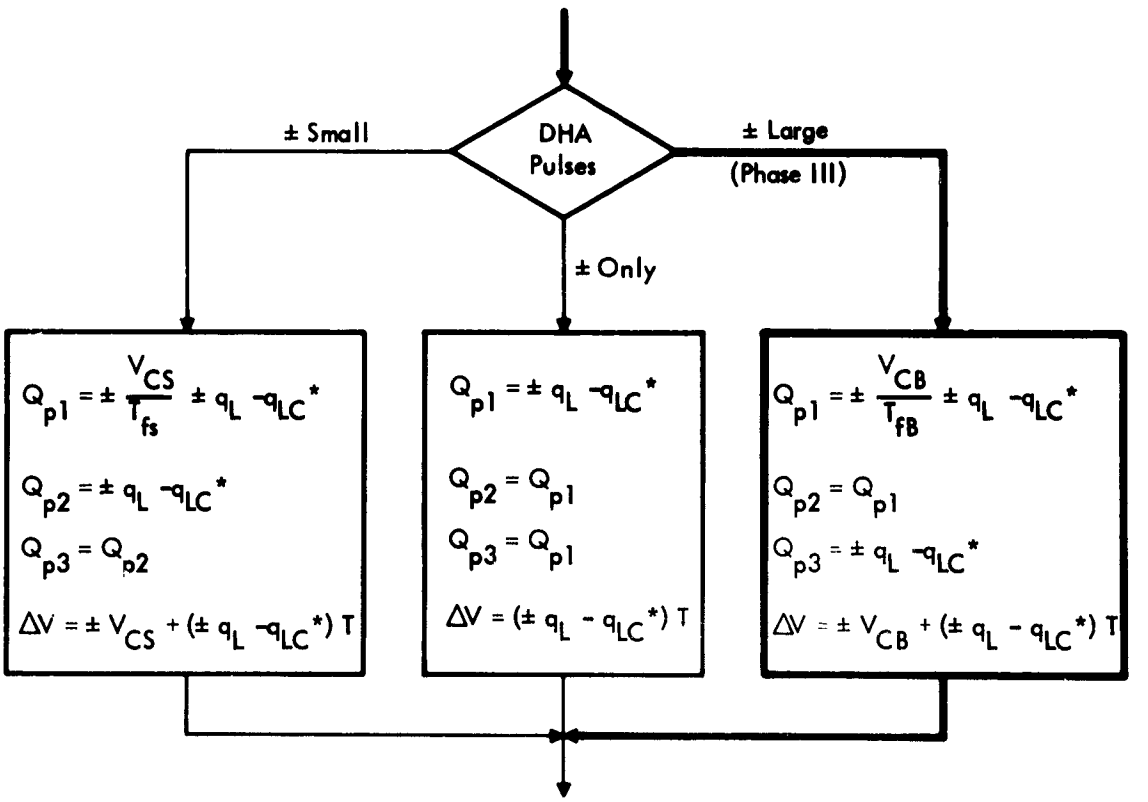

Figure 2-7. Flow Calculations

With reference to the timing chart shown in Figure 2-8, the Q_{p_i} ($i = 1, 2, 3$) are converted from digital to analog at the proper time and fed to an analog integrator to get V_p. To prevent drift in this open-loop integration, the ΔVs are summed to form a digital representation of V_p. A drift correction (Q_{corr}) is added to the Q_{p_i} to force the analog value of V_p to match the digital value V_{dig}, at sampling times (Figure 2-9).

Transfer of the volume commanded during the interval $T_{(n-1)}$ is completed during the time interval $T_{(n)}$. Therefore, to make V_{dig} assume values correct at the analog-to-digital version time, $T_{A/D}$, of V_p, ΔV is divided so that

$$\Delta V = \int_{t_v}^{t_v + T_{(n)}} Q_p \, dt = \Delta V_1 + \Delta V_2$$

where

$$\Delta V_1 = \int_{t_v}^{t_{A/D} + T} Q_p \, dt$$

$$\Delta V_2 = \int_{t_{A/D} + T}^{t_v + T} Q_p \, dt$$

Thus during the nth DHA cycle, the volume added to the integration summer is:

$$\Delta V' = \Delta V_1 (n) + \Delta V_2 (n - 1)$$

or

$$\Delta V' = \int_{t_{A/D}}^{t_{A/D} + T} Q_p \, dt$$

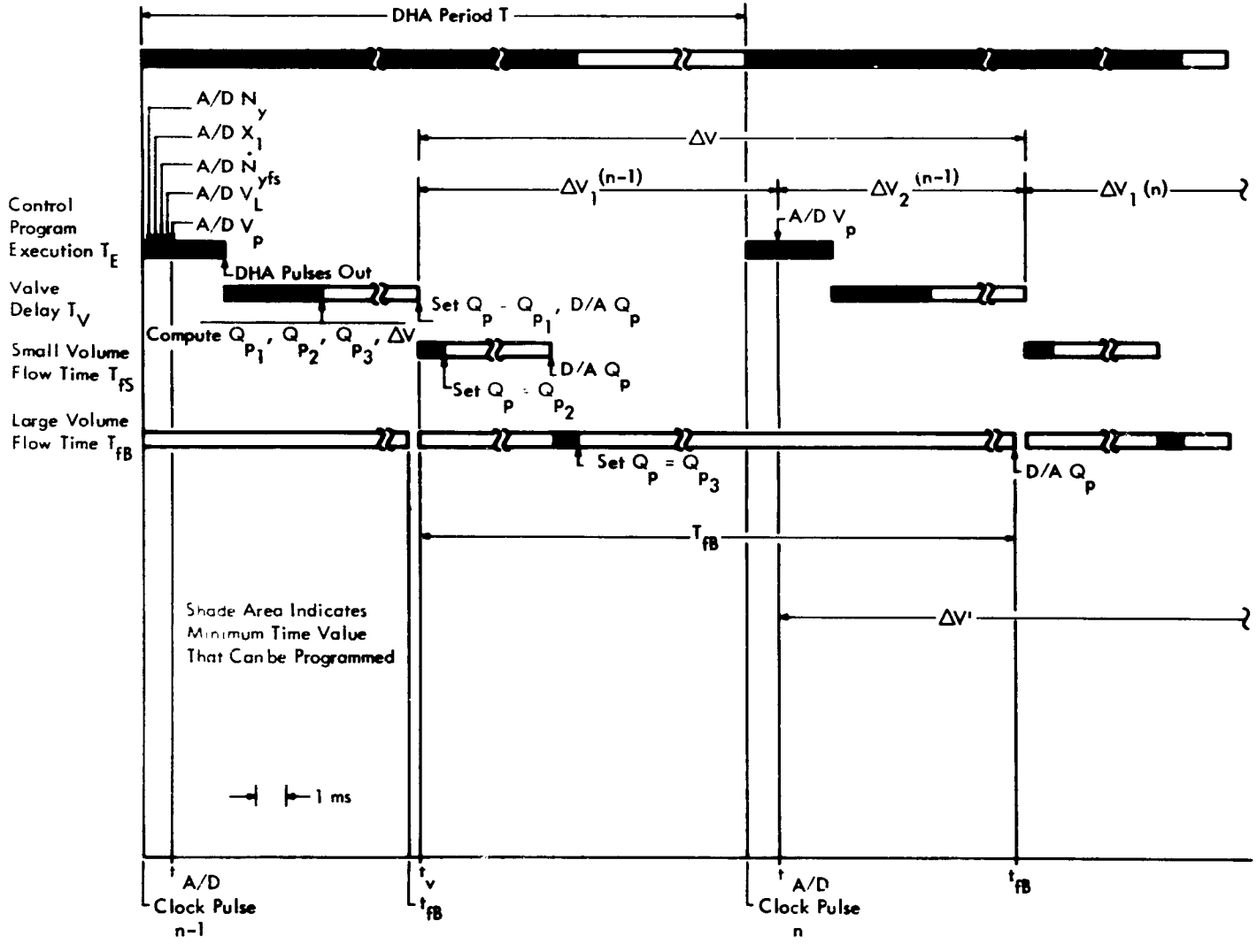

Figure 2-8. Timing Chart

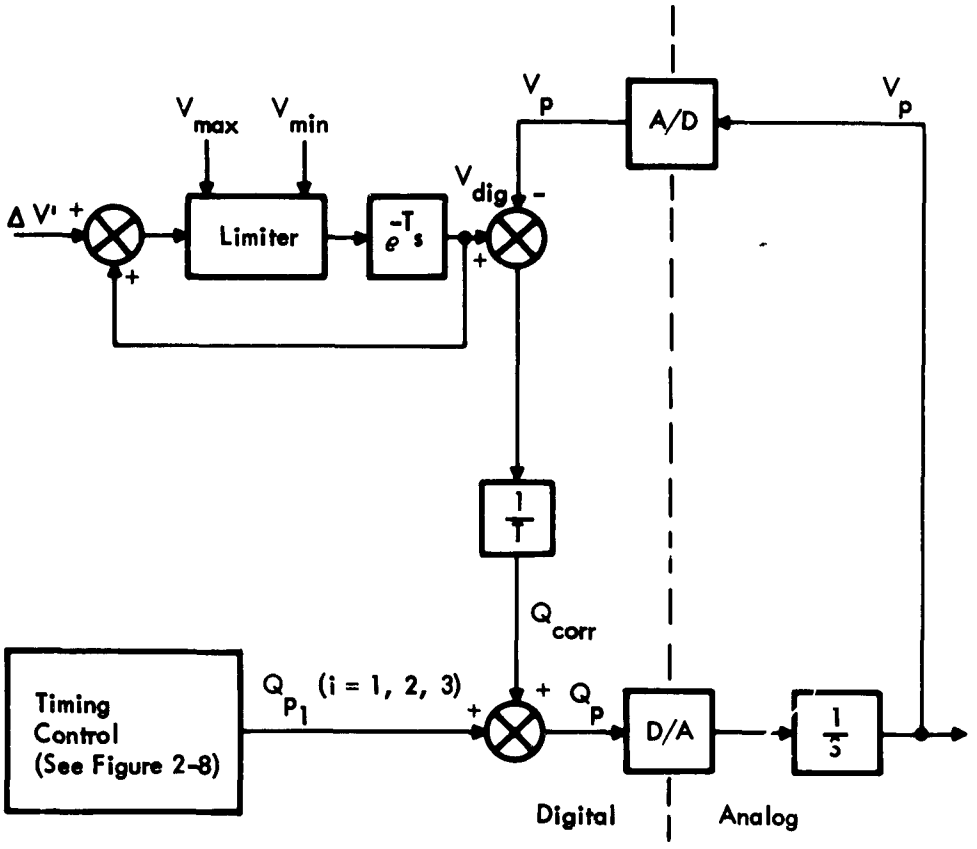

Figure 2-9. Digital Integration

The limiting values, V_{max} and V_{min}, for the digital integrator (Figure 2-9) are variable and are obtained from the following relationships:

$$V_T = V_p - \frac{2q_L}{P_h} \int_0^t P_d \, dt = V_p - V_B$$

which is depicted by block diagram in Figure 2-10. Since V_T has a fixed limit, V_{Lim},

$$-V_{Lim} < V_T < V_{Lim}$$

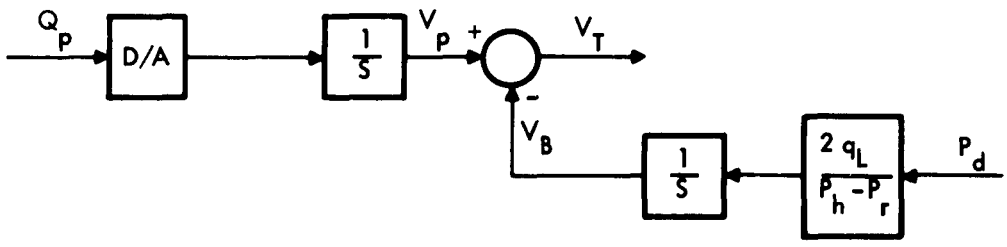

Figure 2-10. Method of Obtaining Limiting Values for the Digital Integrator

or

$$-V_{Lim} < V_p - V_B < V_{Lim}$$

or

$$-V_{Lim} + V_B < V_p < V_{Lim} + V_B$$

Therefore, V_B, an analog quantity, is converted from analog to digital form, and the limits on V_{dig} are computed by the digital computer as

$$V_{min} = -V_{Lim} + V_B$$

$$V_{max} = V_{Lim} + V_B.$$

3. DIGITAL HYDRAULIC ACTUATOR (ANALOG PORTION)

The analog simulation of the actuator dynamics is programmed as in Phase I, (Figure 2-11) with the exception of the coulomb friction. As a result of simulating in real time (Phase I simulation was 1/10 as fast) the limited frequency response, and amplifier phase shift caused the coulomb feedback loop to oscillate when used as a simple bang-bang amplifier as illustrated in Figure 2-12. Hence during a steady state, large-amplitude oscillations of the pressure, P_d, resulted. To overcome this problem, a latching electronic swtich is used at the input of the $\dot{X}$ integrator (Figure 2-13).

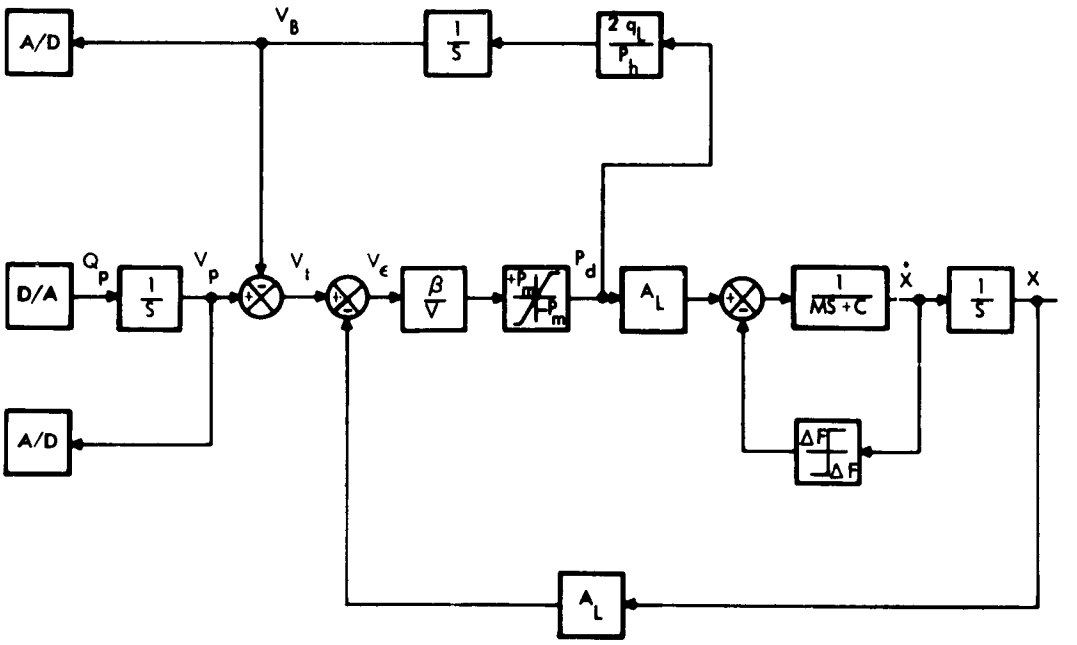

Figure 2-11. Actuator Dynamics

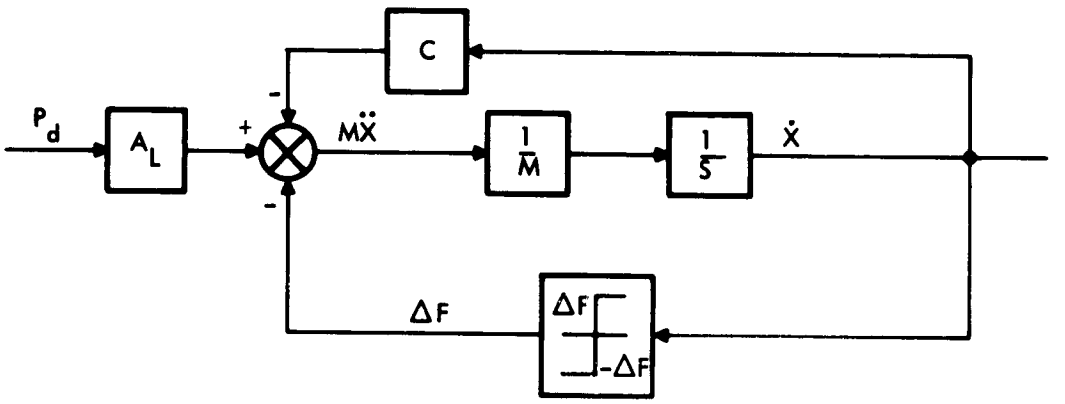

Figure 2-12. Simulation of Coulomb Friction (Phase I)

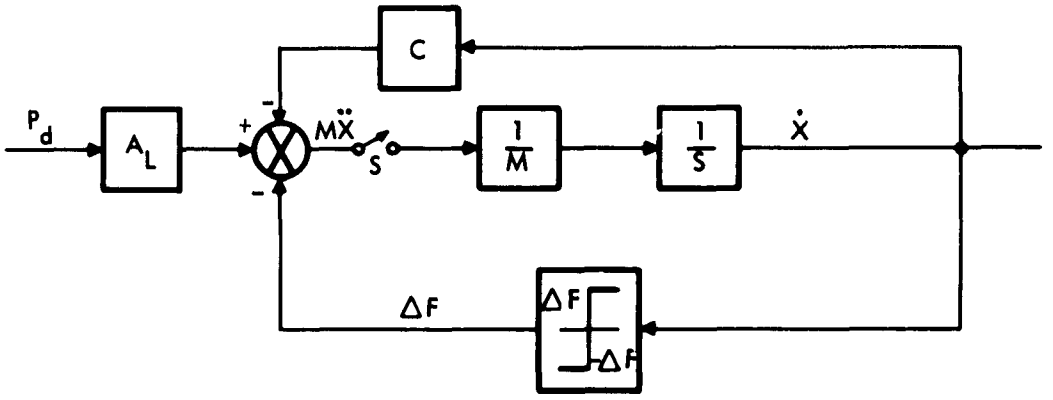

Figure 2-13. Simulation of Coulomb Friction (Phase III)

The logic that operates switch S is:

- S closes and latches whenever $|P_d A_L| \geq F$
- S unlatches when both $|P_d A_L| < F$

$$\dot{X} = 0$$

This prevents ΔF from acting as an accelerating force because of phase shift.

4. COMPARISON

This method of simulating the digital autopilot and DHA for Phase III differed from Phase I. To establish that the results obtained with the present model agreed with the results obtained during Phase I, several simulation runs depicting significant characteristics were rerun. Parameter values used for the reruns were identical to those used for the Phase I Study except for the fluid flow time, T_{fB}. The parameter T_{fB} is not readily modified in the program; therefore, T_{fB} was programmed for the value obtained by test and does not significantly influence the results.

The results attained are compared in Table 2-1 with the results of Phase I. The agreement of the two methods of implementing the equations is further illustrated by the recorded transients shown in Figure 2-14.

Table 2-1

SIMULATION RUNS TO DETERMINE AGREEMENT BETWEEN THE METHODS OF IMPLEMENTING THE MATHEMATICAL MODEL

Model	Results			Parameters							Reference Run (Phase I)
	Stable k_g	Unstable k_g	Input	K ($K_1 t_s$)	q_L in^3/sec	q_{LC} in^3/sec	δ_q deg	T 10^{-3} sec	M Slugs	Quantizer Hysteresis	
Phase I Phase III	5.55 5	5.90 5.55	0	0	0	0	1.09	12.1	3.55	$\delta q/4$	180
Phase I Phase III	5.55 5	5.90 5.55	0	0	0.14	0.01	1.09	12.1	3.55	$\delta q/4$	182
Phase I Phase III	Maximum Stable Step		$N_y = 12$ $N_y = 11$	0.01	0.14	0.01	1.09	12.1	3.55	$\delta q/4$	193
Phase I Phase III	Unstable Step		$N_y = 13$ $N_y = 13$	0.01	0.14	0.01	1.09	12.1	3.55	$\delta q/4$	194
Phase I Phase III	Figure 2-14a Figure 2-14b		$\psi = 1/2$	0.002	0.14	0.01	1.09	12.1	3.55	$\delta q/4$	207

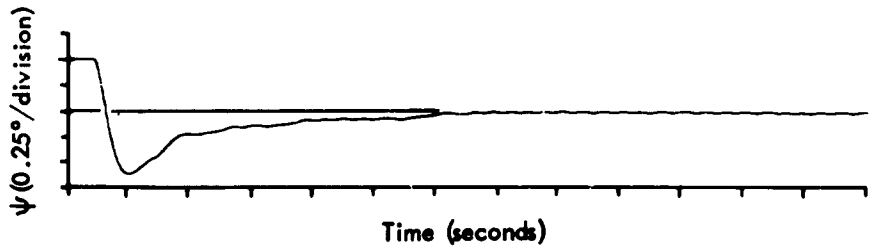

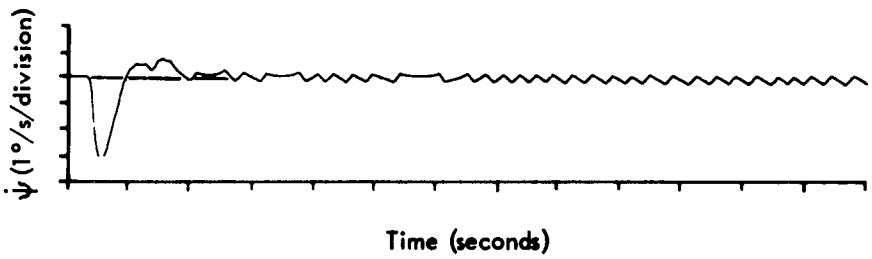

a) Phase I Simulation

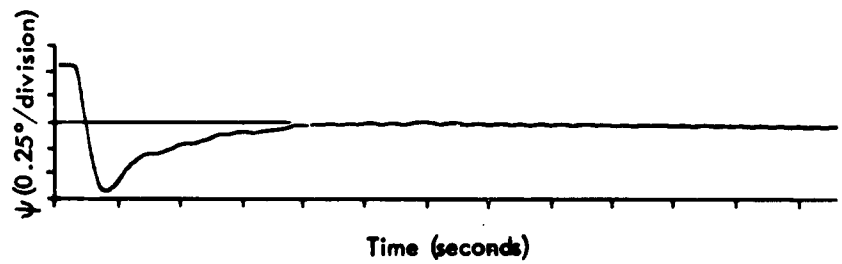

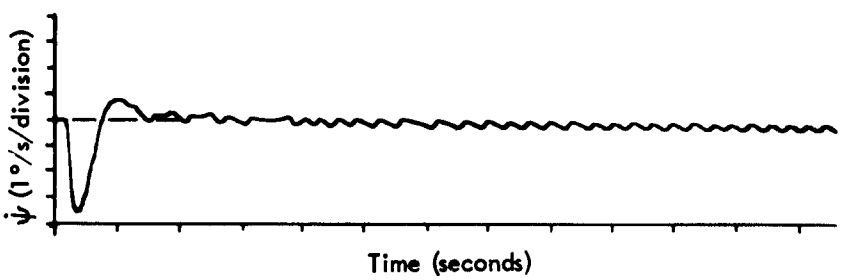

b) Phase III Simulation

Figure 2-14. Recorded Transients for $\psi = -1/2^{\circ}$ (Run 207 Table 2-1)

BLANK PAGE

Section III

MATHEMATICAL MODEL EVALUATION

Performance of the simulated control loop when using the mathematical model of the DHA is compared with the performance when using the laboratory hardware. Accuracy of the model is established by correspondence of the recorded ram motion and agreement of the results for:

- Maximum stable step
- Response to a step command, $N_y = 10$
- Response with an initial yaw condition
- Gain margin for initial conditions less than one quantum
- Limit cycle
- Frequency response and phase shift.

Plant transients presented in this section are of significance only for the purpose of comparison since the ram used did not produce the same force for both directions of motion.

With the DHA in the loop the initial condition of the ram is obtained by allowing the ram to drift from a positive to a negative value. The position is sampled at the operating frequency (82.5 Hz) and the run is started when a zero or negative ram position is detected.

The unpredictable behavior of an unstable plant with zero initial conditions, quantization effects, and the method of initializing the position of the physical load will produce variations in the plant response. Therefore, small variations of the plant transient when using the mathematical model from the transient generated when using the hardware does not necessarily indicate an inaccuracy of the mathematical model.

A. PARAMETER VALUES

Parameter values defining the actuator and load dynamics are shown in Table 3-1. The parameter values were established by test when practicable. Values not measured are indicated. Accurate values are not readily

Table 3-1

PARAMETER VALUES

Parameter	Units	Value	Parameter	Units	Value
ΔF	lb	380	e_b	deg	0.681
M	lb-s^2/in	0.25	Quant. Hys.	deg	$\delta q/4$
R	in	8.125	δ_b	deg	1.09
$*\frac{\beta}{V}$	lb-in^{-5}	26,600	K	—	2^{-7}
*C	lb-s/in	12			
q_L	in^3/s	0.107			
q_{LC}	in^3/s	-0.006			
$q_{LC}{}^*$	in^3/s	-0.0165			
V_{CB}	in^3	0.152			
f_c	Hz	82.5			
T_V	in^{-3}	5.5			
t_f	in^{-3}	10			
P_M	lbf/in^2	+540 -960			
P_R	lbf/in^2	130			
P_h	lbf/in^2	2,130			
A_L	in^2	0.994			
A_L/A_R	—	1.59			

*Value Approximated

B. RESULTS

Simulation results when using the parameter values of Table 3-1 are shown in Table 3-2. Table 3-2 also shows the results when changing the parameter value of Table 3-1 to that indicated.

Table 3-2

PERFORMANCE OF SIMULATED FLIGHT CONTROL SYSTEM

Parameter Value	Maximum Stable Step	Unstable Step	K_G ($N_y = \psi_o = 0$)		Reference: Figure No.	
			Stable	Unstable	$N_y = 10$	Limit Cycle
Hardware Digital Hydraulic Actuator	11 -8	12 -9	4	4.5	3-2 3-8	3-5
Mathematical Model Table 3-1	11 -8	12 -9	4	4.5	3-6	3-7
Mathematical Model with:						
C = 6	11 -9	12 -10	4	4.5	3-9	3-11 a
C = 18	11 -6	12 -7	3.5	4	3-10	3-11 b
$\frac{\beta}{V} = 13,300$	11 -8	12 -9	4	4.5	3-12 a	3-13 a
$\frac{\beta}{V} = 100,000$	11 -8	12 -9	4	4.5	3-12 b	3-13 b
$\Delta F = 0$	11 -9	12 -10	4.5	5		

Recorded transients which further support the accuracy of the mathematical model and the effect when varying the parameters are shown.

As shown by Table 3-1, the maximum stable step is dependent on the sign of the steering pulse command N_y. The difference between the maximum positive and maximum negative stable step is a consequence of the ram force being different for positive and negative motion. The higher negative force produces a larger effective moment due to faster response and increased overshoot. Recorded transients of the ram for positive and negative yaw step commands are shown in Figure 3-1. For the negative step command the ram is seen to be velocity saturated during the positive motion.

Figure 3-2 shows the recorded ram motion of the laboratory model and mathematical model for a yaw step command when closing the simulated loop with the laboratory model (Figure 3-3). It is significant that the transients are parallel. With the mathematical model operated open loop, and error in the leakage rate, q_{LC}, will cause the ram transient for the mathematical model to converge or diverge relative to the transient recorded for the actual ram. Hence the parallel transients verify the value of q_{LC} to be reasonably correct.

Although the agreement is good the transients differ when changing from negative ram motion to positive ram motion, detail A, Figure 3-2. This difference is due to the velocity produced with the mathematical model for negative motion being greater than that achieved with the hardware. A lumped parameter approximation is used to describe damping in the mathematical model. Accuracy of the approximation is decreased when the damping is significantly different for positive and negative motion. With the larger accelerating force for negative commands, Figure 3-4, a larger force acts on the ram before the auxiliary piston is displaced. Until the calibrating piston stroke is completed, the return lines effect damping of the ram motion. Hence, because of the unequal ram force, the damping realized when initiating negative motion is greate than that produced by the mathematical model.

The value used for the damping coefficient (C = 12) better represents the damping for positive motion. This is shown by the agreement when the order of ram motion is reversed, see detail B, Figure 3-2.

Limit cycles produced with the hardware and mathematical model in parallel are shown in Figure 3-5. With the simulated loop closed about the hardware, the higher velocity achieved with the mathematical model for negative commands can be seen. Also of interest is the "stepping" characteristic produced with the mathematical model during drift (see detail A of Figure 3-5). This characteristic is due to the method of implementing coulomb friction. Steps occur when the condition $P_d A_L \geq \Delta F$ is obtained, thus closing the switch (Figure 2-13). Oscillations of P_d which result

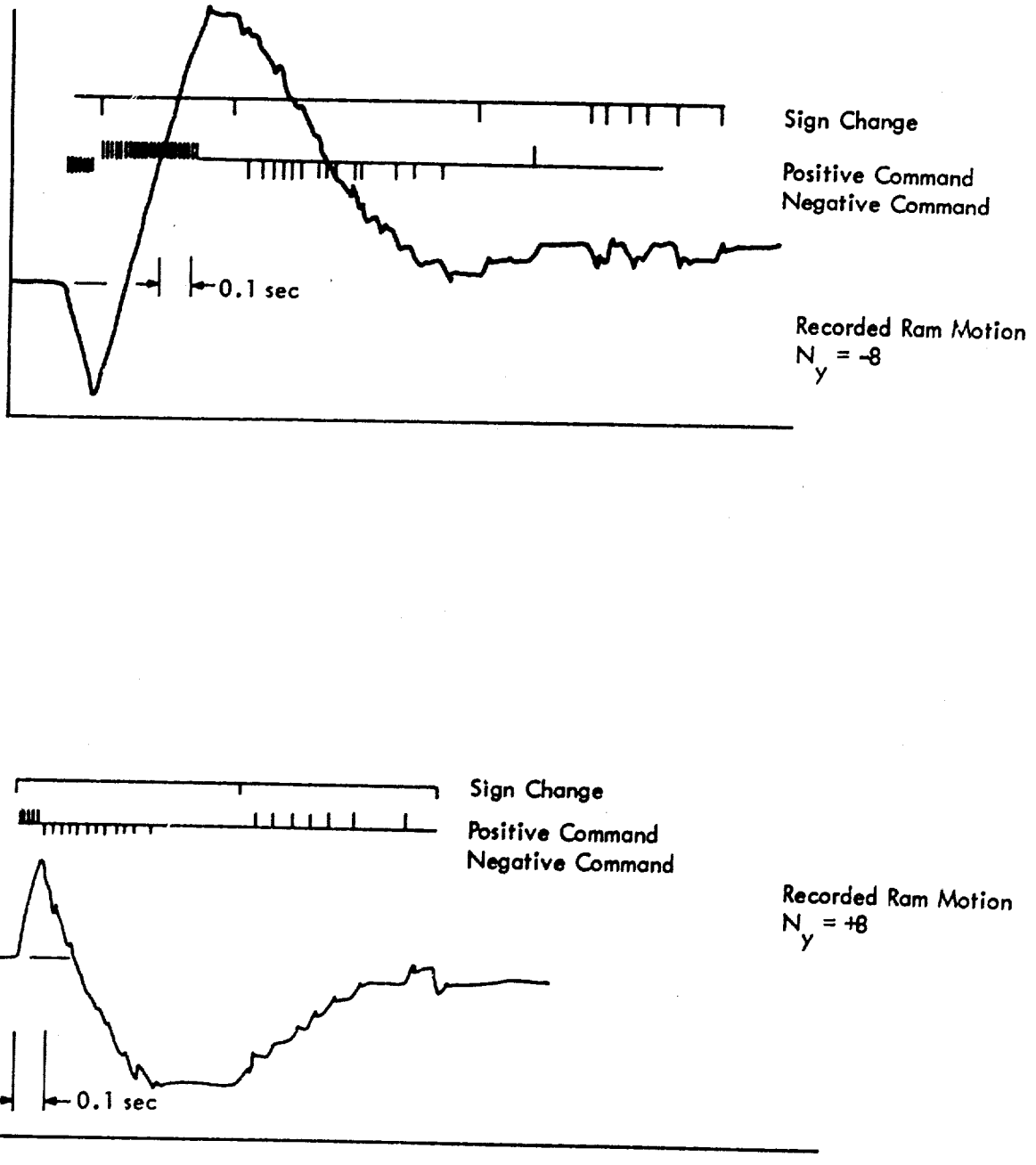

Figure 3-1. Recorded Motion of Ram with Digital Hydraulic Actuator in Simulated Control Loop (ΔF = 60 lbs)

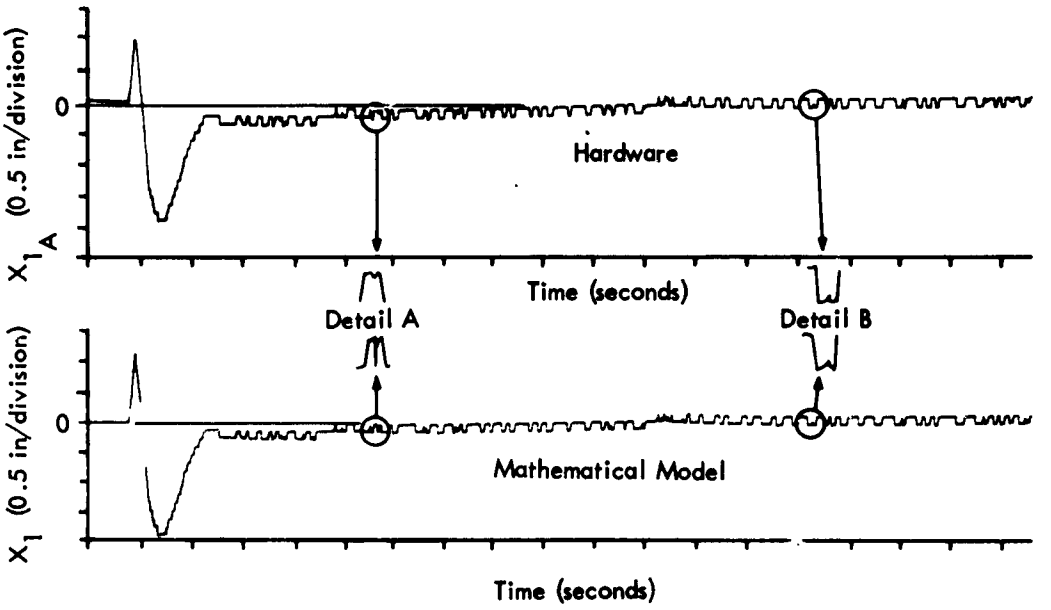

Figure 3-2. Ram Motion for a Yaw Step Command (N_y = 10)

create the conditions required to open the switch, i.e., $P_d A_L < \Delta F$, $X_1 = 0$. The stepping characteristic can also be noted in Figure 3-13 showing the effect of the parameter β/V on the limit cycle. With the increased resonance frequency (larger β/V) the stepping frequency increases.

The ram transient for a yaw step command using the mathematical model in the simulated loop is shown in Figure 3-6. Limit cycle characteristics are shown in Figure 3-7. Comparison with Figures 3-2 and 3-5 shows the recorded ram motion to exhibit the same characteristics as that produced by the hardware. Comparison of the plant transients shown in Figures 3-6 with Figure 3-8 show the response characteristics of the simulated loop with the mathematical model of the DHA to be the same as that achieved with the laboratory hardware.

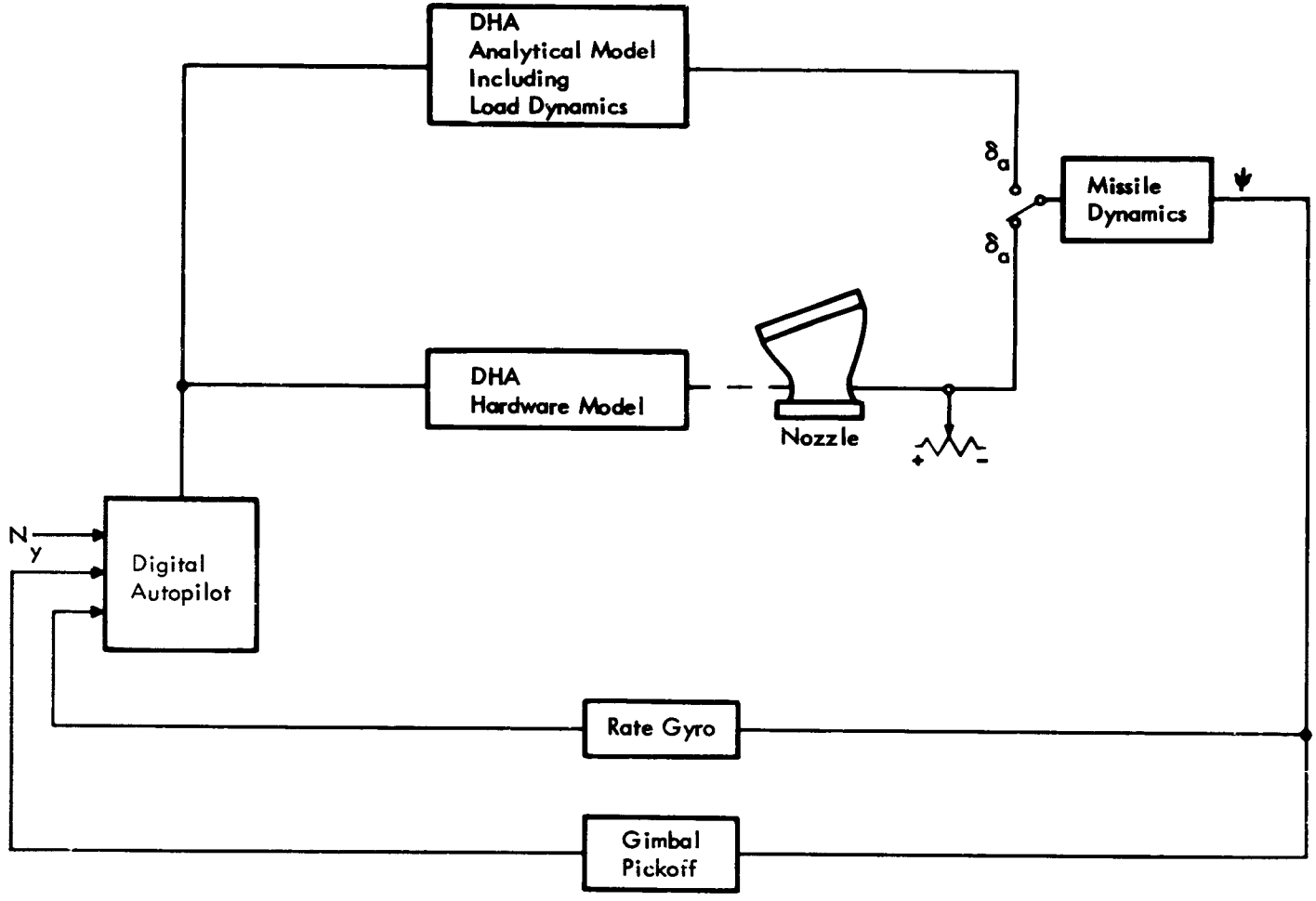

Figure 3-3. Simulation Arrangement

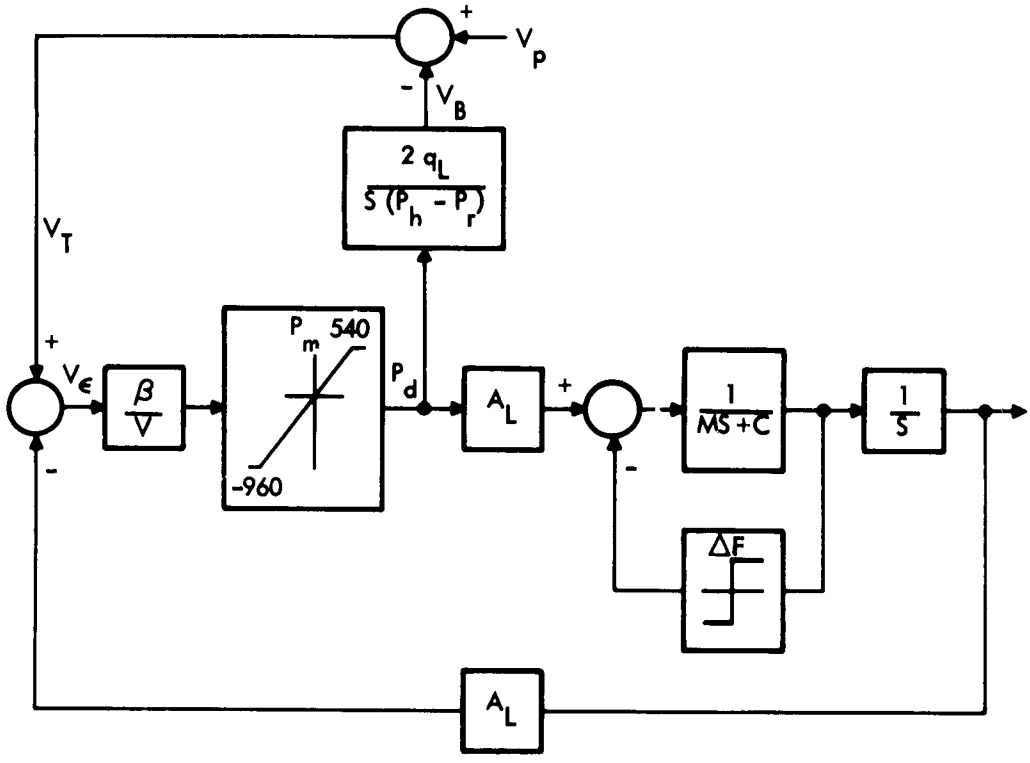

Figure 3-4. Block Diagram for DHA Load Dynamics

1. EFFECT OF THE PARAMETER C

The effect of parameter C on loop performance is shown by the results in Table 3-2. The values of C represent a variation ±50 percent from that used when comparing the mathematical model with the hardware. For both increased and decreased damping, the maximum negative stable step differed from the result obtained with the laboratory model. However, the maximum positive stable step was not changed. As shown by Figure 3-1 negative ram motion is required to stabilize the missile after initiating a positive step command. For the values of damping investigated the relation:

$$\frac{V_c f_c}{A_L} < \frac{P_m A_L - \Delta F}{C}$$

existed with negative motion. Hence the slew velocity required to attain the maximum positive stable step was not effected by the values of C investigated

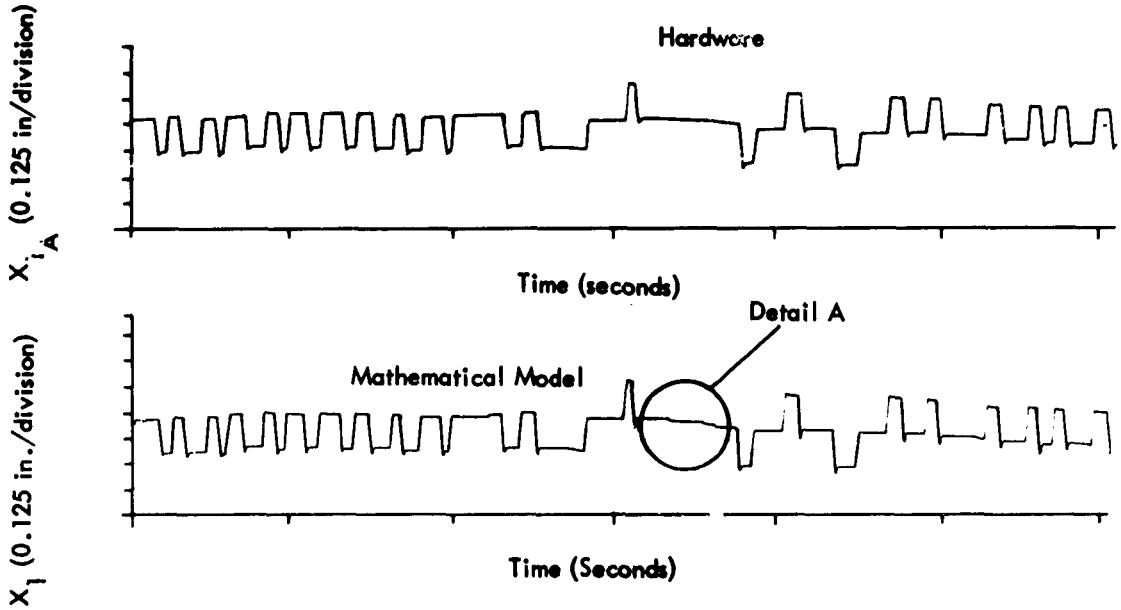

Figure 3-5. Recorded Transients Showing Actual Motion of Digital Hydraulic Actuator and the Motion Generated with the Mathematical Model

Figures 3-9 and 3-10 show the response to a yaw step command for C = 6 and C = 18. The variation of the damping parameter produces no significant change in the transient response. The effect of the damping on the ram motion is shown in Figure 3-11. As to be expected, the overshoot of ram position is greater for decreased damping. However, the limit cycle characteristics as shown in Figures 3-9 and 3-10 do not significantly differ.

2. EFFECT OF THE PARAMETER β/V

The effect of the parameter β/V was determined for values of 13,300 lb/in^5 and 100,000 lb/in^5. As indicated by Table 3-2 the variations had no effect on gain margin or maximum stable step. Transients recorded for a yaw command Ny = 10 are shown in Figure 3-12 for the variations of the parameter β/V. Both transients are in satisfactory agreement with the

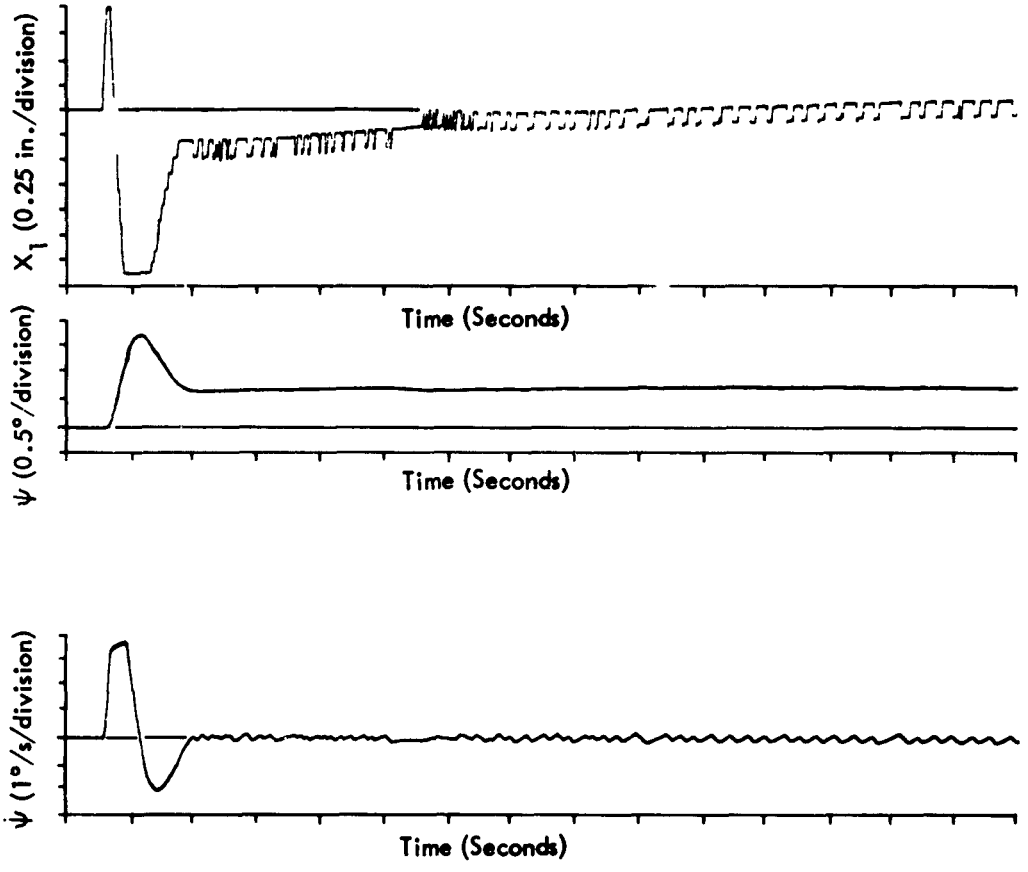

Figure 3-6. Recorded Transients for a Yaw Step Command (Ny = 10) Using Mathematical Model

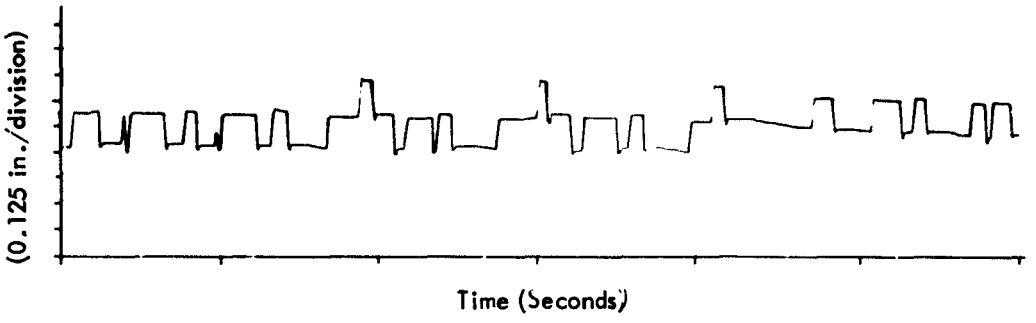

Figure 3-7. Limit Cycle Generated with the Mathematical Model in the Simulated Control System

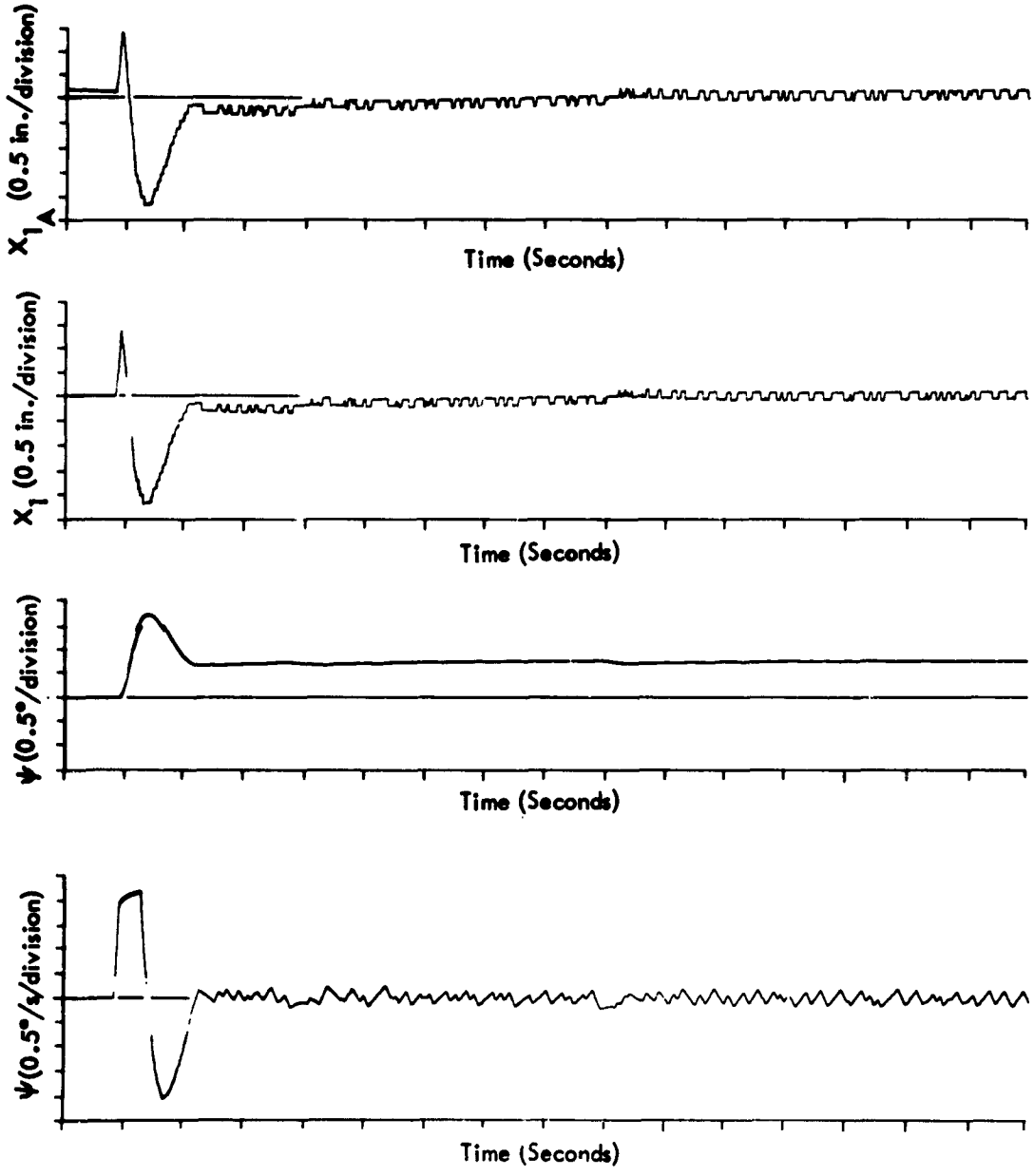

Figure 3-8. Recorded Transients for a Yaw Step Command (N_y = 10) Using Actual Hardware with Mathematical Model Operated Open Loop (Ref - Figure 3-3)

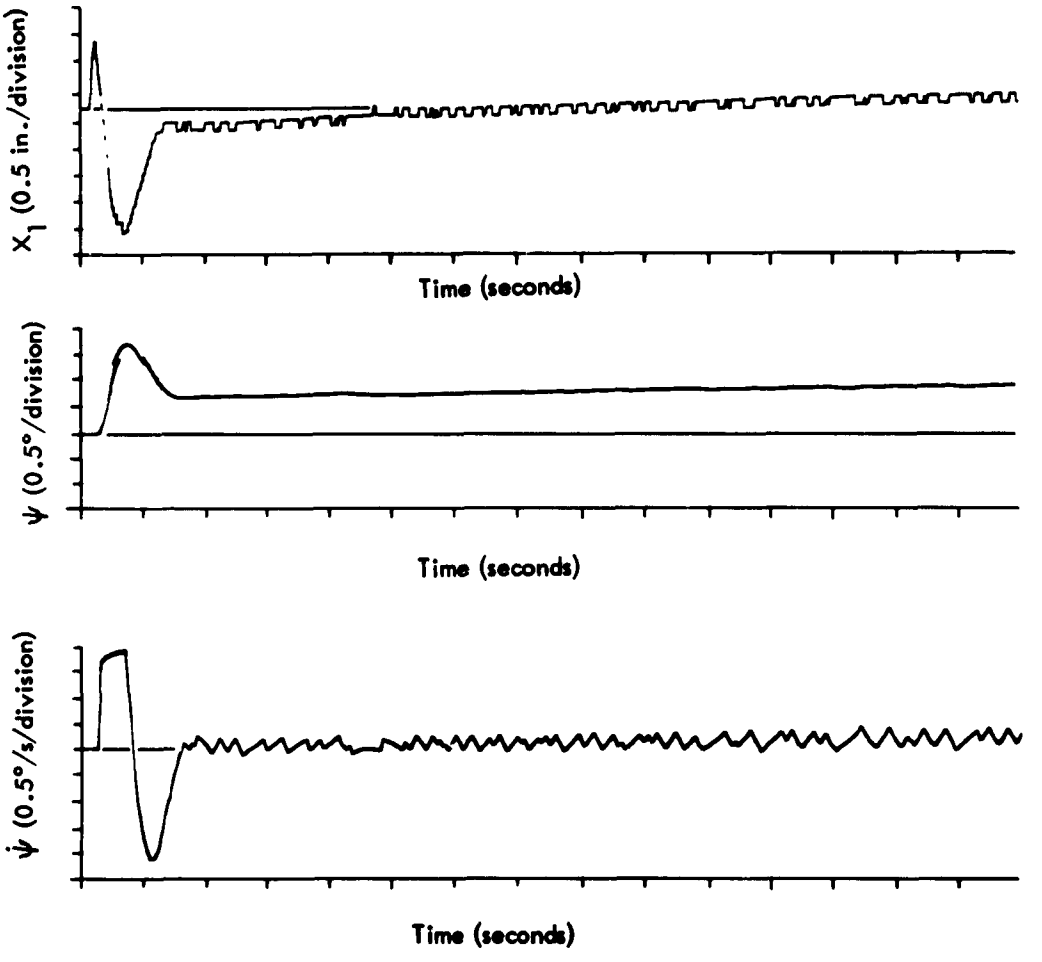

Figure 3-9. Response to a Yaw Step Command with C = 6 lb-s/in

transients recorded for the hardware and the mathematical model. The difference in the settling time of the plant relative to that depicted in Figure 3-6 is noted. However, due to the correspondence between the transients of Figure 3-12 the difference in settling time is attributed to a change of conditions within the simulated loop.

With reference to Figure 3-13, the effect of the parameter β/V on drift characteristics of the ram and ram overshoot is shown. Comparison with Figure 3-7 shows the value for β/V = 26,600 lb/in^5 to provide better agreement with the hardware.

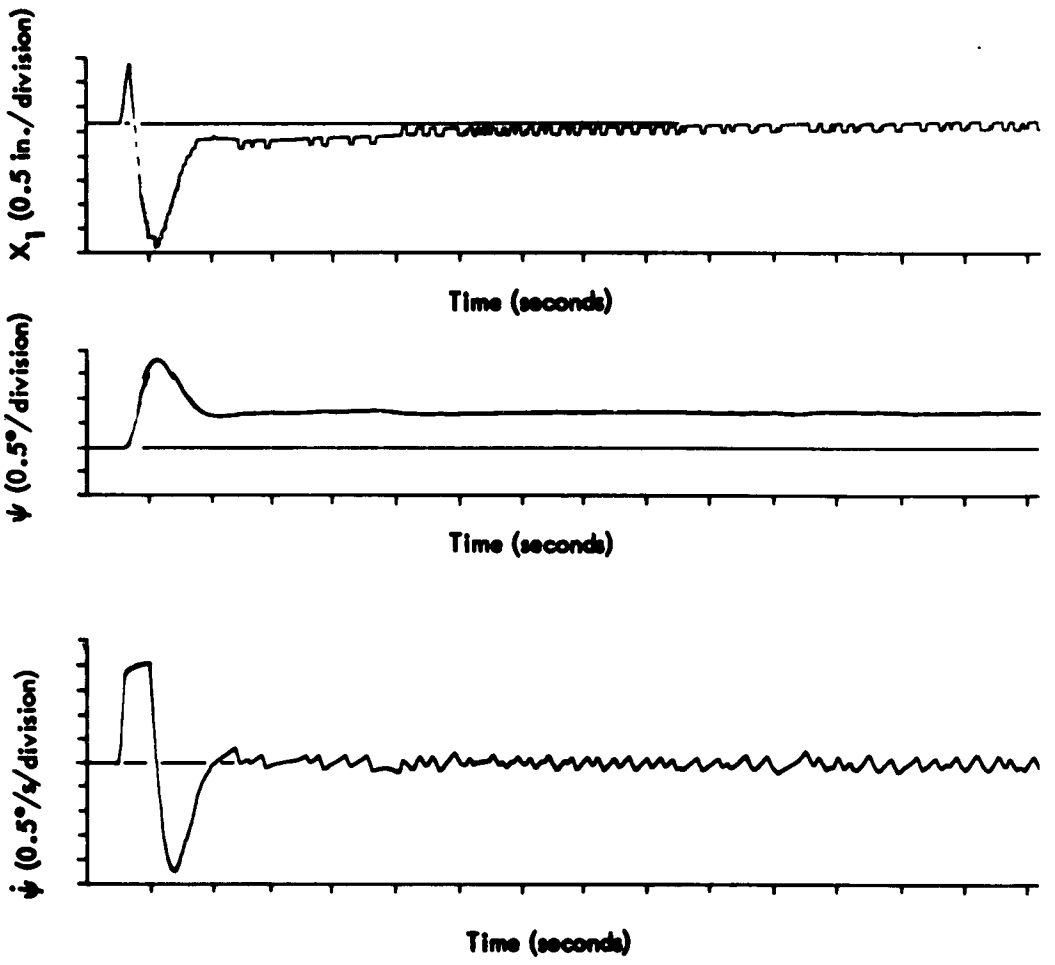

Figure 3-10. Response to a Yaw Step Command with C = 18 lb-s/in

The parameter β/V for the values stated produced little change in the steady state frequency of the ram, see Figure 3-13.

3. GAIN-PHASE

Closed loop frequency response and phase characteristics of the simulated loop were obtained when using the laboratory model and the hardware. Results are depicted in Figures 3-14 and 3-15. Inputs were restricted in amplitude to eliminate the nonlinear effect of velocity saturation. Differences when comparing results are attributed more to the accuracy of measuring the data than to a difference in the models.

The agreement of results further establishes the accuracy of the mathematical model describing the digital hydraulic actuator.

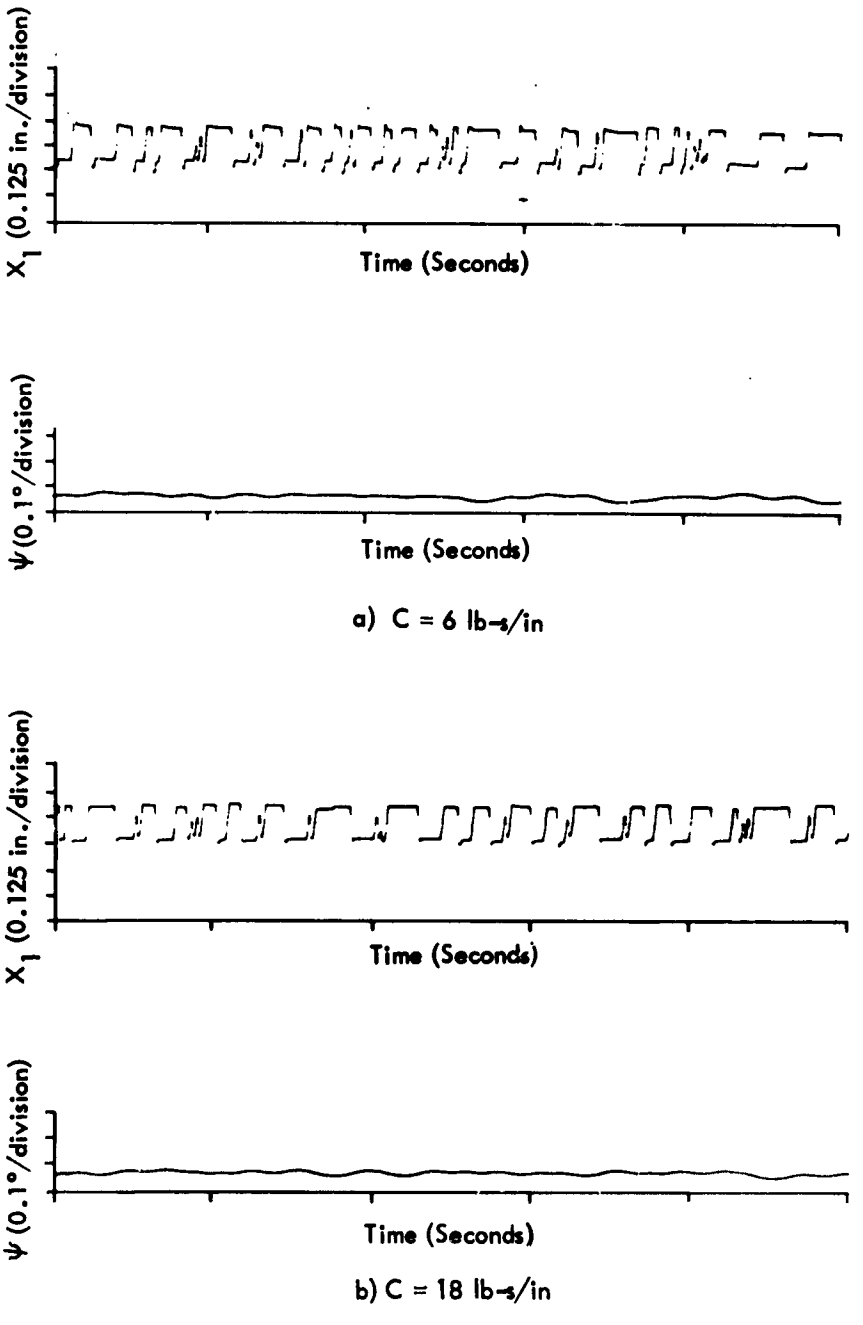

Figure 3-11. Limit Cycle

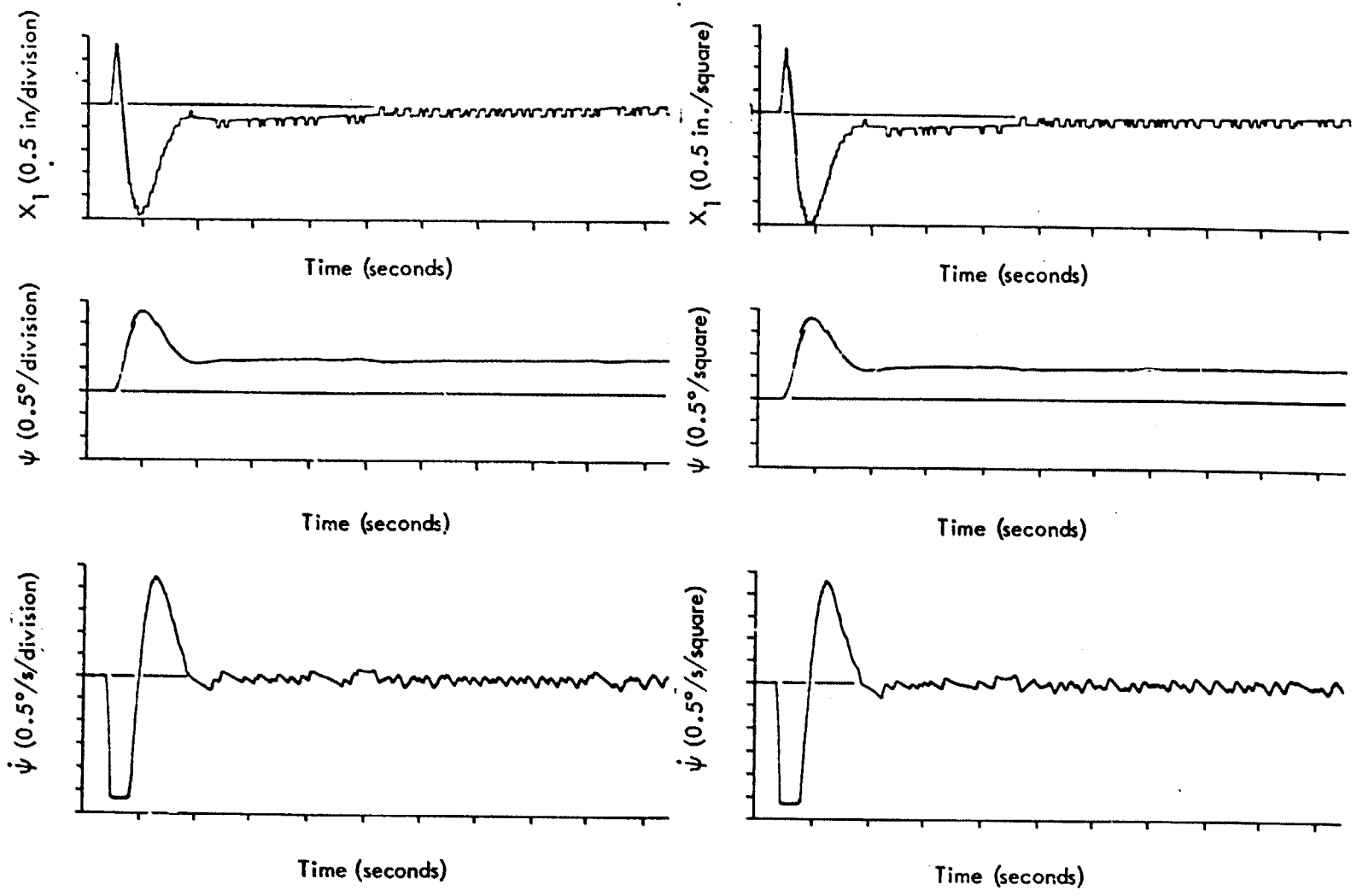

Figure 3-12. Response to a Yaw Step Command for (a) $\frac{\beta}{V} = 13,300$ lb/in^5 (b) $\frac{\beta}{V} = 100,000$ lb/in^5

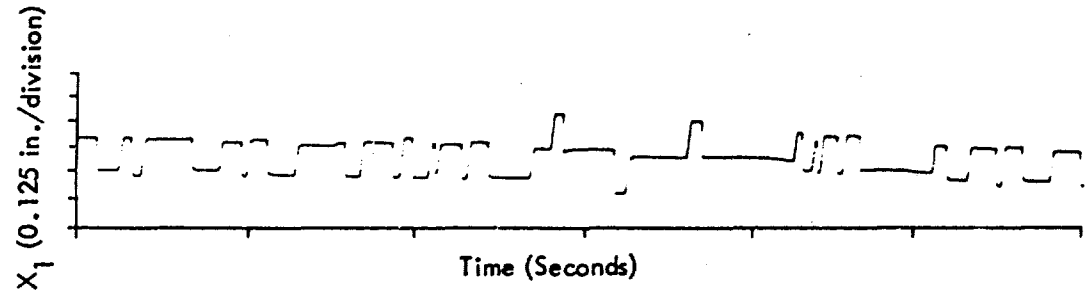

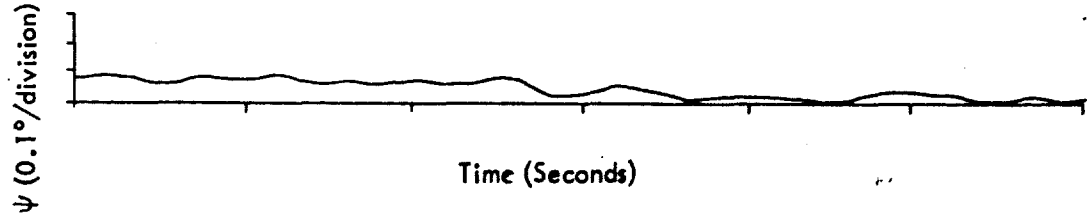

a) $\frac{\beta}{V} = 13{,}300\ \text{lb/in}^5$

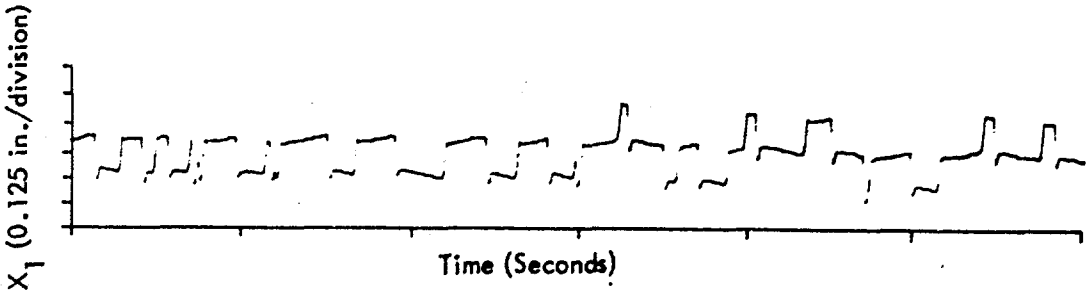

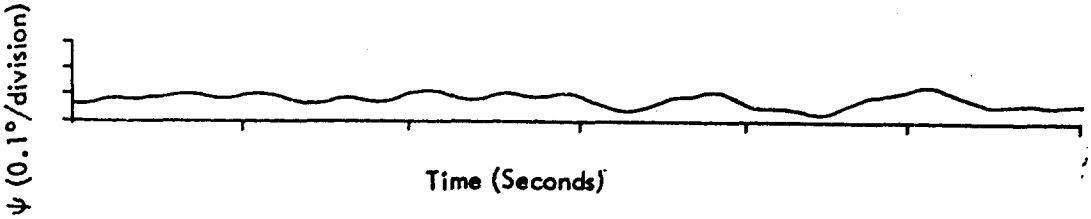

b) $\frac{\beta}{V} = 100{,}000\ \text{lb/in}^5$

Figure 3-13. Limit Cycle

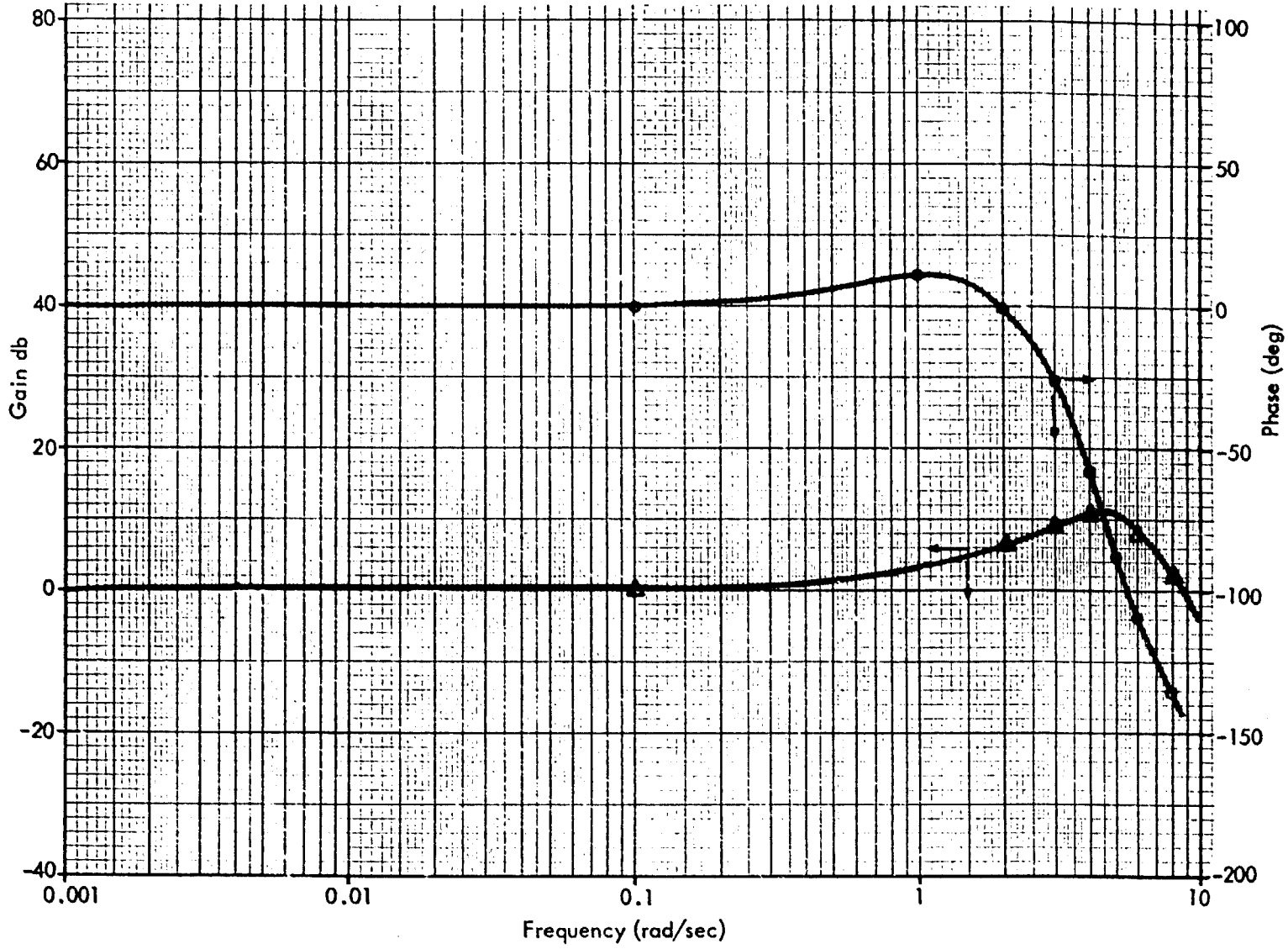

Figure 3-14. Closed Loop Amplitude and Phase Characteristics of Simulated Digital Control System when Closing the Loop with the Laboratory Model

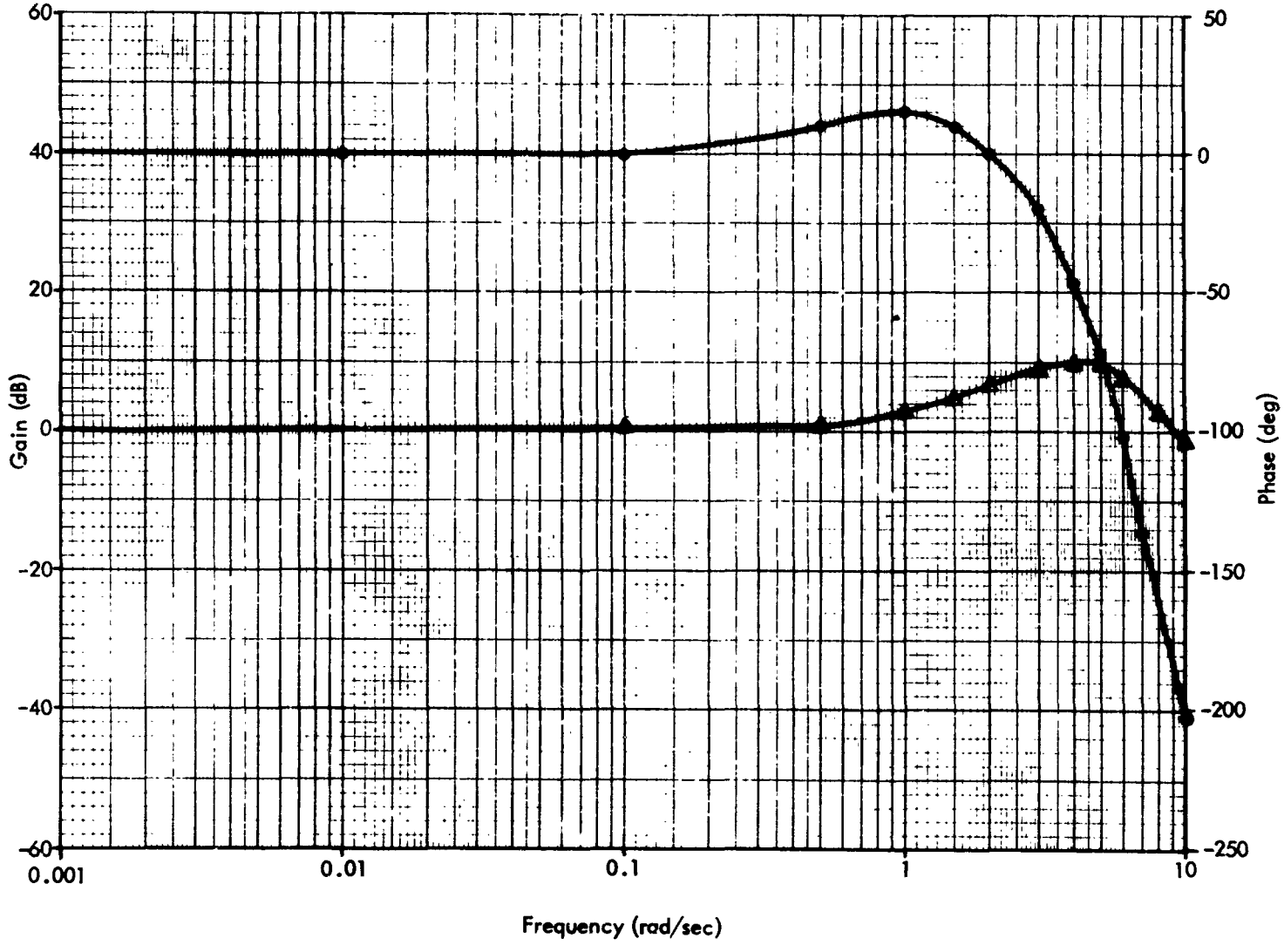

Figure 3-15. Closed Loop Amplitude and Phase Characteristics of Simulated Digital Flight Control System Using Mathematical Model (See Table 3-1)

Section IV

DIGITAL FLIGHT CONTROL SIMULATION

A. DESCRIPTION

Performance of the Polaris missile was determined when using a DHA which provides the same force for both directions of motion. A nozzle torque independent of velocity, producing an axial load of 600 pounds, is assumed. Results were obtained with the mathematical model for the actuator parameters of the actual hardware and a ram area ratio of 1.885:1. The equivalent mass load differs from that used when evaluating the mathematical model due to the longer moment arm used with the hardware. Parameter values are summarized in Table 4-1.

The effect of the leakage parameters and the gain, K, of the autopilot compensation is shown. Performance is evaluated by comparison with the performance of the analog flight control simulated during Phase I.

B. RESULTS

Simulation results for the parameter values of Table 4-1 are shown in Table 4-2. Also shown are results for the parameter values indicated.

1. EFFECT OF LEAKAGE PARAMETERS

As shown by the results of Table 4-2 system performance of the flight control system was not decreased for the assumed values of the leakage parameters, q_L, and q_{LC}. A worst-case condition was assumed by using the larger of the values for both q_L and q_{LC}. Values greater than shown could be used, however, the variation from that of the actual hardware is believed to represent a reasonable tolerance. Figure 4-1 shows the recorded transients for a yaw step command using the parameter values of Table 4-1. The transient of X_1 in Figure 4-1, is typical of that recorded for the leakage conditions shown in Table 4-2.

The recorded transients for an initial condition $\psi_o = -1/2$ degree are shown in Figure 4-2 for the parameter values of Table 4-1. Results for a no

Table 4-1

PARAMETER VALUES FOR SIMULATION OF DIGITAL FLIGHT CONTROL

Parameter	Units	Value	Parameter	Units	Value
ΔF	lb	600	e_b	deg	0.681
M	lb-s^2/in	0.296	Quant. Hys.	deg	$\delta q/4$
R	in	8.00	δ_b	deg	1.09
$\frac{\beta}{V}$	lb-in^{-5}	26,600	K	—	2^{-7}
C	lb-s/in	12			
q_L	in^3/s	0.107			
q_{LC}	in^3/s	-0.006			
q_{LC}^*	in^3/s	-0.0165			
V_{CB}	in^3	0.152			
f_c	Hz	82.5			
T_V	in^{-3}	5.5			
T_f	in^{-3}	10			
P_M	psi	+750			
P_R	psi	130			
P_h	psi	2130			
A_L	in^2	1.00			
A_L/A_R	—	1.885			

leakage condition are shown in Figure 4-3 and for the worst-case leakage in Figure 4-4. Power during steady state can be expressed by:

$$W = X_1 A_L P_h \frac{A_R}{A_L} f_c,$$

where f_c is the actuator frequency.

Table 4-2

SUMMARY OF RESULTS -
SIMULATION OF DIGITAL FLIGHT CONTROL

Parameter Value	Maximum Stable Step	Unstable Step	Stable K_G ($N_y = \psi_o = 0$)	Unstable K_G	Reference Figure No.	
					$N_y = 10$	$\psi_o = -\frac{1}{2}$
Table 4-1	10	11	4.0		4-1	4-2
$q_L = .150$	10	11	4.5	5.0		
$q_{LC} = -.0165$	+11 -10	12 -11	4.5	5.0		
$q_L = q_{LC} = 0$	10	11	4.5	5.0		4-3
$q_L = .150$ $q_{LC} = -.0165$	11 -10	12 -11	4.5	5.0		4-4
$K = 12^{-16}$	11	12	4.5	5.0	4-5	
$K = 2^{-5}$	7	8	4.0	4.5		4-6
$K = 2^{-9}$	11	12	4.5	5.0	4-9	4-10

With reference to Figures 4-2 through 4-4, the frequency, f_o, during steady state averaged from 6 to 11 Hz. The lowest average frequency was obtained with the condition: $q_L = q_{LC} = 0$. However, for the no leakage condition the peak to peak amplitude of ψ approached 0.07 degree as compared to approximately 0.03 degree with leakage. The variation of ψ and f_o produced with the assumed worst case leakage, did not noticeably differ from the variation obtained with the hardware parameters.

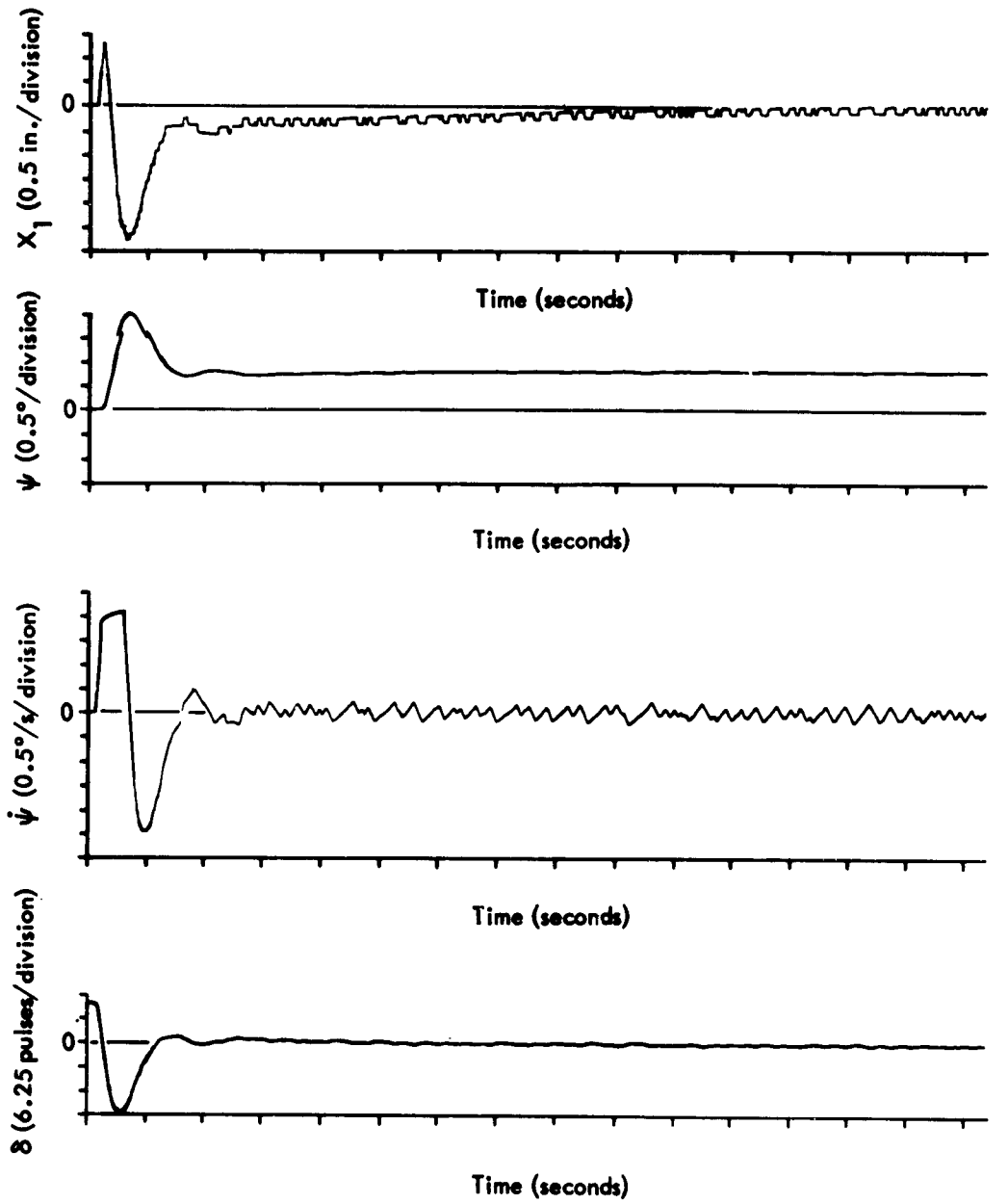

Figure 4-1. Recorded Transients for a Yaw Step Command
N_y = 10 (See Table 4-1)

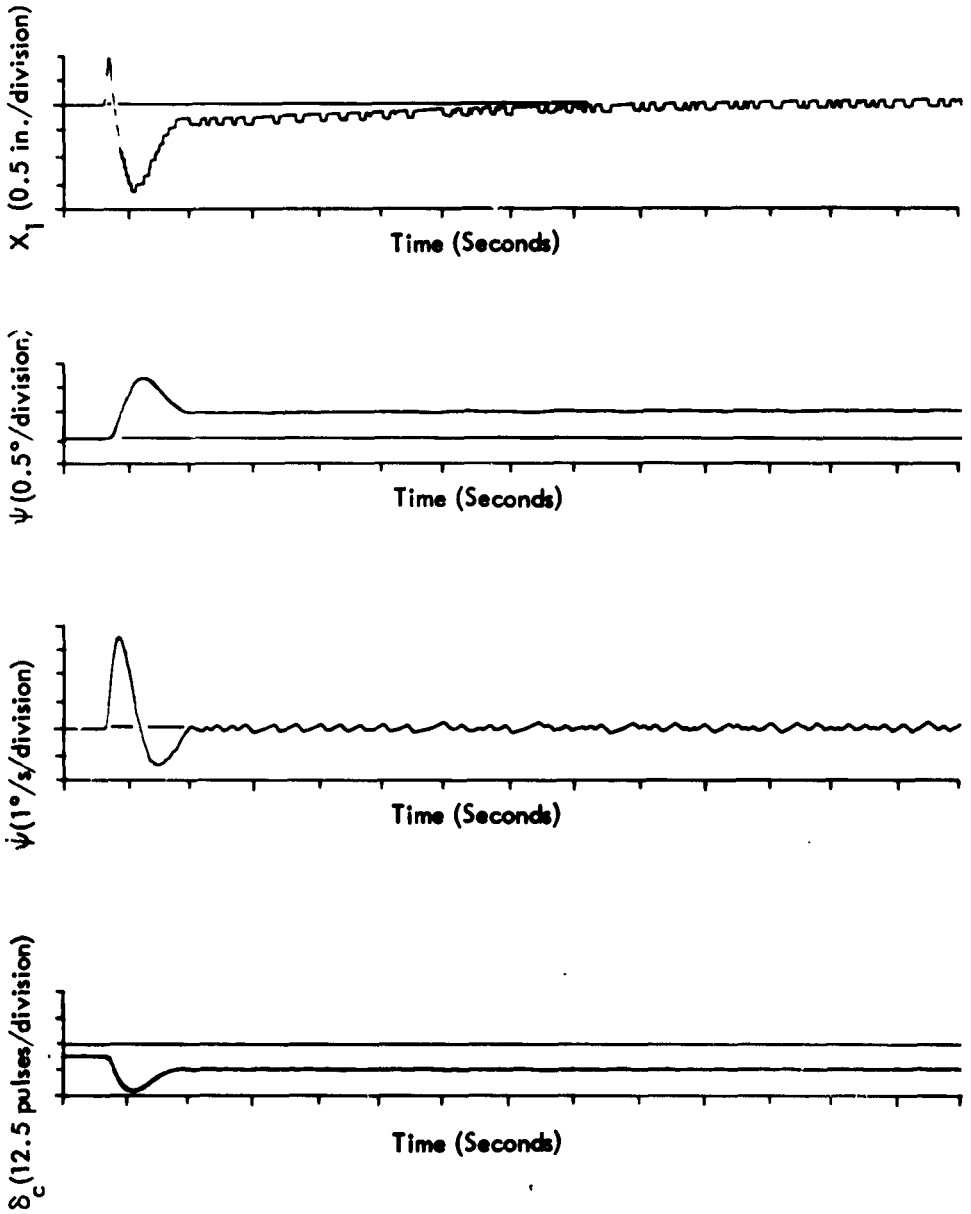

Figure 4-2. Recorded Transients for an Initial Yaw Condition, $\psi_o = -1/2°$ (Ref: Table 4-1)

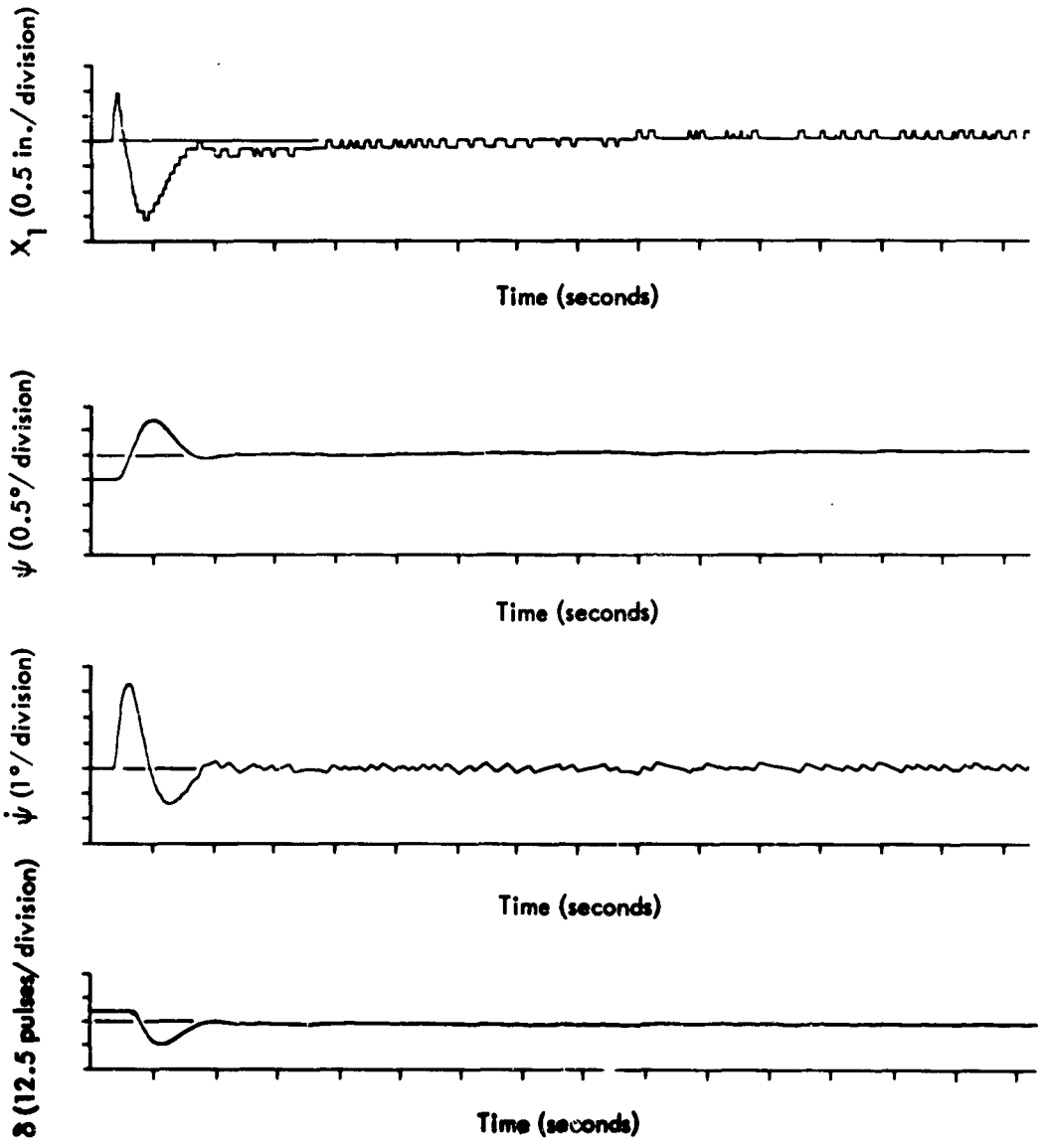

Figure 4-3. Recorded Transients for an Initial Yaw Condition (ψ_o = -1/2°) and no Leakage (q_L = q_{LC} = 0)

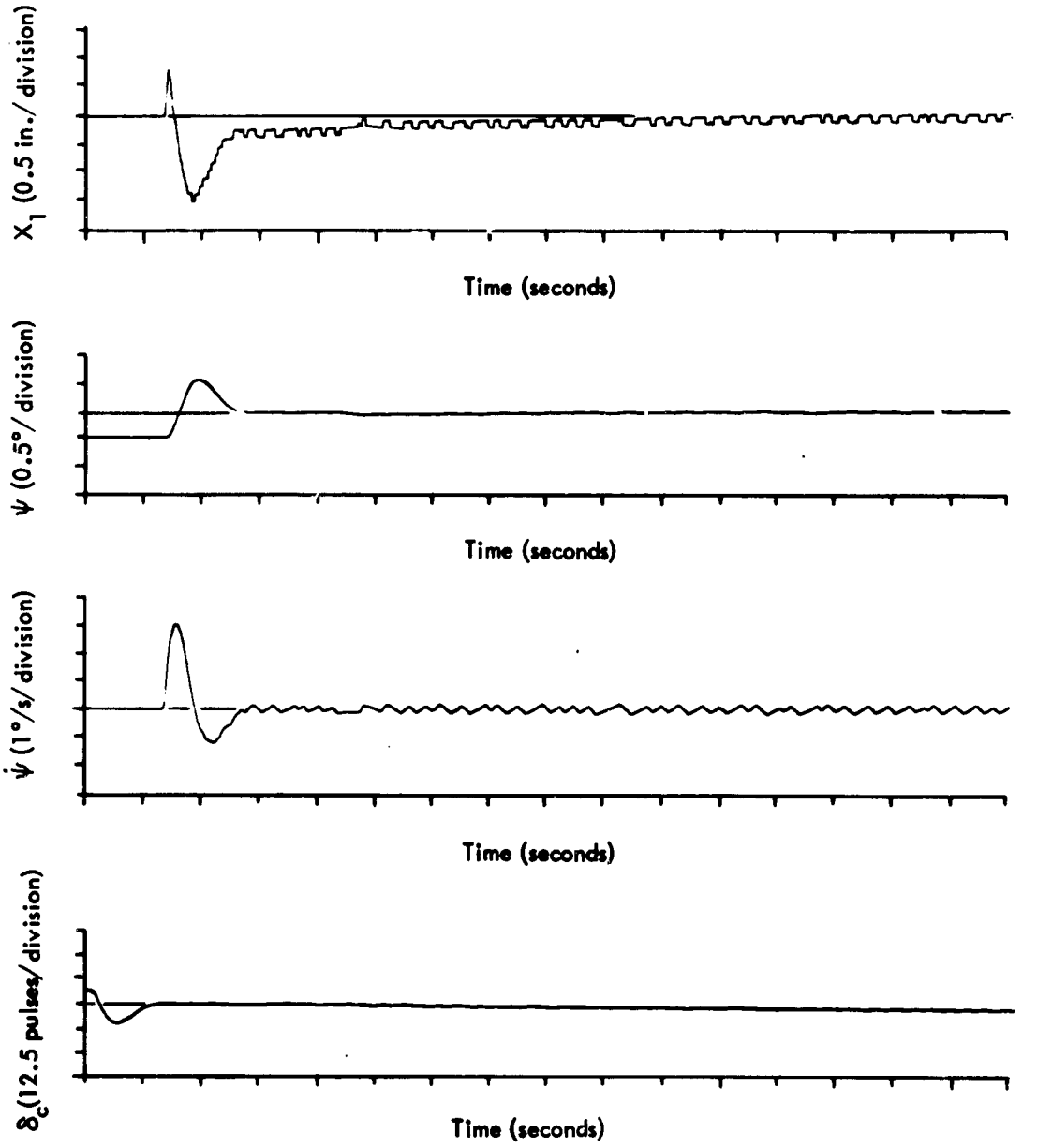

Figure 4-4. Recorded Transients for an Initial Yaw Condition (ψ_o = -1/2°), Assuming the "Worst" Case Leakage (q_L = 0.150 in^3/s, q_{LC} = -0.0165 in^3/s)

2. EFFECT OF COMPENSATION GAIN, K

System performance and response characteristics of the missile can be readily modified by changing the gain, K, of the autopilot compensation. Transients for $K = 2^{-16}$ are shown in Figure 4-5 and for $K = 2^{-5}$ in Figure 4-6. As K approaches zero ($K = 2^{-16}$) a steady state error of ψ results due to the presence of leakage. For large K ($K = 2^{-5}$) the missile transient is highly oscillatory.

3. COMPARISON WITH ANALOG FLIGHT CONTROL

Table 4-3 shows the performance of the analog flight control system simulated as part of the Phase 1 study. Transients for a yaw step command and an initial yaw condition are shown respectively in Figures 4-7 and 4-8. Similar performance and transient characteristics are achieved with the digital flight control with the compensation gain K equal to 2^{-9} (Figures 4-9 and 4-10). The maximum stable step for the analog system is 0.075 degree larger, a difference of 8 percent. This is attributed to the change in implementation, (see Table 2-1). With the digital flight control, oscillations of ψ during steady state approached a peak-to-peak value of 0.04 degree, a consequence of a nonlinearities and quantization. Because of the dynamics of the vehicle, the effect of the oscillations of ψ on the flight path angle is attenuated.

As discussed in Reference 1, the no-input condition used to investigate gain of the digital flight control is not analogous to the no-input condition used with the analog flight control. A 0.109 degree oscillation of the nozzle exists during the steady-state condition of the digital system. Hence, the maximum gain of the analog system is higher. The gain of the analog system approaches that of the digital system when measured with an input of $N_y = 1$. Although maximum gain of the digital system is lower, the gain changed required to produce instability provides a credible margin.

4. GAIN-PHASE

The frequency response and phase shift characteristics of the closed loop system is depicted in Figure 4-11 when using the parameter values of Table 4-1. To minimize the effect of velocity saturation the input was restricted to small signals.

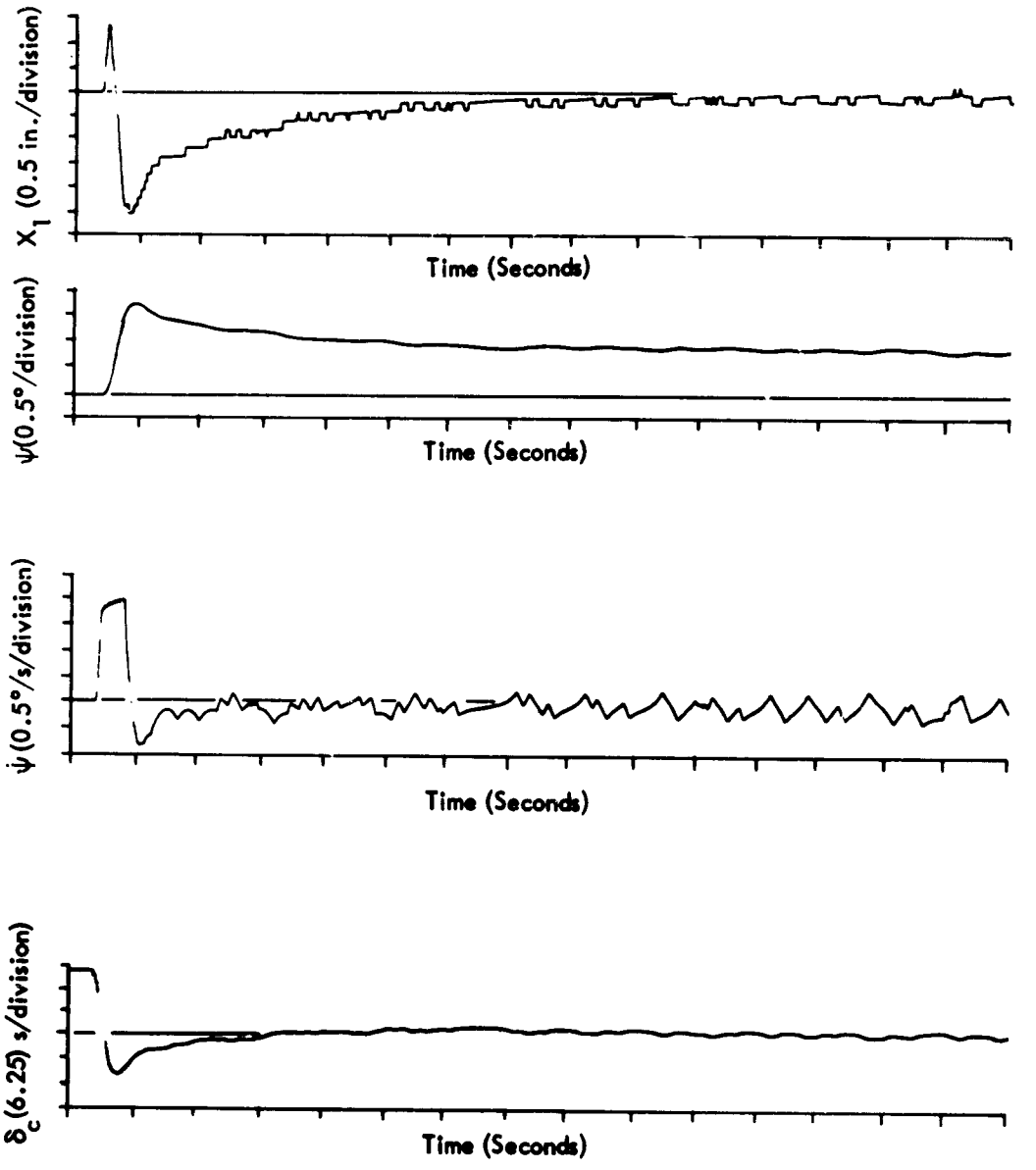

Figure 4-5. Recorded Transients for a Yaw Step Command (Ny = 10) Showing Steady State Error of ψ when K → 0 ($K = 2^{-16}$)

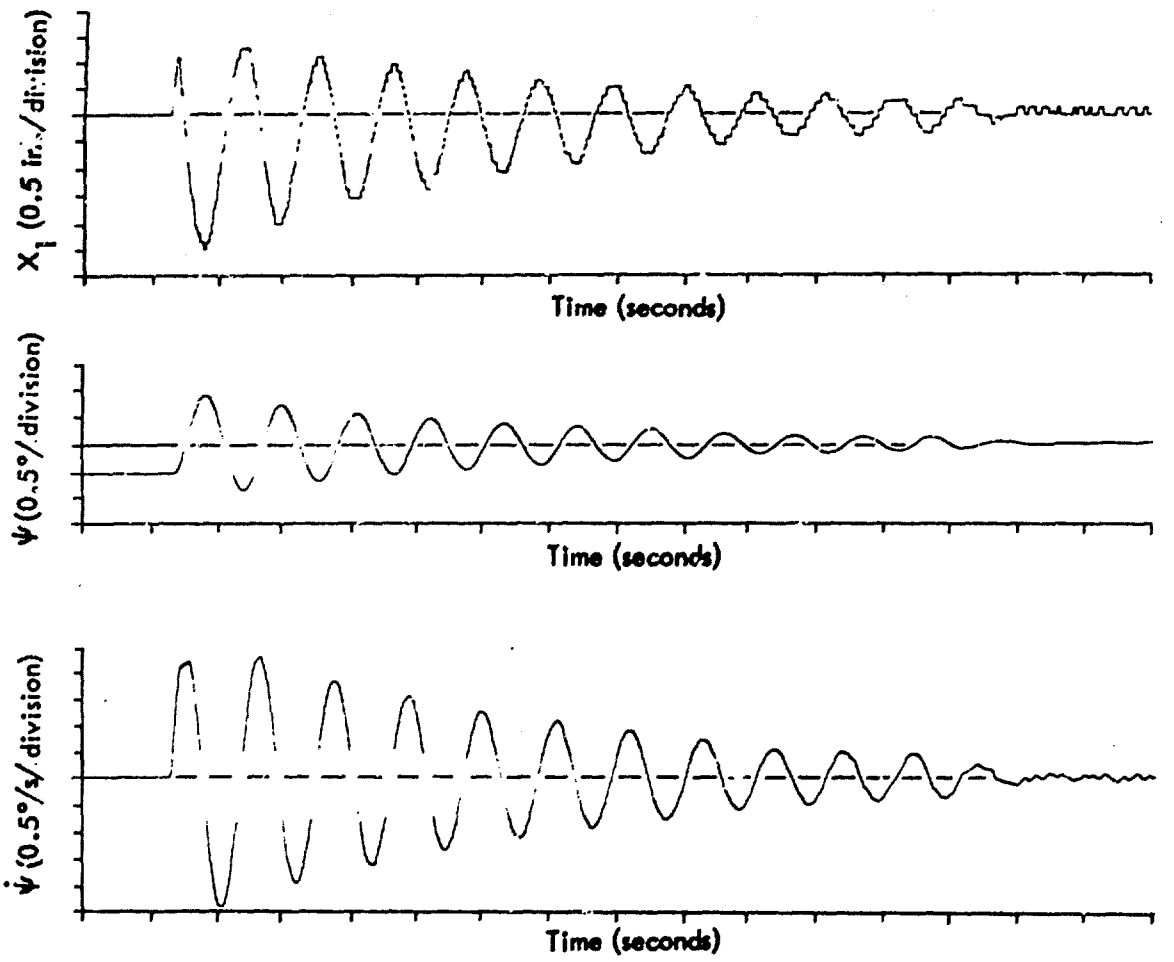

Figure 4-6. Recorded Transients for a Yaw Condition (ψ_o = -1/2°) with K = 2^{-5}

Table 4-3

RESULTS OF ANALOG FLIGHT CONTROL SIMULATION (PHASE I)

Run	Input	Results	Time Histories
C-13A	None	Stable with $K_g = 18.2$	
C-13B	None	Unstable with $K_g = 18.9$	
C-14	Step of $N_y = 12$	Stable	
C-15	Step of $N_y = 13$	Unstable	
C-16	Initial $\psi_o = 0.5°$	Stable	Figure 4-8
C-17	Step of $N_y = 10$	Stable	Figure 4-7
C-18	Step of $N_y = 1$	Stable	
C-19A	Step of $N_y = 1$	Stable with $K_g = 7.0$	
C-19B	Step of $N_y = 1$	Unstable with $K_g = 7.25$	
C-20A	Step of $N_y = 2$	Stable with $K_g = 4.5$	
C-20B	Step of $N_y = 2$	Unstable with $K_g = 4.75$	

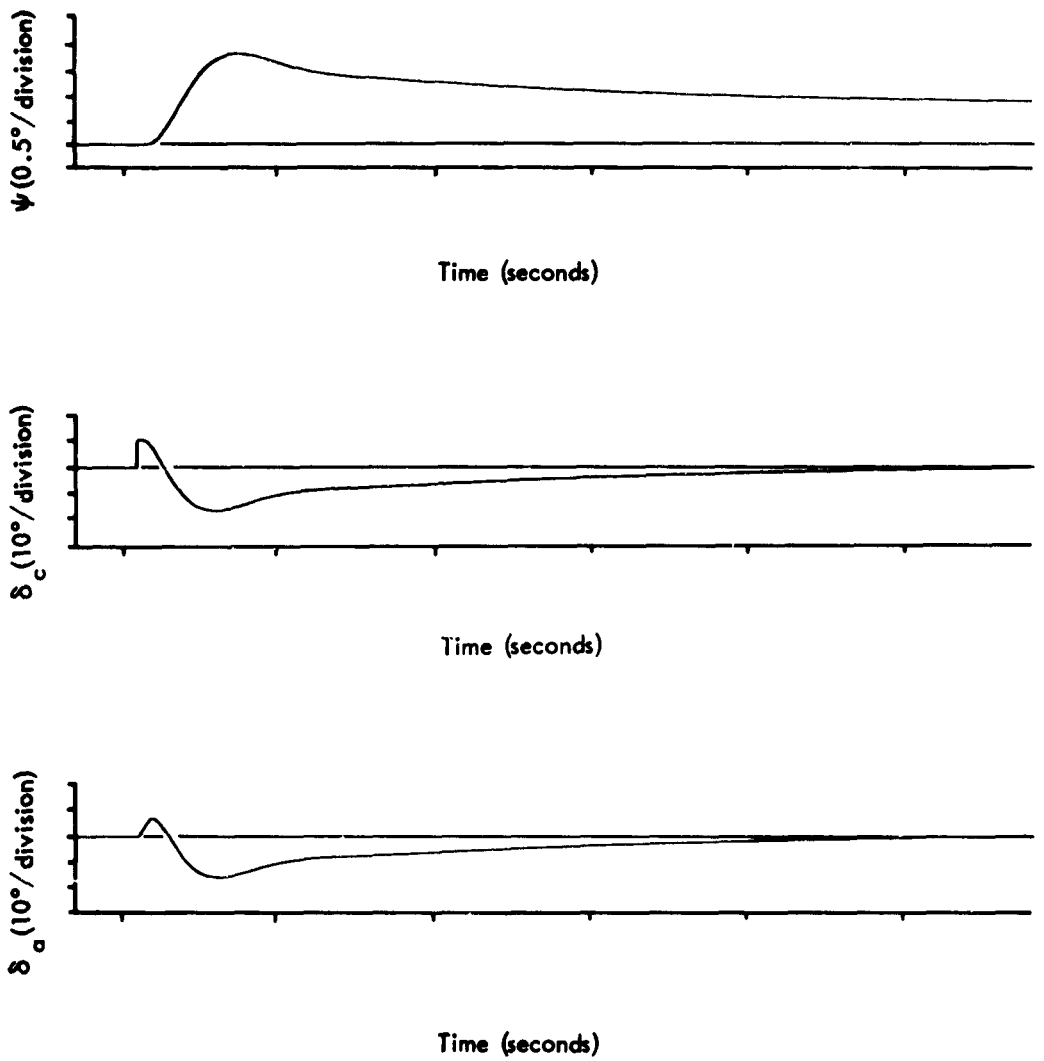

Figure 4-7. Recorded Transients Using Analog Flight Control for a Yaw Step Command (N_y = 10)

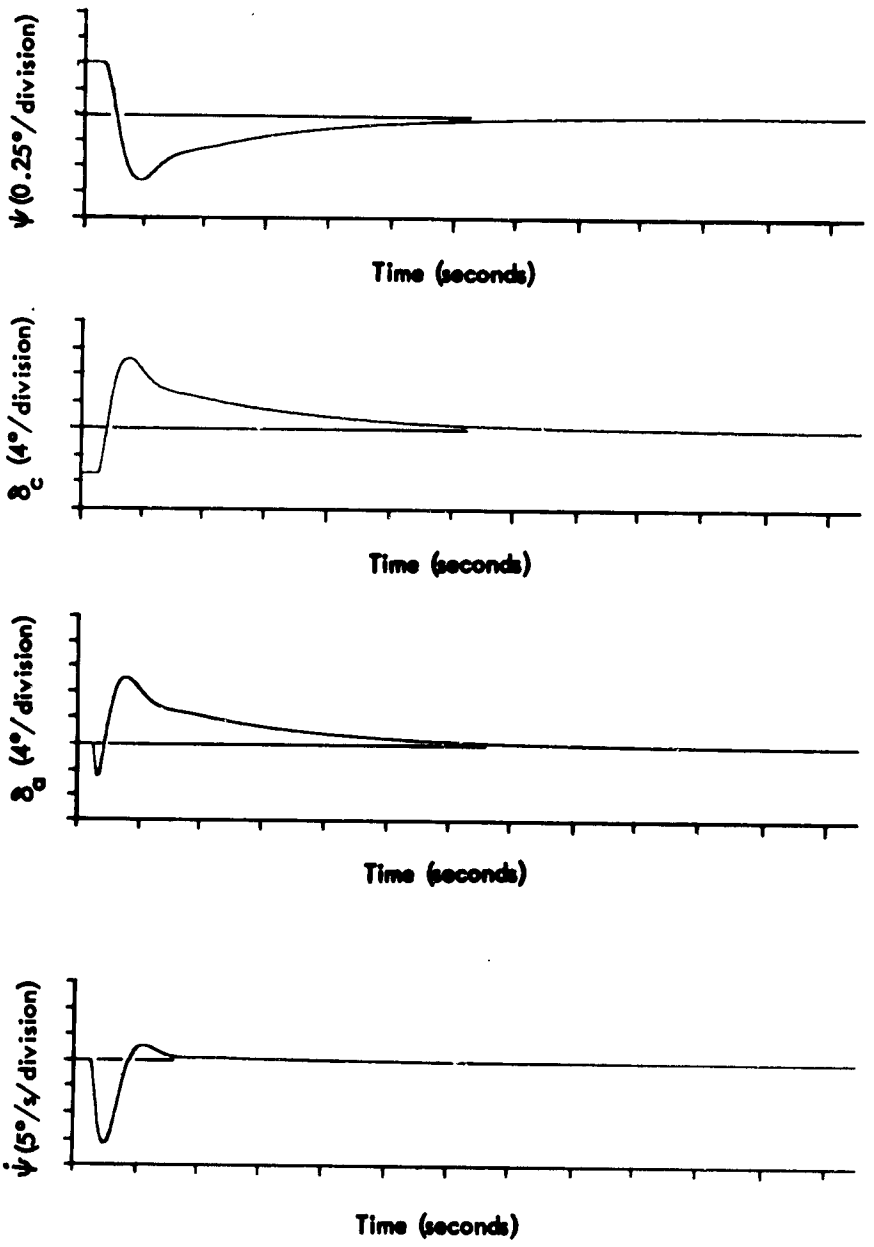

Figure 4-8. Recorded Transients Using Analog Flight Control System for an Initial Yaw Condition ($\psi_0 = +1/2°$)

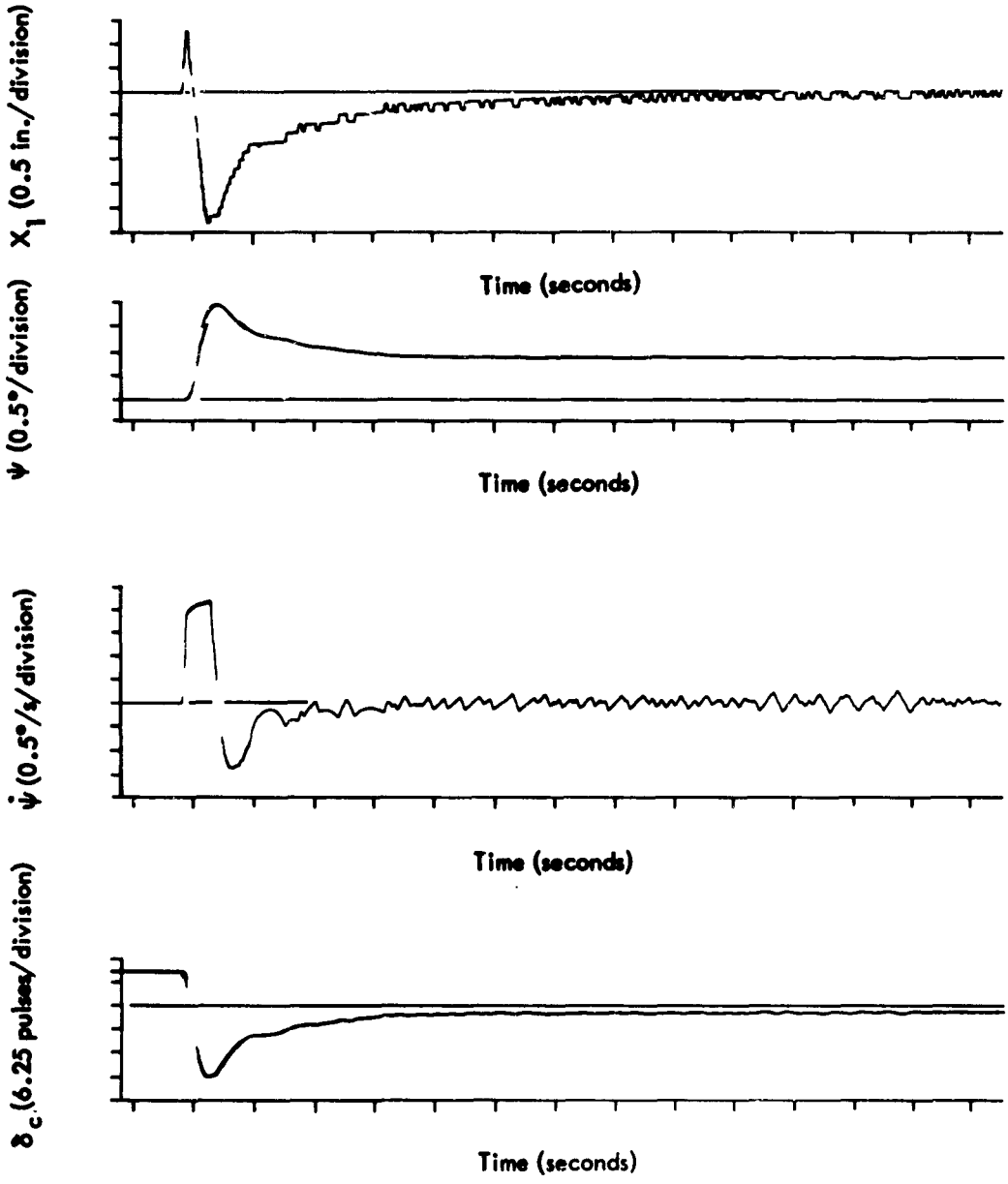

Figure 4-9. Recorded Transients for a Yaw Step Command (N_y = 10) with K = 2^{-9} (Ref - Table 4-1)

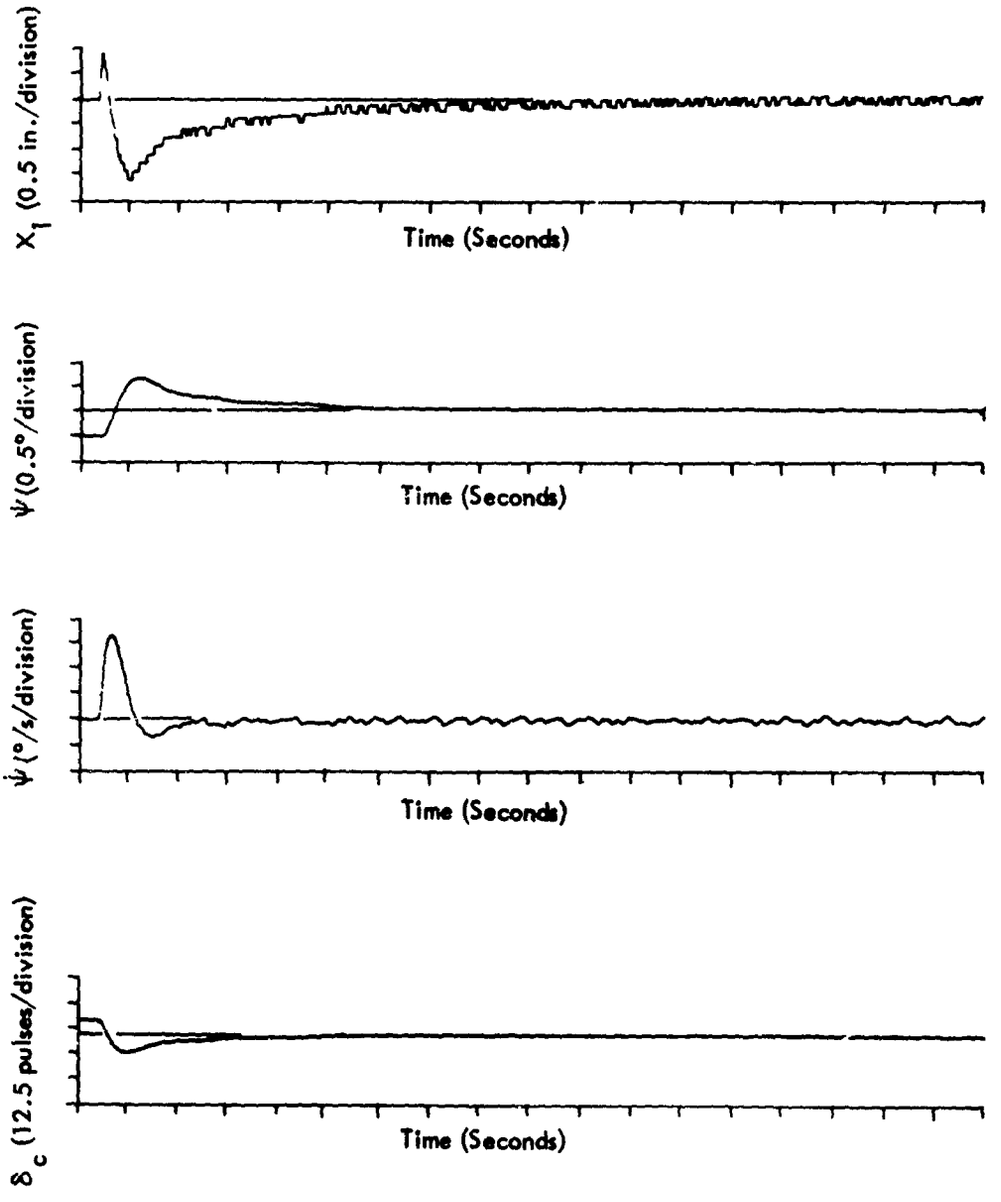

Figure 4-10. Recorded Transients for an Initial Yaw Condition (ψ_o = -1/2°) with K = 2^{-9} (Ref - Table 4-1)

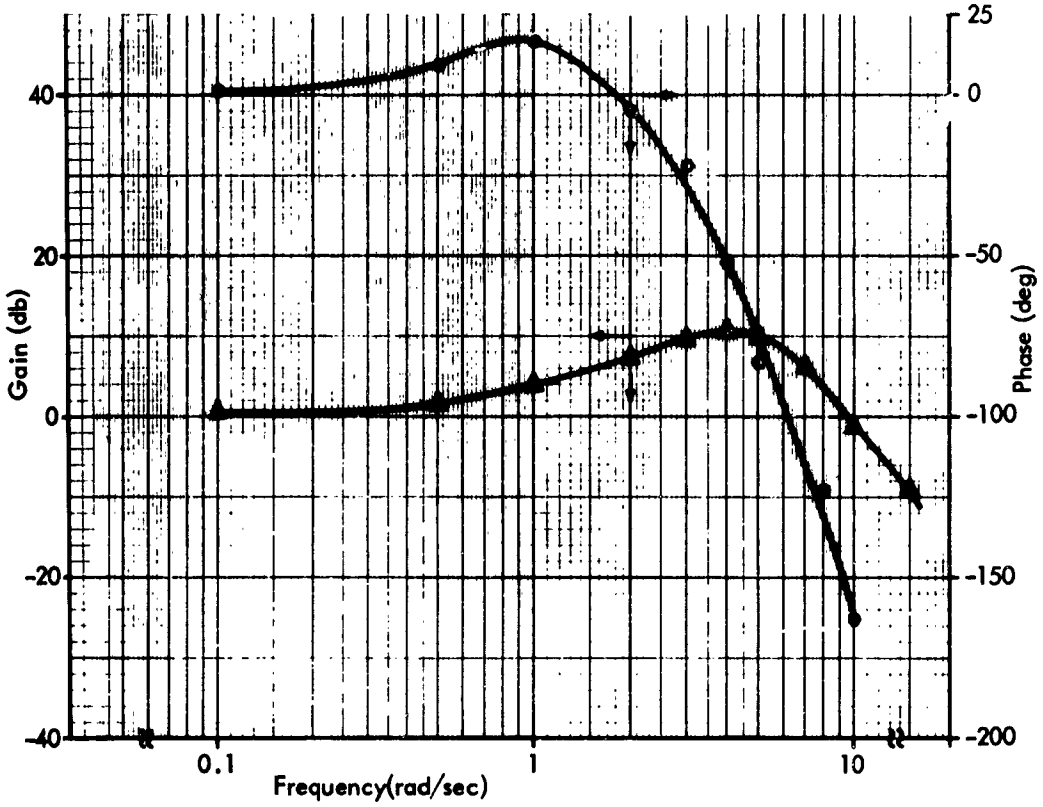

Figure 4-11. Closed-Loop Amplitude and Phase Characteristics of Simulated Polaris Digital Flight Control

Section V

LINEARIZED MODEL

As a first approximation, a linearized model provides a convenient means of determining the suitability of the DHA to a given application. To ascertain the validity of using a linear model, the mathematical model of Figure 2-3 is reduced to a linear form. Performance of the linear model is compared to the performance of the simulated system when closing the loop with the laboratory model. Validity is established by the agreement of performance characteristics for frequency response, phase shift, and step response.

A. DEVELOPMENT

Figure 5-1 shows the block diagram of the digital flight control system when load dynamics are neglected. Restricting the commands so that the input to the non-linear block never exceeds one quantum and neglecting quantization Figure 5-2 is equivalent to Figure 5-1. By use of the identity shown in Figure 5-3 the model can be represented by the diagram of Figure 5-4 which also includes the approximation:

$$\frac{1 - e^{-T_f S}}{T_f S} \cong e^{\frac{-T_f S}{2}}.$$

Zero-order holds can be formed in the feed forward path and minor loop by combining the integration of the DHA with the first difference computation. The sampling frequency is approximately two orders of magnitude higher than the frequency of the missile poles. Hence, a sample and hold can be approximated by the time delay, $e^{\frac{-TS}{2}}$. Using this approximation and rearranging the terms yields the linearized model shown in Figure 5-5.

The linearized model is based on small signal inputs, i.e., velocity saturation does not exist. The magnitude of missile poles are small relative to the poles of the actuator. As a consequence loop dynamics even in the presence of slow saturation are dominated by the characteristics of the missile. Therefore, the linearized model can be used with inputs which produce

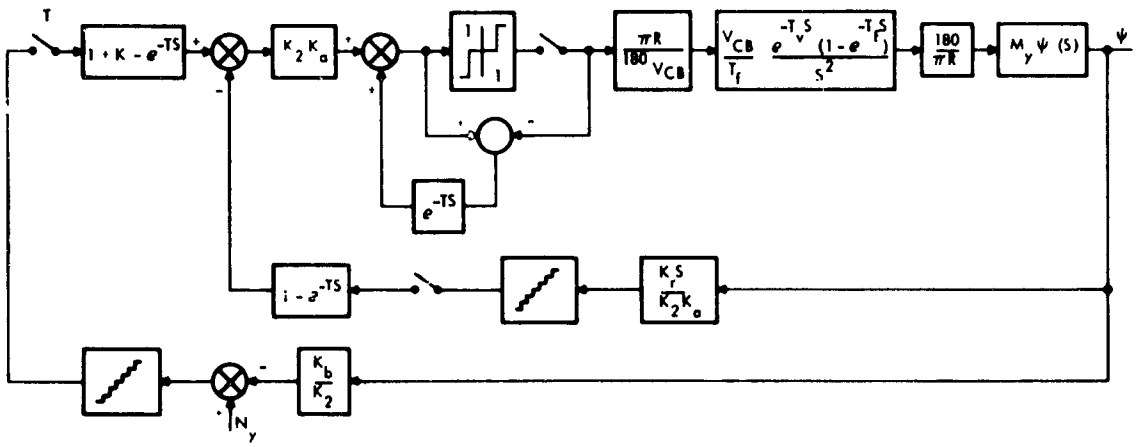

Figure 5-1. Block Diagram of Digital Flight Control System Neglecting Load Dynamics

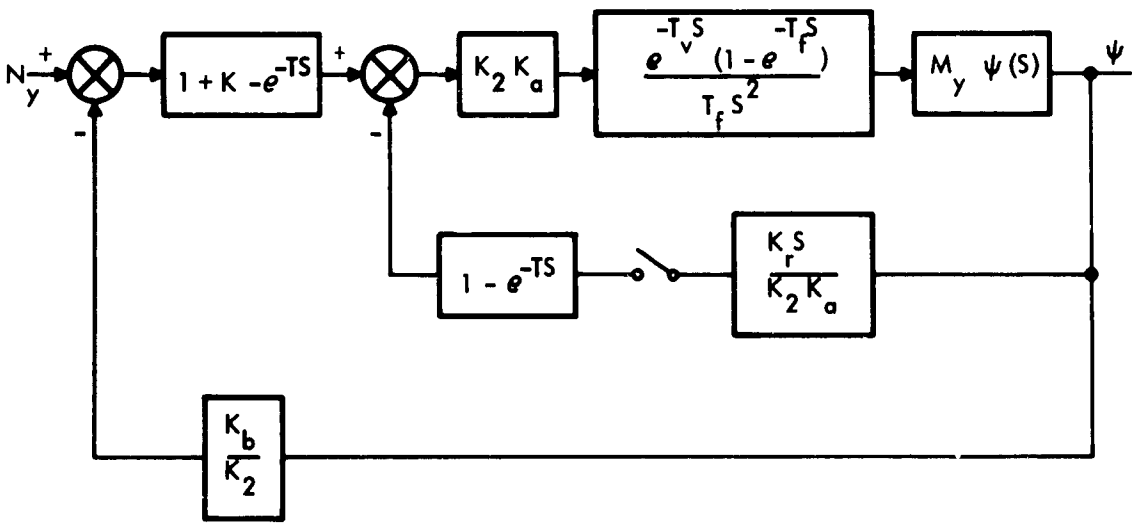

Figure 5-2. Block Diagram Equivalent of Figure 5-1 When Neglecting Quantization and Restricting Input to Small Signals

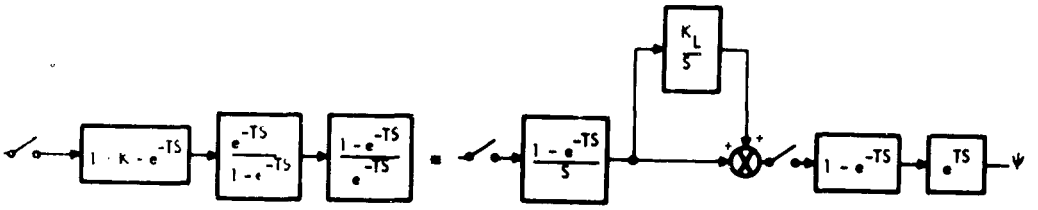

Figure 5-3. Identity Used to Reduce Figure 5-2 to Figure 5-4

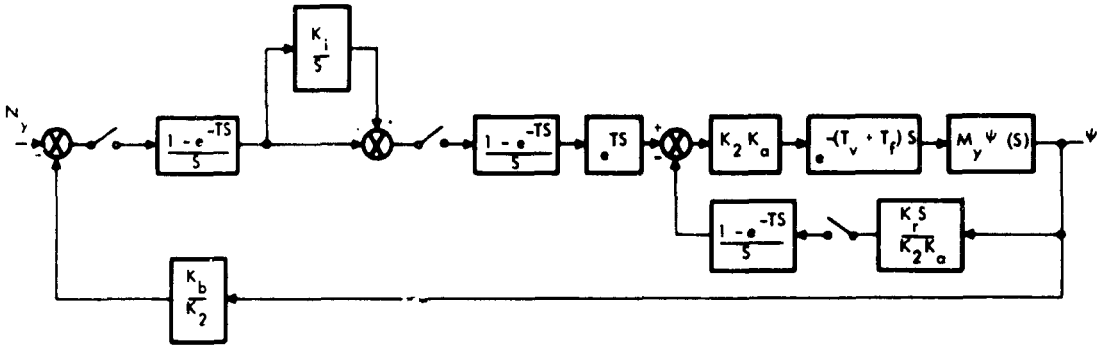

Figure 5-4. Equivalent Form of Figure 5-2

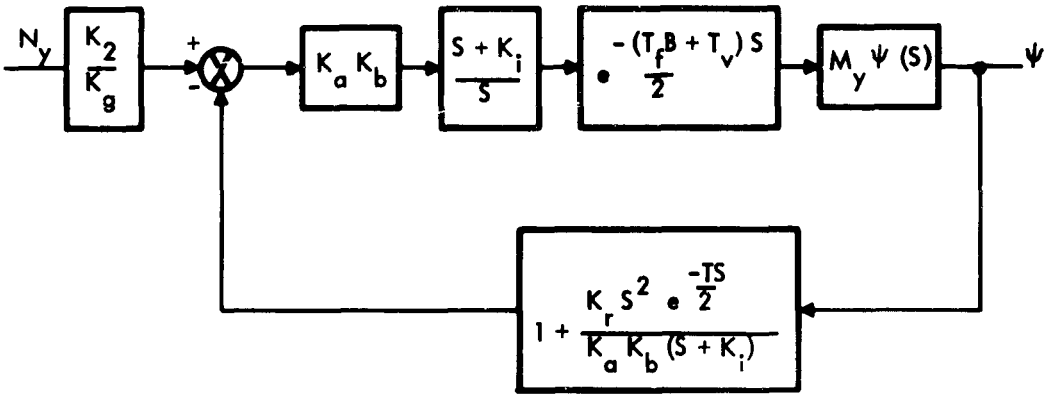

Figure 5-5. Linearized Model of Digital Flight Control System

velocity saturation. The magnitude of the input, however, is limited by the stability condition:

$$\left[T_\Sigma \sin\zeta\, l_e\right] \delta_{max} > C_{N\beta}\, \bar{q} S\, l_{p\beta}(t)$$

and $$\left[T_\Sigma \sin\zeta\, l_e\right] \delta(t) > C_{N\beta}\, \bar{q} S\, l_{p\beta}\dot{\beta}(t) \text{ for sgn } \delta(t) = -\operatorname{sgn}\beta(t)$$

B. RESULTS

Results presented in Figure 5-6 and 5-7 were obtained using the linearized model of Figure 5-5. Although not included in this report, satisfactory results were also achieved with a model which included the approximation:

$$e^{-\tau S} = \frac{1}{\tau S + 1}$$

which was used to obtain the response curve of Figure 5-7. Comparison of Figure 5-6 and 5-7 with Figures 4-11 and 4-1 shows the linearized model to be a good approximation.

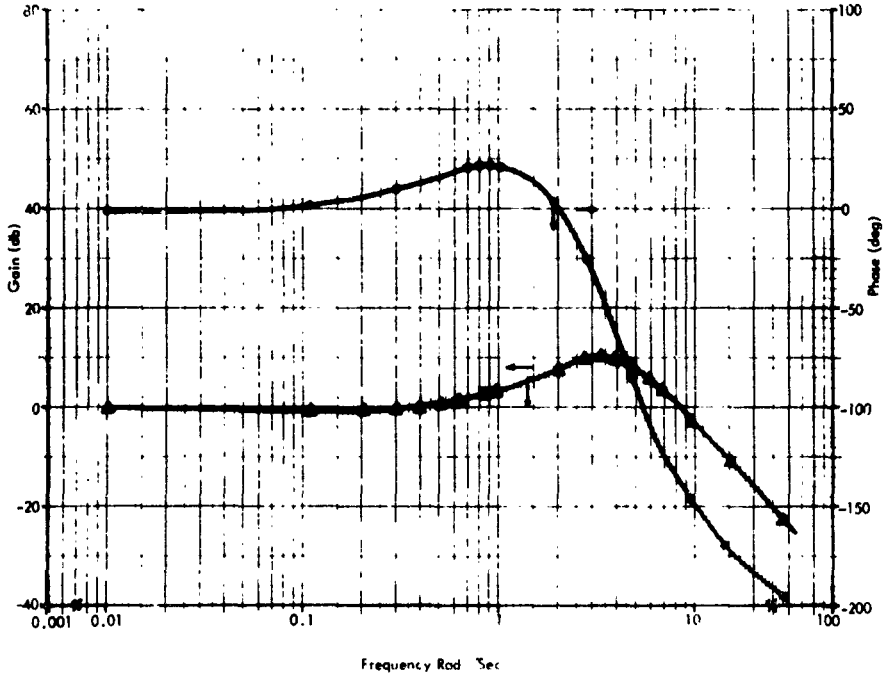

Figure 5-6. Closed Loop Amplitude and Phase Characteristics of Linearized Model (Ref Fig. 5-5)

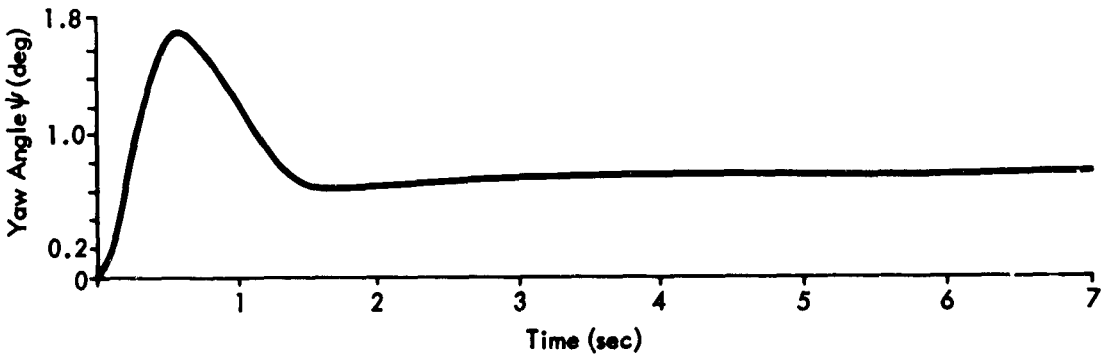

Figure 5-7. Computed Response to a Yaw Command (N_y = 10) Using Linearized Model (Figure 5-5)

REFERENCES

1. "Digital Hydraulic Actuator Study Final Report (U)," Contract No. Nonr 4375(00), IBM CD No. 3-260-6036, August 1964.

2. Raider, Scott, "Digital Hydraulic Study Engineering Summary Report Phase II", Contract No. Nonr 4375(00), IBM No. 66-928-7.

3. "Digital Hydraulic Actuator Phase III Proposal," IBM No. 65-947-085, August 1965.

4. Raider, Scott, "A Digital Hydraulic Actuator," IBM No. 65-825-1467, April 1965.

5. "Polaris A3 Preliminary Flight Performance Report, Polaris A3P (MK 3 MODO) Missile (U)," 15 March 1962.

Appendix A

DIGITAL HYDRAULIC ACTUATOR OPERATIONAL CONCEPT

Appendix A

DIGITAL HYDRAULIC ACTUATOR OPERATIONAL CONCEPT

The digital hydraulic actuator (DHA) design concept used in this study is shown in Figure A-1. Calibrated fluid volumes, transferred by displacing the calibrating piston, are summed to achieve a load position corresponding to a digital command. Auxiliary pistons permit the calibrated volume to be displaced at a rate independent of the mass load.

For simplicity, the operation of the DHA (Figure A-2) will be described neglecting the auxiliary pistons. The high pressure is directed to force the volume piston to its extreme upper position. When the actuating valve is moved down, the fluid pressure will move the volume piston to its extreme bottom position and displace fluid into the actuating cylinder. This in turn will cause the output ram to move a calibrated distance to the right. Because of the larger area on the left side of the ram piston, the high-pressure fluid on the right side of the cylinder will be forced into the high-pressure line. A restriction placed in this line will damp the output ram. Further movement of the actuating valve will cause the output ram to continue discrete motions to the right.

To see how motion to the left is achieved, assume that both valves are again in the upper position, but this time move the direction valve down. The return pressure will now propagate to the bottom side of the volume piston, causing the volume piston to move down. This will withdraw one calibrated volume from the actuating cylinder, and the output ram will be forced to the left by the high pressure on the right side of the actuator cylinder. Motion to the left is continued by moving the actuating valve. Hence, the output ram is moved to the right by moving the direction valve up, or, if it is already in its upper position, by changing the position of the actuating valve. Output ram motion to the left is achieved by moving the direction valve down, or, if it is already down, by changing the position of the actuating valve.

Accuracy requires that the valve iteration interval, T_C, be greater than the time required to transfer the calibrated volume, V_C. The maximum valve iteration rate, f_C, for a given pressure is thus dictated by the magnitude of the mass load. The addition of auxiliary pistons (Figure A-1) permits the calibrated volume to be displaced at a rate independent of the mass load.

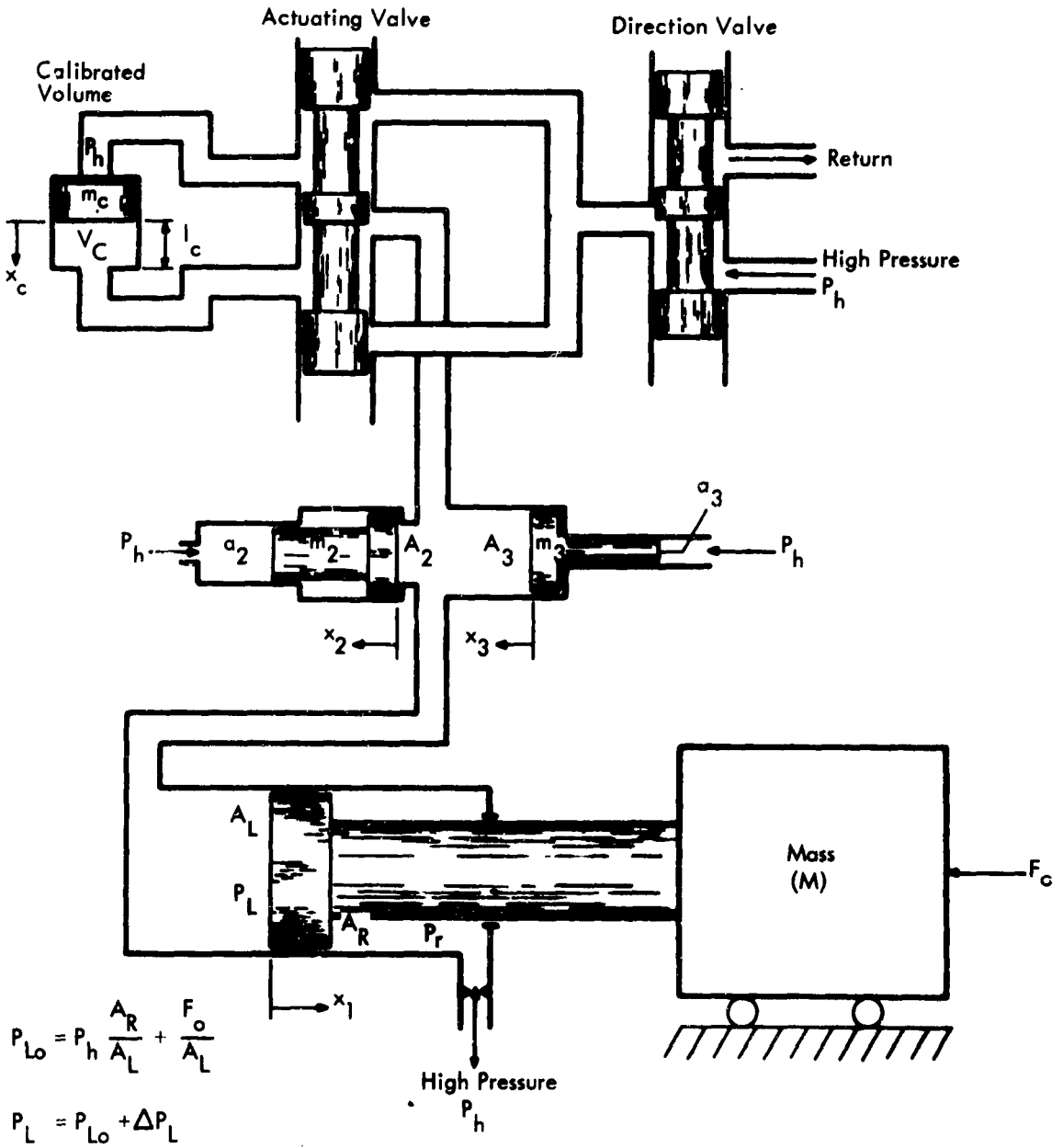

$$P_{Lo} = P_h \frac{A_R}{A_L} + \frac{F_o}{A_L}$$

$$P_L = P_{Lo} + \Delta P_L$$

$$\Delta P_L = -\frac{\beta}{V_o} \Delta V$$

Figure A-1. Schematic of the Basic Digital Hydraulic Actuator

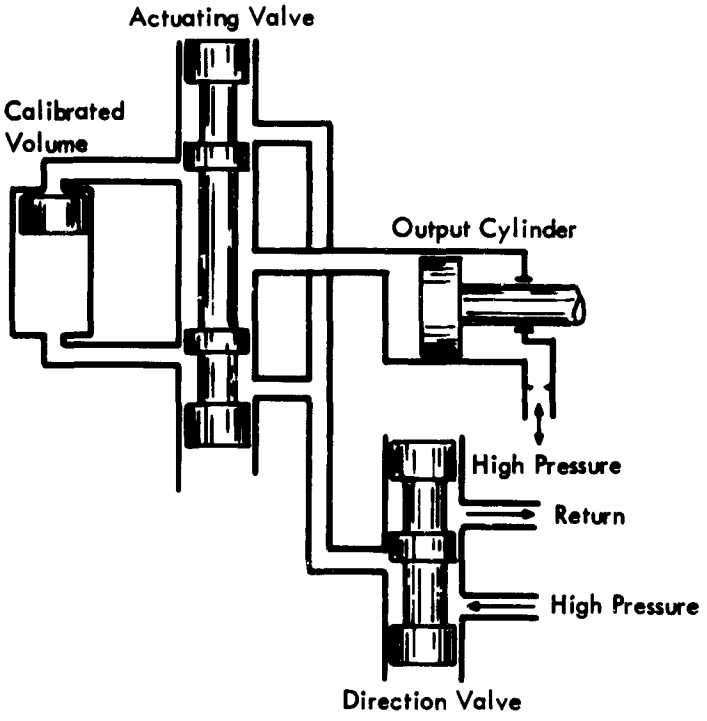

Figure A-2 Digital Hydraulic Actuator

Hence, the iteration rate is limited only by: (1) the maximum switching speed of the valve; (2) the time required to transfer V_C; and (3) the time required to decay the transient pressures displacing the volume piston. Since the mass of each auxiliary piston is much less than that of the mass load, fluid transfer time is greatly reduced. Consequently, the mass rate, m_r, acting to displace the mass, M, approaches a step function.

If the actuating valve is positioned so that high pressure, P_h, forces the calibrating piston from the position shown in Figure A-1 to the bottom position, a calibrated volume of fluid, V_C, will be displaced. The volume displaced can be considered as being divided into three unequal parts:

- A volume necessary to increase the transient total internal pressure, P_L, from

  $$P_h \frac{A_R}{A_L} \quad \text{to} \quad P_h \frac{a_2}{A_2} .$$

- A volume which displaces the ram piston the right.

- A volume which displaces the auxiliary piston of area A_2.

Because the mass, M, driven by the ram piston is large relative to the mass of the auxiliary piston, the response of the auxiliary piston is high. Hence, the larger portion of the displaced volume is used to displace the auxiliary piston. The ram piston, initially accelerated by a portion of the volume displaced by the calibrating piston, is further displaced by the transfer of the volume stored by the auxiliary piston due to P_h acting to restore auxiliary piston 2 to its rest position. Motion of the ram piston is completed when the volume required to increase P_L is transferred to ram piston motion, thus returning P_L to its original value, $P_h A_R/A_L$. Hence, the ram piston displacement X_1 is:

$$X_1 = \frac{V_c}{A_L} .$$

Additional calibrated volumes displaced by the calibrating piston are stored by displacing auxiliary piston 2.

Over-travel of the ram piston as it moved to the right reduced P_L. As a consequence, auxiliary piston 3 is displaced, thus limiting P_L to minimize the effect of cavitation. Displacement of auxiliary piston 3 creates a pressure differential that acts to return the auxiliary piston to its rest position. Hence, over-travel of the ram piston is limited. Auxiliary piston 3 is restored to its rest position and returns the ram piston to a position such that

$$X_1 = \frac{V_c.}{A_L}$$

Positioning the sign valve so that the return is connected to the calibrated volume permits the ram piston to be displaced to the left. Displacing the actuating valve allows P_L to displace the calibrating piston. Due to the magnitude of the mass, M, the initial volume of fluid required to displace the calibrating piston is furnished by the motion of auxiliary piston 3. Operation is therefore identical in principle to the motion of the ram piston to the right. However, when ram piston motion is to the left, auxiliary piston 3 provides the storage capability and auxiliary piston 2 returns the ram piston to its commanded position when over-travel occurs.

Hydraulically actuated pilot valves operate both the sign and actuating valves. In addition, by using hydraulic power to move the pilot valve, the magnet is not required to perform any work, and this permits the use of small, low-power magnets controlled by electrical commands. Energized, the magnets act as latches, holding the spool of the pilot valve at a fixed position. When de-energized, a magnetic latch permits the hydraulic force to move the

pilot spool, which in turn allows a hydraulic force to move the main spool. A schematic diagram of the pilot and actuator valves is shown in Figure A-3. The pilot valve is shown held in its left hand position by magnetic latch A. Hydraulic pressure acts through the pilot valve to the end of the actuator valve, forcing it to the extreme right. It also acts through the actuator valve to the left end of the pilot spool. De-energizing magnetic latch A allows the hydraulic pressure to move the pilot to the extreme right-hand position, where it is held by latch B. Moving the pilot to the right-hand position switches the pressure to the right-hand end of the actuator valve and connects the left end to the sump. The actuator valve is therefore moved to the extreme left. In an extreme left position, the pressure switches to force the pilot to the left. The left end of the pilot is now connected to the sump, and movement of the pilot is prevented by magnetic latch B. De-energizing latch B allows both valves to move back to the initial position.

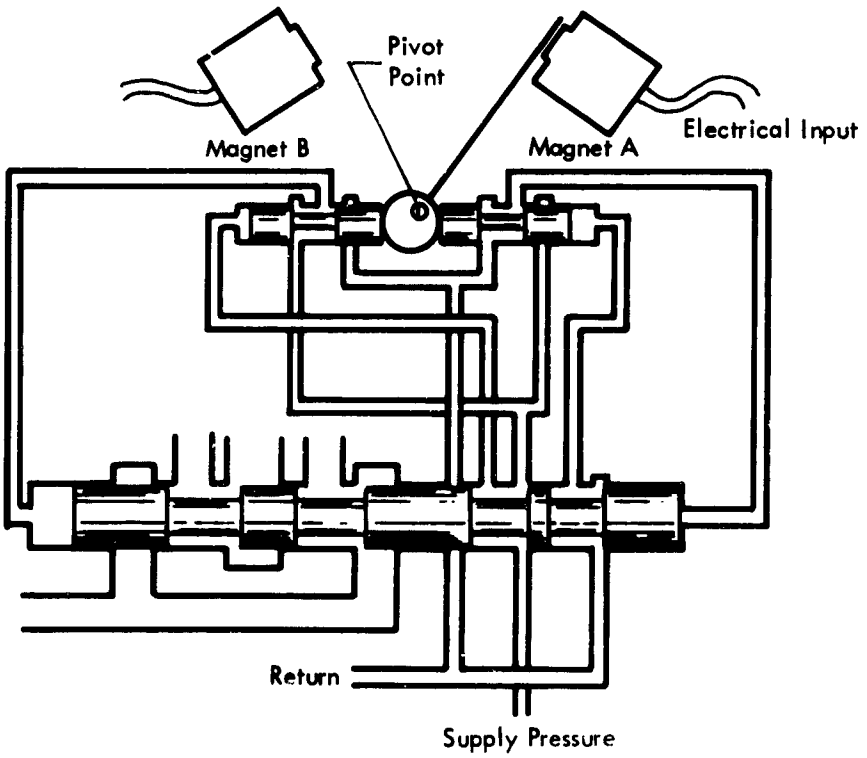

Figure A-3. Pilot Drive Schematic

Appendix B

CIRCUITS

CONTROL LOGIC

Description of Symbols

Symbol	Description	Type – IBM No.
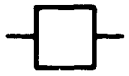	Inverter	370348
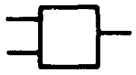	2-Input NAND Inverter	370216
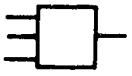	3-Input NAND Inverter	370378
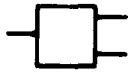	Trigger	37022
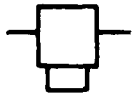	Singleshot	370262
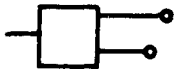	Driver	371633
	Load Card	37032

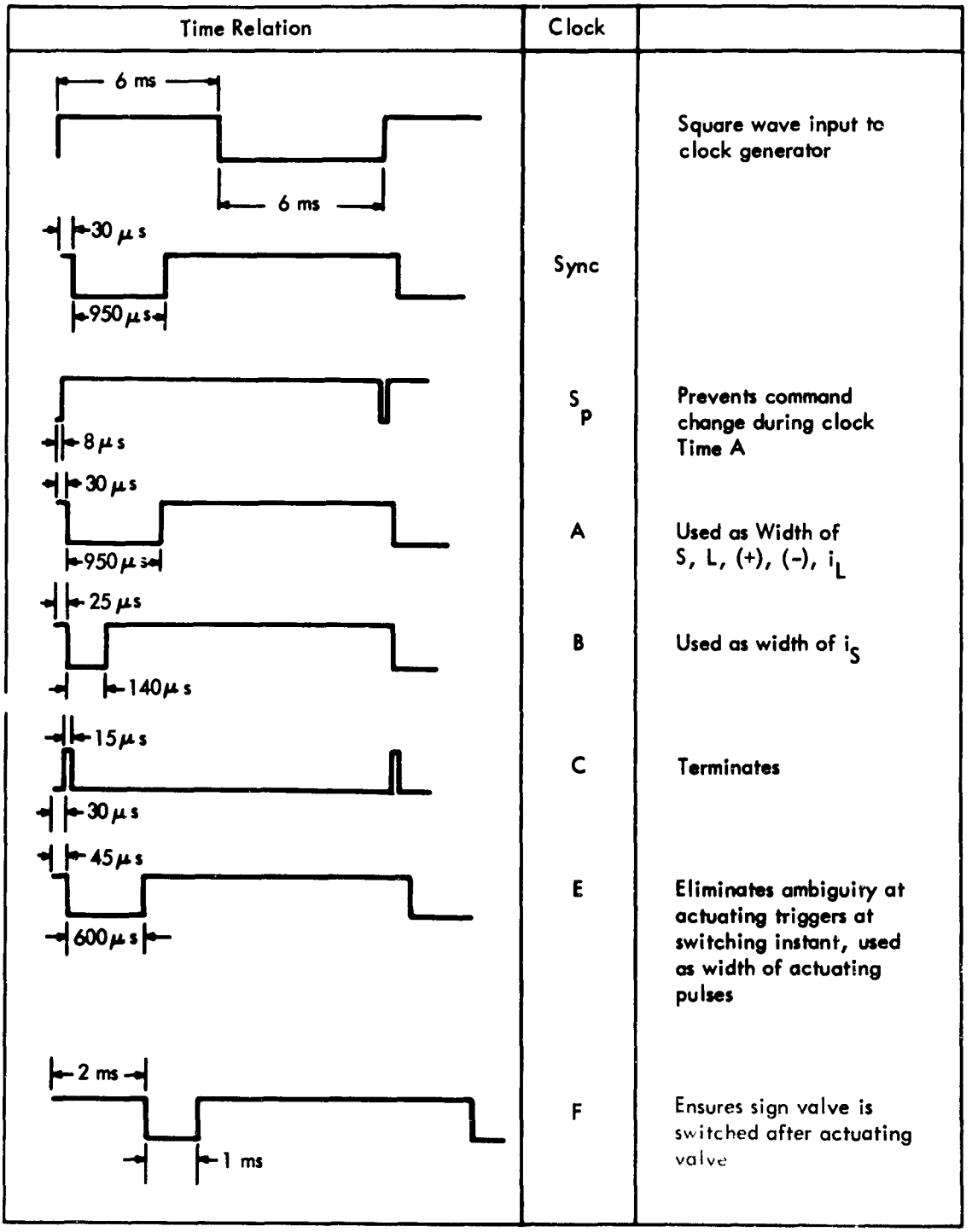

Figure B-1. Clock Pulses - Function and Time Relation (Revised)

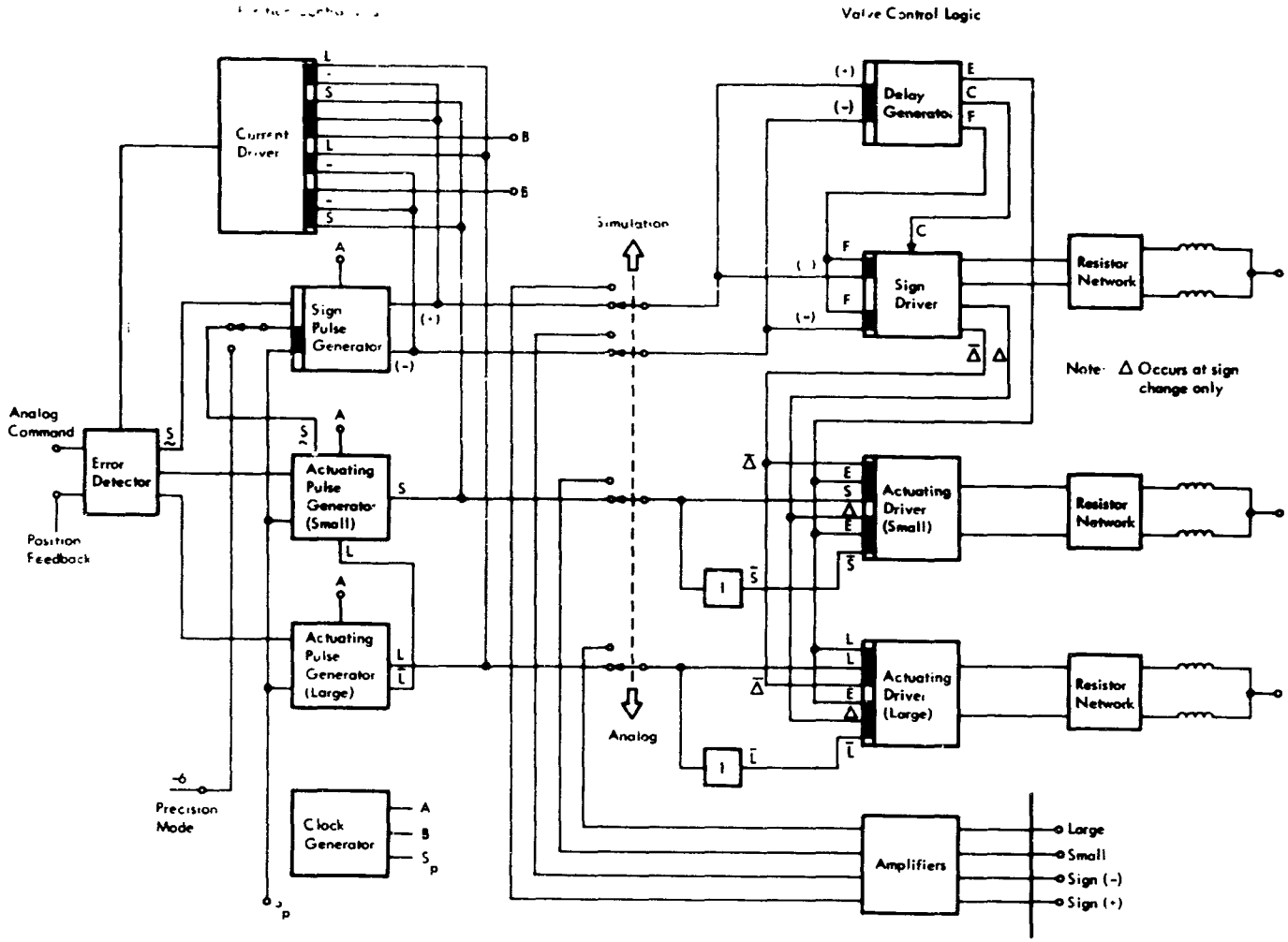

Figure B-2. Central Logic

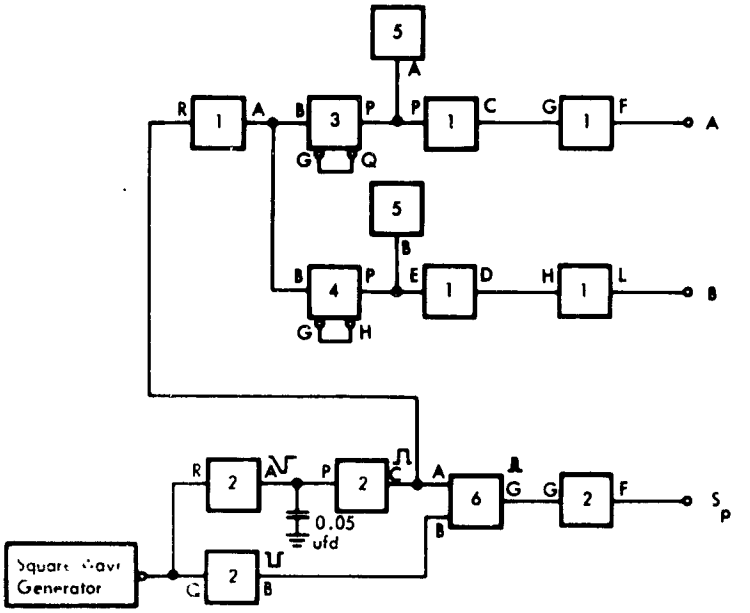

Figure B-3. Clock Generation

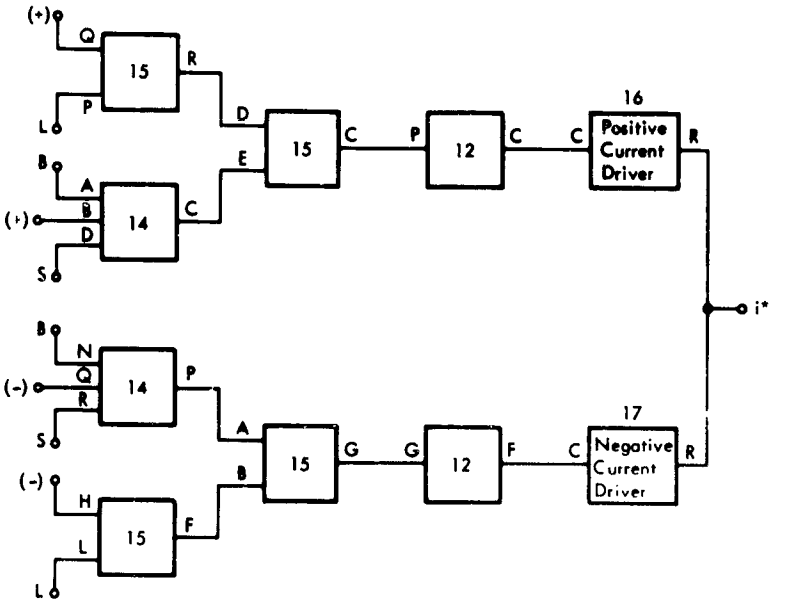

Figure B-4. Current Driver

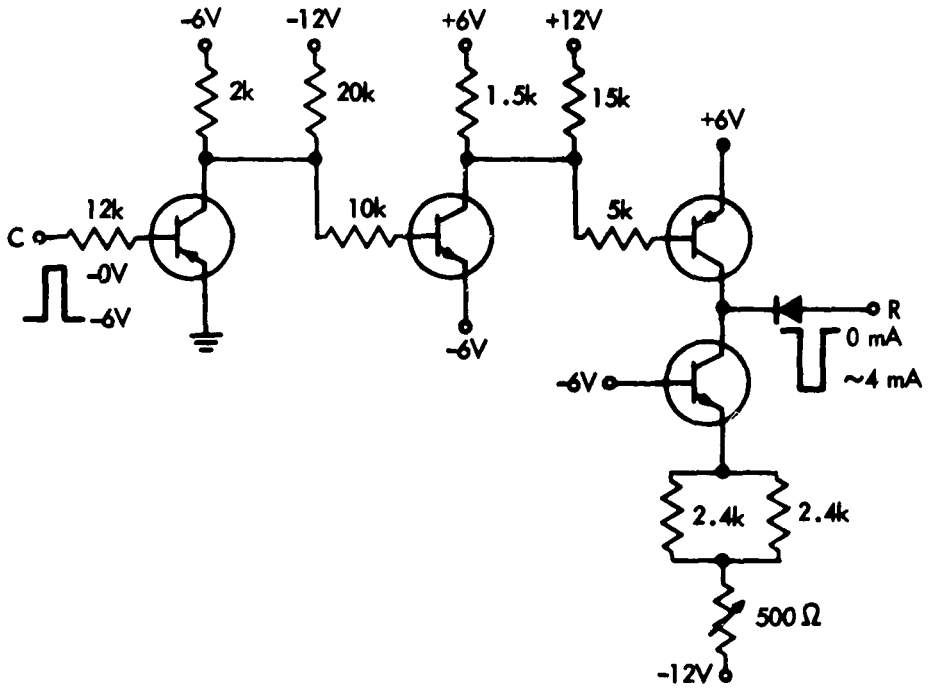

Figure B-5. Negative Current Driver

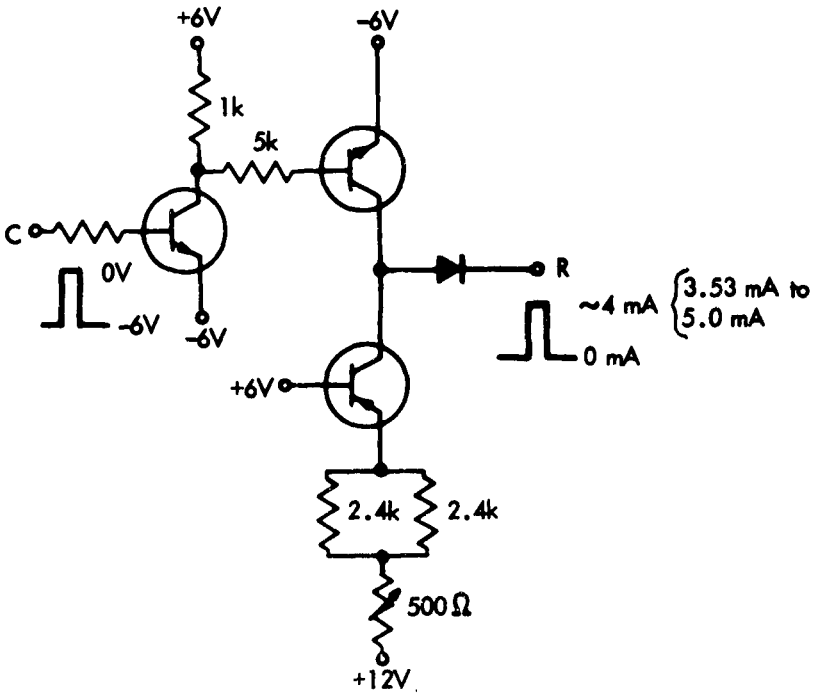

Figure B-6. Positive Current Driver

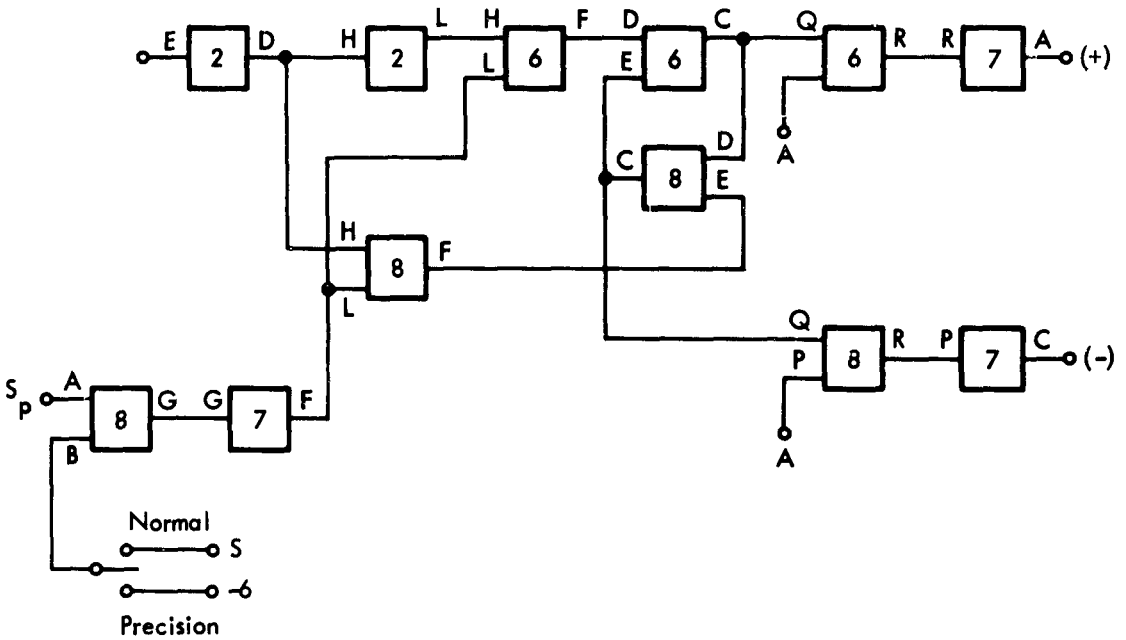

Figure B-7. Sign Pulse Generation

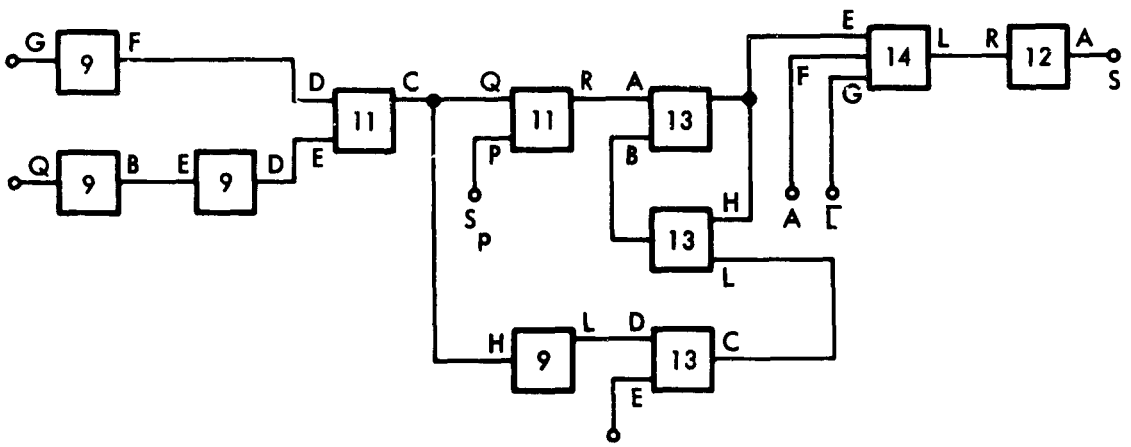

Figure B-8. Small Pulse Generation

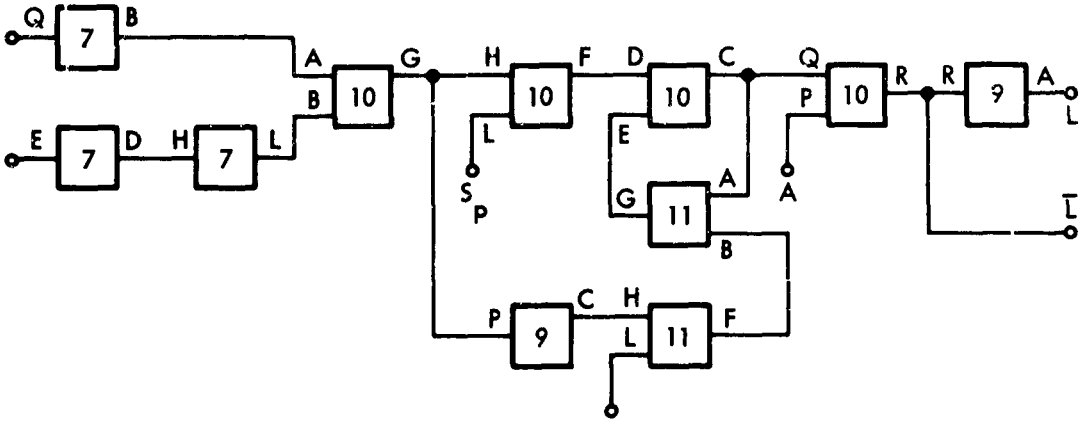

Figure B-9. Large Pulse Generation

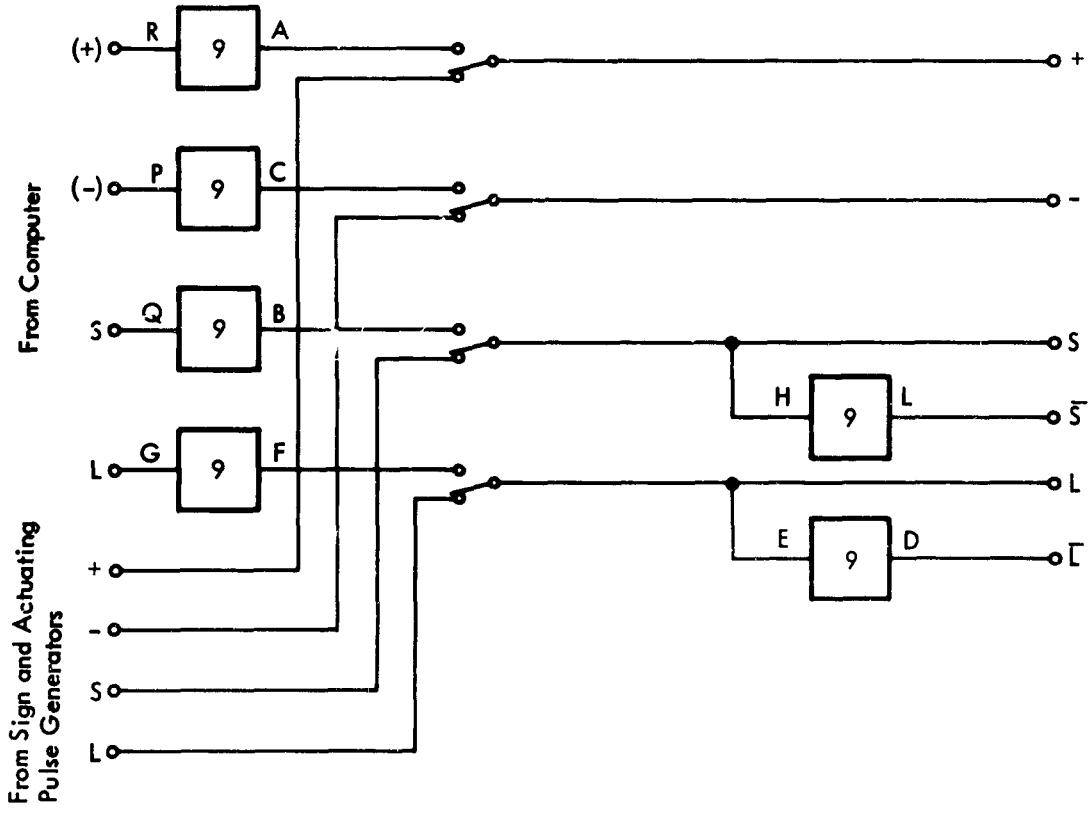

Figure B-10. Amplifiers and Command Inverters

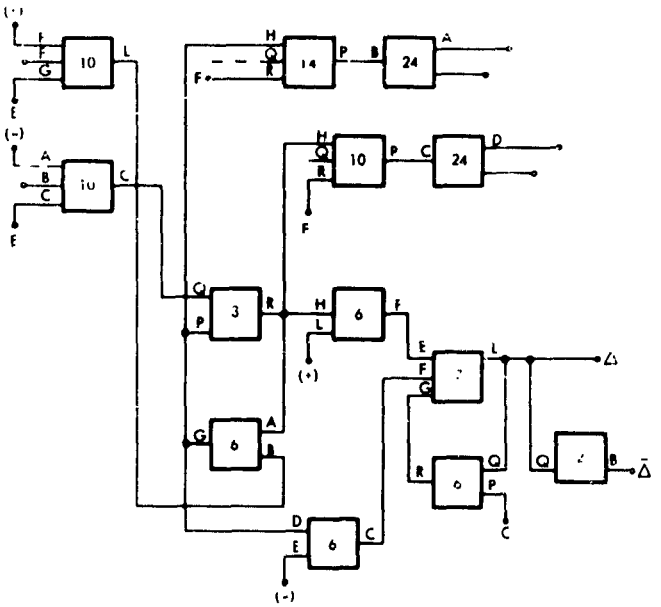

Figure B-11. Sign Driver

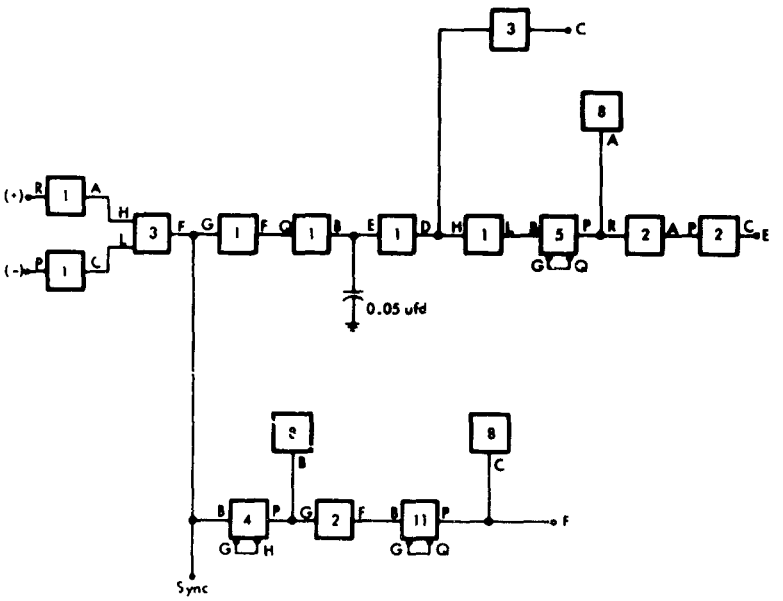

Figure B-12. Delay Generation Logic

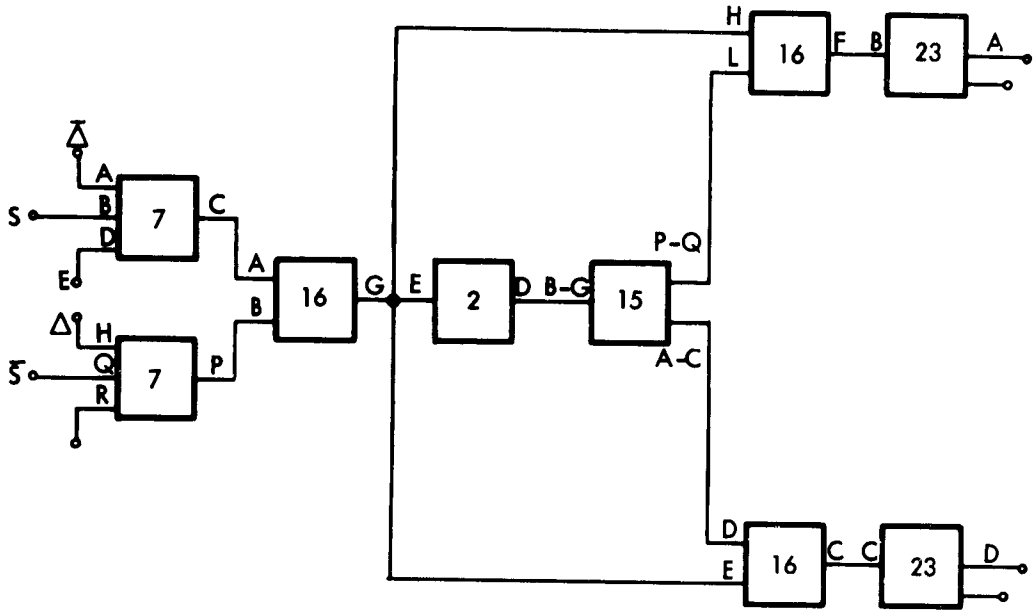

Figure B-13. Small Actuating Driver

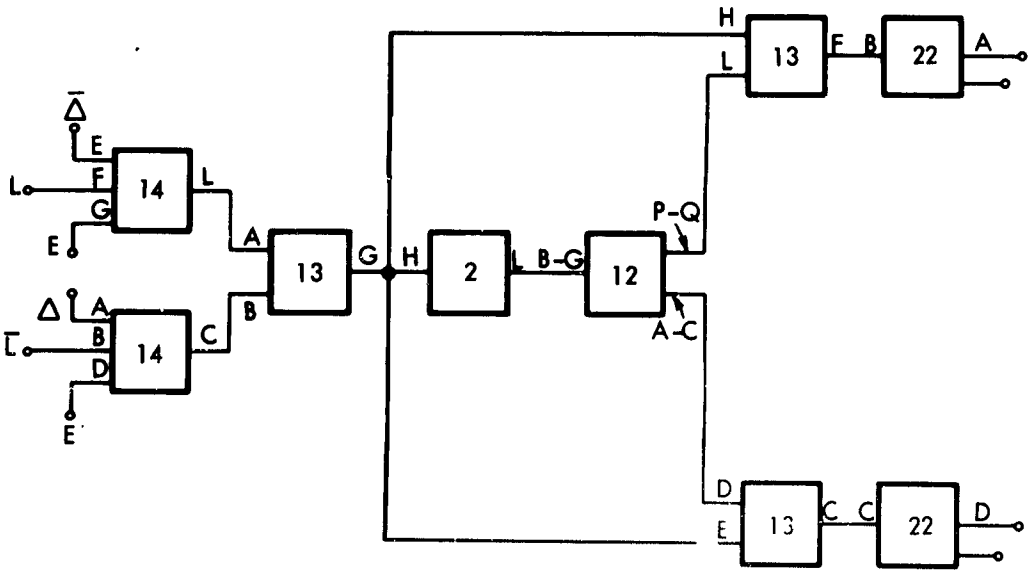

Figure B-14. Large Actuating Driver

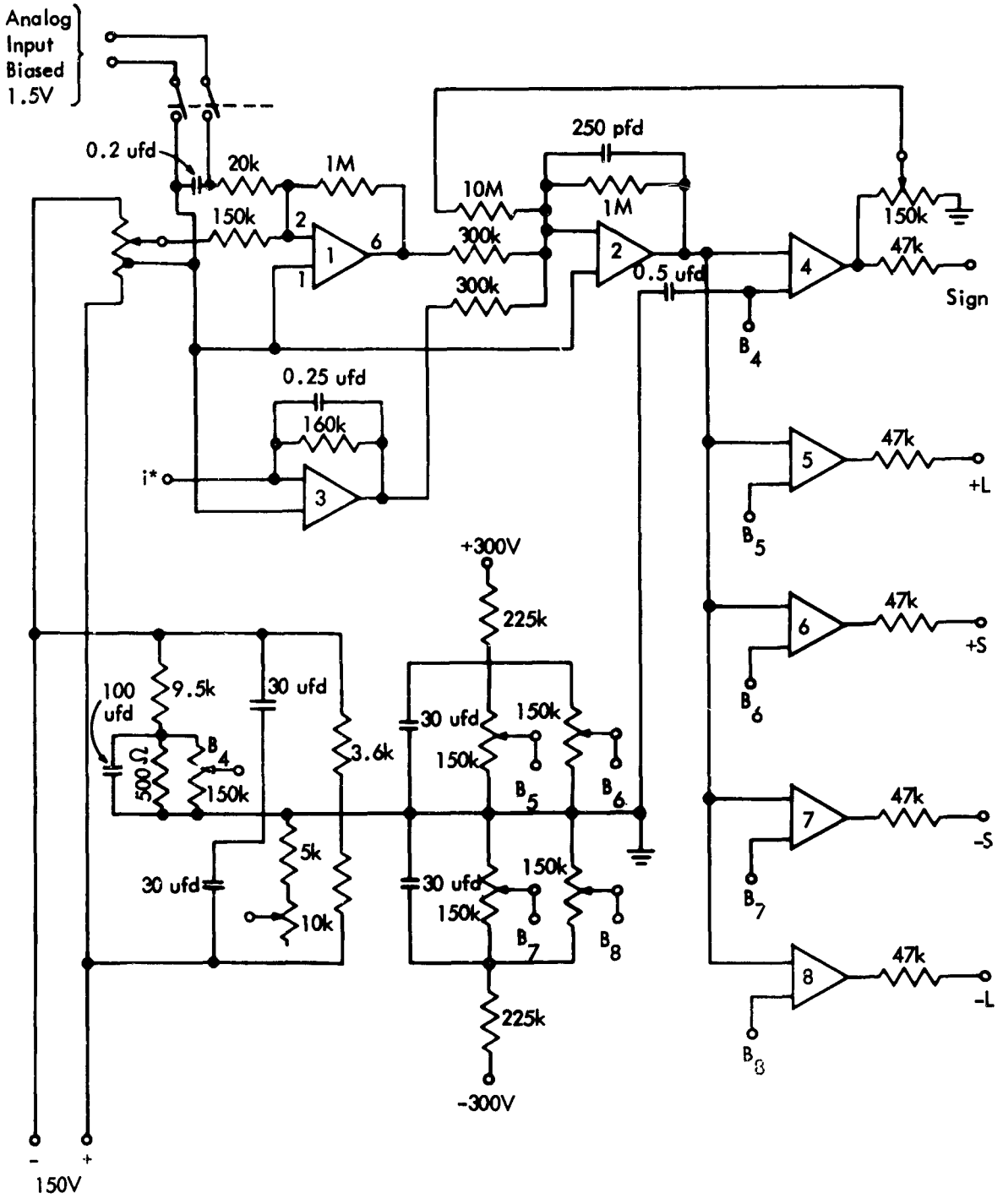

Figure B-15. Error Detector

Appendix C

LIST OF SYMBOLS

Appendix C

LIST OF SYMBOLS

Symbol	Dimension	Definition
A_c	in^2	Area of Calibrating Piston
A_L	in^2	Area of Ram Piston Exposed to P_L
A_R	in^2	Area of Ram Piston - Rod End
A_2	in^2	Area of Auxiliary Piston 2 Exposed to P_L
a_2	in^2	Area of Auxiliary Piston 2 Exposed to P_s
A_3	in^2	Area of Auxiliary Piston 3 Exposed to P_L
a_3	in^2	Area of Auxiliary Piston 3 Exposed to P_s
C	$lb - s/in^{-1}$	Viscous Damping Coefficient
$C_{N\beta}$	—	Gradient of Normal Force Coefficient with Respect to Angle of Sideslip
e_b	deg	Error Required to Produce Input - Large
e_s	deg	Error Required to Produce Small Volume Command
FB	—	Feedback
ΔF	—	External Force
K	—	Forward Path Gain of Integration Compensation - Equal to $K_i T$

Symbol	Dimension	Definition
K_a	–	Pitch and Yaw Attitude Autopilot Gain
K_b	–	Weighting Factor for Yaw Body Angles
K_g	–	Variable Gain Used to Determine Gain Margin
K_i	s^{-1}	Forward Path Gain of Autopilot Integration Compensation
K_L	deg s^{-1}	Leakage Rate Gain
K_r	s	Yaw Rate Autopilot Gain
K_2	deg/pulse	Proportionality Factor for Guidance Yaw Command and Pulses
ℓ_p	ft	Aerodynamic Control Arm
ℓ_e	ft	Axial Control Arm
M	lb - s^2/in^{-1}	Lumped Mass of Output Ram Piston Including Load Inertia
M_y	radians/ pound	Missile Transfer Function ψ/T_y
N_y	–	Algebraic Sum of Yaw Steering Pulses
N_{yFB}		$\frac{K_B}{K_2}\psi$
$N_{y\epsilon}$		$N_y(t) + N_{yFB}$
P_d	lb/in^2	Pressure Change of P_L
P_h	lb/in^2	High Pressure
P_L	lb/in^2	Transient Total Internal Pressure

Symbol	Dimension	Definition
P_m	lb/in^2	Maximum Deviation of P_L
P_r	lb/in^2	Return Pressure
P_s	lb/in^2	Supply Pressure
q	$in^3 - s^{-1}$	Flow
Q_{corr}	in^3/s	Correction Required to Make Analog Integrated Value V_B Equal to Integrated Value, V_{dig}
Q_{p_i}	in^3/s	Flow for Specified Parts of the Period T
Q_p	in^3/s	Summation Q_{P_L} and Q_{corr} at Sample Time
$\overline{q}$	lbf/in^2	Dynamic Pressure
q_{LC}^*	in^3/s	$q_{LC} + \frac{2}{P_h - P_r} \left[P_h \frac{A_R}{A_L} - \frac{P_h + P_r}{2} \right] q_L$
q_{LC}	in^3/s^{-1}	Error Rate Leakage
q_L	in^3/s^{-1}	Leakage Rate Gain
r_1	$lb\ s/in^{-5}$	Flow Resistance
R	in	Moment Arm
S	s^{-1}	Laplace Transform Variable
$\overline{S}$	ft^2	Missile Reference Area
T	s	Sampling Period
T_D	s	Delay

Symbol	Dimension	Definition
T_v	s	Valve Operation Period
T_{fB}	s	Fluid Flow Period (Large Volume)
T_{fs}	s	Fluid Flow Period (Small Volume)
T_z	lb	Thrust Along Yaw Axis
$T\Sigma$	lb	Nominal Total Thrust
ΔV	in^3	Volume Transferred Over Interval t_v to $(t_v + T)$
$\Delta V'$	in^3	Volume Transferred Over the Interval $t_{A/D}$ to $(t_{A/D} + T)$
V_{dig}	in^3	Digital Summation of $\Delta V'$
ΔV_1	in^3	Volume Transferred Over the Interval t_v to $(t_{A/D} + T)$
ΔV_2	in^3	Volume Transferred Over the Interval $(t_{A/D} + T)$ to $(t_v + T)$
V_p	in^3	Analog Integrated Value of the Flow Q_p
V_B	in^3	Leakage Volume Change Due to the Pressure P_d
V_T	in^3	Total Volume Producing Ram Motion
V_ϵ	in^3	Volume Generating Pressure P_d

Symbol	Dimension	Definition
V_{CS}	in^3	Displacement Volume of Calibrating Small Piston
V	in^3	Oil Volume of Digital Hydraulic Actuator
V_{CB}	in^3	Displacement Volume of Calibrating Piston - Large
V_T	in^3	Total Volume Producing Ram Motion
X_1	in	Displacement of Output Ram Piston
X_{1A}	in	Actual Displacement of Output Ram Piston
δ_a	deg	Actual Nozzle Rotation
δ_β	deg	Feedback Gain
δ_c	rad	Desired Nozzle Position
δ_n	deg	Feedback Gain
δ_p	deg	Feedback Gain
δ_L	deg	Feedback Gain
$\dot{\delta}_{LC}$	deg s^{-1}	Error Rate Leakage
β	lbf/in^2	Bulk Modulus
$\beta(t)$	rad	Angle of Sideslip
δ_q	deg	One Quantum
ζ	deg, rad	Rotatable Nozzle Cant Angle
ψ	deg, rad	Yaw Angle
ϵ	deg	Desired Change of Nozzle Position

APPENDIX D

DISTRIBUTION LIST
NONR 4375(00)

Appendix D

DISTRIBUTION LIST - NONR 4375(00)

Chief of Naval Research
Department of the Navy
Washington, D. C. 20360
Attn: Code 461 (2)

Commander
Naval Air Systems Command
Department of the Navy
Washington, D. C. 20360
Attn: AIR-5301 (1)
AIR-5303 (1)
AIR-3033B (1)
AIR-53321G (1)

Commander
Naval Ordance Systems Command
Department of the Navy
Washington, D. C. 20360
Attn: ORD(SP-2702) (1)
ORD(SP-2731) (1)
ORD-62311 (1)

Commander
Naval Ships Systems Command
Department of the Navy
Washington, D. C. 20360
Attn: 6178D04 (1)

U.S. Naval Postgraduate School
Department of Electrical Engineering
Monterey, California 93940
Attn: Dr. G. Thaler (1)
Dr. H. A. Titus (1)

National Aeronautics & Space Administration
Washington, D. C. 20546
Attn: REC (1)

Air Force Flight Dynamics Laboratory
FDLC
Wright-Patterson AFB
Dayton, Ohio 45433
Attn: F. R. Taylor (1)

Commanding Officer
U.S. Naval Ordance Test Station
China Lake, California 94313
Attn: D. P. Augency (1)

Defense Documentation Center
Cameron Station, Building 5
5010 Duke Street
Alexandria, Virginia 22314 (20)

Security Classification

DOCUMENT CONTROL DATA - R&D

(Security classification of title, body of abstract and indexing annotation must be entered when the overall report is classified)

1 ORIGINATING ACTIVITY *(Corporate author)* IBM Corporation, Federal Systems Division Electronics Systems Center, Owego, New York	2a REPORT SECURITY CLASSIFICATION Unclassified 2b GROUP

3 REPORT TITLE

DIGITAL HYDRAULIC ACTUATOR STUDY
Phase III, Final Report

4 DESCRIPTIVE NOTES *(Type of report and inclusive dates)*

Final Report

5 AUTHOR(S) *(Last name, first name, initial)*

Scott, George W.

6 REPORT DATE November 1966	7a TOTAL NO OF PAGES 99	7b NO OF REFS 5
8a CONTRACT OR GRANT NO 4375(00) b. PROJECT NO c d	9a ORIGINATOR'S REPORT NUMBER(S) 66-L03-005 9b. OTHER REPORT NO(S) *(Any other numbers that may be assigned this report)*	

10 AVAILABILITY/LIMITATION NOTICES

11 SUPPLEMENTARY NOTES	12 SPONSORING MILITARY ACTIVITY Air Programs, Office at Naval Research

13 ABSTRACT

To further support the practicability of the digital hydraulic actuator as a control component, IBM has successfully demonstrated operation of the Phase III laboratory model in a simulated digital flight control system. Performance using the laboratory model is compared with the performance when using a mathematical model. Recorded transients and the values obtained for a maximum stable step and gain change are presented. The effect of varying the actuator parameters and the validity of a linearized model is also established. Agreement of the results shows the mathematical model to accurately represent the actual hardware. Hence, this study verified the results of both Phase I and Phase II.

DD FORM 1 JAN 64 1473

Security Classification

14 KEY WORDS	LINK A		LINK B		LINK C	
	ROLE	WT	ROLE	WT	ROLE	WT
Actuators						
Digital Control Valve						
Digital Hydraulics						
Digital Control						

INSTRUCTIONS

1. ORIGINATING ACTIVITY: Enter the name and address of the contractor, subcontractor, grantee, Department of Defense activity or other organization *(corporate author)* issuing the report.

2a. REPORT SECURITY CLASSIFICATION: Enter the overall security classification of the report. Indicate whether "Restricted Data" is included. Marking is to be in accordance with appropriate security regulations.

2b. GROUP: Automatic downgrading is specified in DoD Directive 5200.10 and Armed Forces Industrial Manual. Enter the group number. Also, when applicable, show that optional markings have been used for Group 3 and Group 4 as authorized.

3. REPORT TITLE: Enter the complete report title in all capital letters. Titles in all cases should be unclassified. If a meaningful title cannot be selected without classification, show title classification in all capitals in parenthesis immediately following the title.

4. DESCRIPTIVE NOTES: If appropriate, enter the type of report, e.g., interim, progress, summary, annual, or final. Give the inclusive dates when a specific reporting period is covered.

5. AUTHOR(S): Enter the name(s) of author(s) as shown on or in the report. Enter last name, first name, middle initial. If military, show rank and branch of service. The name of the principal author is an absolute minimum requirement.

6. REPORT DATE: Enter the date of the report as day, month, year; or month, year. If more than one date appears on the report, use date of publication.

7a. TOTAL NUMBER OF PAGES: The total page count should follow normal pagination procedures, i.e., enter the number of pages containing information.

7b. NUMBER OF REFERENCES: Enter the total number of references cited in the report.

8a. CONTRACT OR GRANT NUMBER: If appropriate, enter the applicable number of the contract or grant under which the report was written.

8b, 8c, & 8d. PROJECT NUMBER: Enter the appropriate military department identification, such as project number, subproject number, system numbers, task number, etc.

9a. ORIGINATOR'S REPORT NUMBER(S): Enter the official report number by which the document will be identified and controlled by the originating activity. This number must be unique to this report.

9b. OTHER REPORT NUMBER(S): If the report has been assigned any other report numbers *(either by the originator or by the sponsor)*, also enter this number(s).

10. AVAILABILITY/LIMITATION NOTICES: Enter any limitations on further dissemination of the report, other than those imposed by security classification, using standard statements such as:

(1) "Qualified requesters may obtain copies of this report from DDC."

(2) "Foreign announcement and dissemination of this report by DDC is not authorized."

(3) "U. S. Government agencies may obtain copies of this report directly from DDC. Other qualified DDC users shall request through _____."

(4) "U. S. military agencies may obtain copies of this report directly from DDC. Other qualified users shall request through _____."

(5) "All distribution of this report is controlled. Qualified DDC users shall request through _____."

If the report has been furnished to the Office of Technical Services, Department of Commerce, for sale to the public, indicate this fact and enter the price, if known.

11. SUPPLEMENTARY NOTES: Use for additional explanatory notes.

12. SPONSORING MILITARY ACTIVITY: Enter the name of the departmental project office or laboratory sponsoring *(paying for)* the research and development. Include address.

13 ABSTRACT: Enter an abstract giving a brief and factual summary of the document indicative of the report, even though it may also appear elsewhere in the body of the technical report. If additional space is required, a continuation sheet shall be attached.

It is highly desirable that the abstract of classified reports be unclassified. Each paragraph of the abstract shall end with an indication of the military security classification of the information in the paragraph, represented as *(TS), (S), (C), or (U)*.

There is no limitation on the length of the abstract. However, the suggested length is from 150 to 225 words.

14 KEY WORDS: Key words are technically meaningful terms or short phrases that characterize a report and may be used as index entries for cataloging the report. Key words must be selected so that no security classification is required. Identifiers, such as equipment model designation, trade name, military project code name, geographic location, may be used as key words but will be followed by an indication of technical context. The assignment of links, roles, and weights is optional.